Robotic timber connection

Van Laar, J.

Award date:
2021

Department of the Built Environment
Master Architecture, Building and Planning
Specialization Structural Design

Robotic Timber Connection

Master Thesis

Joren van Laar

Supervisors:
prof. ir. -ing. P. (Patrick) Teuffel
Chairman Innovative Structural Design
ir. A.P.H.W. (Arjan) Habraken
Assistant Professor Innovative Structural Design
ir. A.H. (Arjen) Deetman
Doctoral candidate

Final version

Eindhoven, April 2021

Abstract

Formerly craftsman architecture was a popular section in the building sector. Besides the strength of a joint, also the assembly and appearance were important. However, when mass production became more important, the hand-made detail almost disappeared in architecture. Only in some countries it is still an occasionally used connection design. In recent years computational design and production possibilities increased tremendously, which made a lot possible. Craftsman architecture in the original form, fabricated by human hands, is still labour intensive. Though with robotic fabrication similar complex joints can be executed with higher accuracy in less time. On this development the research goal is established:

"Design and develop a timber connection, fabricated and assembled by a robot, without using mechanical fasteners or adhesives."

To reach the set goal several steps have been walked through. First of all, a study has been done in the existing joints. It is found that connections made without mechanical fasteners or adhesives mostly transfer compressive forces, sometimes some tensile forces, but almost never bending moments. Also the number of elements that come together in one node is limited, mostly with a maximum of two or three elements. With this information an ideal structural scheme of which the joint will be part is found. A *Warren* truss is chosen because there are only compressive and tensile forces, and the maximum number of elements that come together in one node is three, if the bottom and top members are executed as one continuous member. With this information, a joint is designed and modelled in Abaqus. The weaknesses found in Abaqus are analyzed and a new joint is found. As a result the *Rotating Gooseneck connection* is found as the most ideal shape for the joint. The joint is designed parametrically so that parameters can be altered. This is used in the structural optimization to find the strongest ratio of the parameters. Eventually the found optimal joint is examined in two practical applications.
Afterwards the joint will be fabricated and assembled. A theoretical fabrication and assembly is discussed first, then the real fabrication is elaborated. Found limitations are implemented in finding an alternative approach to make the joint. Finally in a similar way a model is made for a laboratory tensile test. Due to fabrication issues the results of the laboratory test are not completely trustworthy. Tough, the tested joint seems to have a strength that is close to the calculated strength.

Preface

When I was looking for a graduation topic I knew I wanted to do something out of the box. The graduation project is provisionally the last project with a lot of freedom for a long time. When I spoke with Arjan Habraken about graduating, he told me two robots were coming to the TU/e on a short notice. There was no clear assignment, but I had to think of applying the robot(s) in a structural way. Initially it was hard to find a good starting point, but after watching a lot of videos of woodworkers making complex joints I came to the realization that I could use this as a base. It led to my graduation subject: Robotic Timber Connection. This master thesis is written for the completion of the master track Architecture, Building and Planning, with the specialization Structural Design, at the Eindhoven University of Technology.

Still in the starting phase of my graduation project, I joined some lectures of a course where the final product was made by a robot. At that time we thought we were the next to start doing tests with the robot, but then came the COVID-19 pandemic. It literally scrambled the planning and the approach had to be adjusted. This resulted in a numerical and theoretical research, the experimental part was left out for a long time. Ideally the three approaches were done simultaneously to compare results with each other instantly. Now, only in the final phase the findings could be tested by the robot and in a structural test.

My supervision committee consists out of Patrick Teuffel, Arjan Habraken and Arjen Deetman. I would like to thank them for their guidance every two weeks during the FAMO-meetings. They gave me the freedom to do what I had in mind, but mentioned the risks and always helped me to continue in the right direction. During these FAMO-meetings my fellow students also gave feedback, of which I am also grateful. Furthermore I would like to thank the complete staff of the laboratory in Vertigo at the TU/e. They always found time for me when I had to finish something in time. Also, they thought of more practically clever solutions, when I had something in mind that would not work out in practice. Besides I would like to express my gratitude to MetsäWood (the Netherlands) and DUPAC (Belgium) for providing me the materials and their properties that I needed for the laboratory test.

Finally I would like to thank my family for their unconditional mental, but definitely also financial, support during the complete graduation project. Moreover I would like to thank my friends for maintaining a good balance between study and leisure. At last I would like to show my appreciation for my girlfriend, who has been there for me every day and helped me going on, even if things were not going as planned.

Joren van Laar — Eindhoven, April 2021

Contents

Chapter 1

Introduction

1.1 Introduction to the graduation topic

In the late 19^{th} century craftsman architecture was very popular in the building sector. There was a great desire to incorporate hand-made details and organic elements into the family homes. In some countries you can still see the use of the craftsman carpentry in houses, for example in Japan. Japanese joinery is well-known for its special cut connections that not only provide strength and perfect contact, but also have a beautiful appearance (Hayashi et al., n.d.). In traditional Japanese wooden structures it was particularly important, because structural elements were usually visible from outside. Another advantage is that these joints made it possible to disassemble and reassemble the whole structure. This gave the opportunity to replace damaged or rotten structural elements, which contributes to a durable structure. Despite all of these benefits, as the demand for houses increased, and the amount of master craftsmen decreased, the carpentry connections were not the most effective way to build houses anymore. Less labour intensive methods were preferred to keep up with the increasing demand.

In recent years computational design and production possibilities increased tremendously. Existing computational design technologies became more advanced and new software showed up as well. More advanced design technologies lead to more complex designs. These complex designs also need better production possibilities, without the help of new technologies the advanced designs are difficult to manufacture. With the introduction of CNC (Computer Numerical Control) machining and robots the possibilities became infinite. More complex shapes could be made with higher accuracy.

Nowadays it would be possible to create craftsman joinery with the help of robots. However, traditional carpenters used approximately 180 different tools to create each complex connection (Locher, 2010). These were basically extensions of their hands which made all angles and corners possible to be made. A robot could use multiple tools as well, although the efficiency decreases a lot when the robot has to change tools often. Contrary to human beings a robot needs more time to change the end effector. Multiple end effectors could be mounted to the robot simultaneously, but there is a limit for this. It will be impossible to attach 180 different tools. Moreover, proceedings would be really hard for a robot to be executed. Therefore making the craftsman connections would need another approach when carried out by a robot.

Milling devices (see figure 1.1a) are better alternatives to make these connections with robots. They can be used very accurately and a lot of different shapes can be milled. Yet, a

milling tool will have a certain diameter, so sharp edges can hardly be made. Hence, traditional carpentry joints cannot be copied and executed by a robot. Consequently, in contrast to traditional joinery which avoided curvature, contemporary fabrication must adjust angular designs to allow for filleted internal-corners (Heesterman and Sweet, 2018). An example of joinery with more curvature is shown in figure 1.1b. What also can be seen is that internally it is not possible to cut square corners. By using router bits with a very small diameter, square corners can be approached. Milling a complete connection with such a small router bit means it will cost a lot of time. To work efficient multiple router bits need to be used then, or the design should be adjusted for the robot.

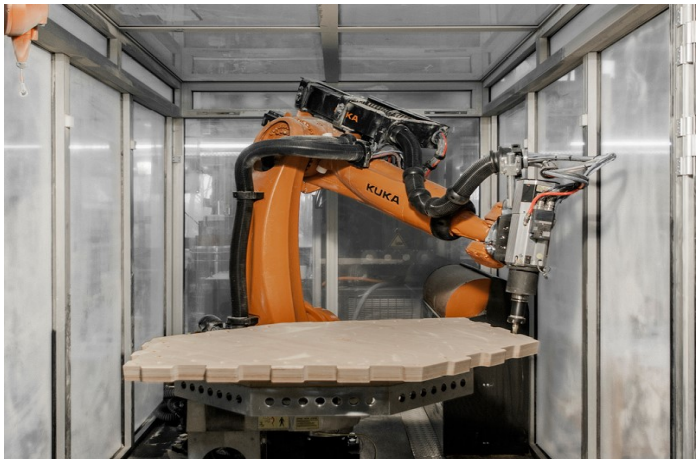

(a) Milling robot

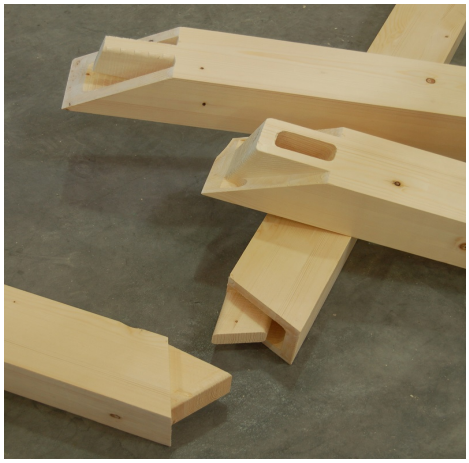

(b) Milled connection

Figure 1.1: Possibilities with robots

1.2 Research goal

In this graduation thesis a structural element will be made where the connections will be manufactured by a robot. Besides, the assembly will also be done by a robot. The elements should be able to be used in a structural application. Both design and execution is a computational process where individual steps will be automated. To formulate the research goal in one sentence:

"Design and develop a timber connection, fabricated and assembled by a robot, without using mechanical fasteners or adhesives."

1.3 Boundary conditions

For the design of the connections several conditions are set. First of all the robot should be able to make the joint without any human interfering. So a timber element will be mounted in a fixed position and the robot mills the complete connection. Then the robot should also assemble the milled elements to form a complete structure. Another requirement is that only timber elements are used. No mechanical fasteners or adhesives are allowed to construct the connection. Finally the assembled structure should also be able to be disassembled. All these conditions contribute to a more sustainable and durable structure.

When designing a connection without mechanical fasteners or adhesives it is very hard to create a connection that is able to withstand bending moments. The connection shown

in figure 1.1b is designed to transfer some bending moments, but the resistance will not be sufficient when applied in a structural application. To evaluate the opportunities, first traditional existing joint are examined.

1.4 Lay-out of thesis

In this thesis all of the previous discussed items will be examined. First existing carpentry connections will be analyzed. Knowing the advantages and disadvantages of certain joints will give more insight in useful applications for such a connection. With the known possibilities of a carpentry joint a structural scheme can be examined. Using the ideal structural scheme for the joint will result in a stronger and stiffer structure. With the help of the developed knowledge gained by the master craftsmen a new connection is designed. This will be designed parametrically with computational design so it is possible to alter the shape. Several alternations will be analyzed further to find the strongest possible shape of the joint. After a shape has been found, the design will be further optimized in the structural design. First the optimal material will be discussed, then the dimensions of the joint can be optimized. To make sure the structure is secured, a locking mechanism will be explained briefly. For the optimized connection two possible applications will be further calculated in a structural report. Both results will be compared to analyze in the influence of the changes. One of the applications will eventually also be executed by a robot. The executed version will be scaled so that it doable for the robot. For this execution several steps must be prepared to eventually mill the connection. After the designed elements have been milled, a laboratory test will be executed on the joint. It is important to see whether the theoretically and numerically found optimized joint behaves like it is expected. Eventually conclusions will be adduced and recommendations for further research are explained.

Chapter 2

Preliminary study

2.1 Types of connections

When looking at types of connections in timber, there is an infinite amount of joints. In the building traditions of timber construction, the Japanese joinery was one of the most inspiring types of joinery, which is still used in Japan a lot. Other parts of the world had different approaches for woodworking, but most of them used mechanical fasteners and adhesives in their designs. In the Japanese joinery this is really avoided, so therefore their connections will be analyzed firstly. Afterwards more topic connections that are still used nowadays will be explored.

2.1.1 Japanese joinery

In the field of timber connections, the Japanese joinery is one of the most coveted ones. The traditional Japanese connections consist out of wood only. Furthermore Japanese joints can be disassembled. Apart from being made by robots, these joints meet all the requirements. So firstly some Japanese joints will be analyzed. The book *Wood joints in classical Japanese architecture* (Sumiyoshi and Matsui, 1991) describes two different kinds of joints.

Splicing joints

First there are splicing joints, these are joints that connect two elements that are positioned in the same direction. For example two beam halves or two column halves, some examples of splicing joints are shown in figure 2.1. The splice beams in figure 2.1a can be used to join ground sills, girders or beams, where the splice beam in figure 2.1b is mostly used for ground

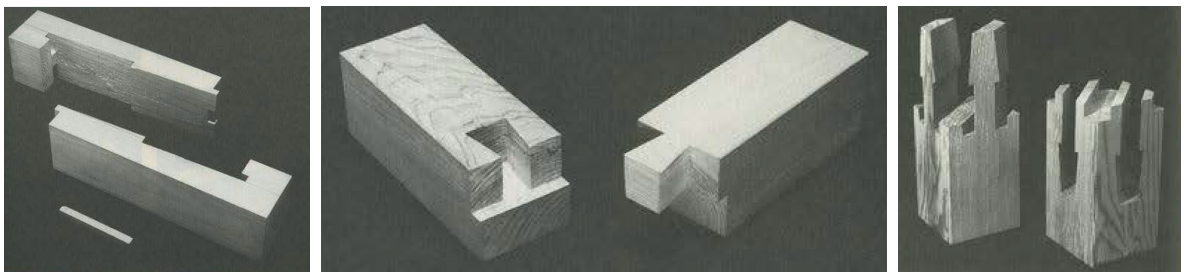

(a) Oblique scarf splice (b) Stepped dovetail splice (c) Column splice

Figure 2.1: Japanese splice joints

sills only. The column splice in figure 2.1c is used in columns, as the name already indicates. Splicing joints are mainly made for compressive forces but are able to withstand some tensile forces. These connections cannot be used to create larger structures, only larger elements. They are not used to connect different members with each other.

Connecting joints

On the other hand there are connecting joints, these are joints that connect different members, for example a beam with a column. In figure 2.2 some of the connecting joints are shown. There are some clear differences between the joints. In figure 2.2a for example, a wedge needs to be driven in as deep as possible to avoid rattling. The connection can be disassembled by removing the wedge. The second joint, figure 2.2b, works differently. Instead of inserting a wedge to lock the connection, the end of the member locks itself. The dovetail is inserted in the larger opening of the mortise and then it is shifted sideways to a narrower slot which has the inverted shape. Now the connection is already locked in the direction of the forces, only a plug will be inserted in the larger opening to ensure the joint will not easily come apart. The last example in figure 2.2c is an example that is used often in Japanese joinery. At first sight the connection members do not seem to fit into each other. When the double tenon is inserted in the same angle as the tapered surface, it does fit perfectly. A lot of 'impossible' joints were designed by Japanese carpenters. A disadvantage of the connection in this example is that the tenon can slide out of the mortise when pulled in the right angle.

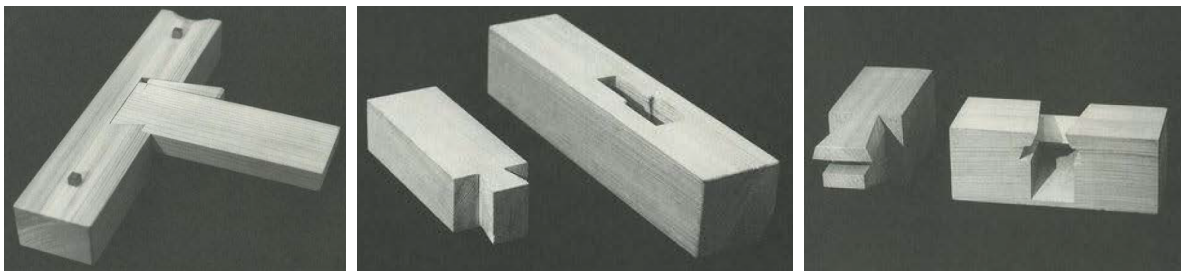

(a) Half dovetailed joint (b) Housed dovetailed joint (c) Sumiyoshi double tenon

Figure 2.2: Japanese connecting joints

Similar to the splicing joints, the connecting joints are mostly used to transfer compressive forces, however with some adjustments in the geometries they would be able to take some tensile forces. Though, the shape of the joints is mainly used to interlock the tenon in the mortise, not to resist high tensile forces.

2.1.2 Current woodworking joints

Nowadays woodworking joints made by hand still work with more or less the same categories of joints. First there are lengthening joints, which are used for increasing the effective length of timber elements. Then there are widening joints, these increase the effective width of timber or board elements. These first two joints can be compared to the splicing joints in the Japanese joinery. The third kind of joints are the framing joints, these are used to terminate or change direction of the timber element. This is similar to the connecting joints.

As explained in the previous section, the lengthening and widening joints are used to increase the size of an individual element. So it is not used to combine multiple elements. For this reason only the framing joints are analyzed in this chapter. In the book *Carpentry and*

joinery 1 (Porter and Tooke, 2001) several framing joints are explained, some of the relevant joints are explained here.

Housing joints

First there are housing joints, these are often used in the construction of shelf and cabinet units, partitions, and sectional timber framed buildings. In figure 2.3a four different housing joints are shown. With exception for the dovetailed joint, all of these joints generally require nailing. Similar to the Japanese joints, the dovetail mainly acts to interlock the connection, not to provide tensile strength. When a relatively high tensile force will act in the vertical element, the connection will most probably fail.

Halving joints

Halving joints are mostly used where timber members are required either to cross or lap each other. The halving joints shown in figure 2.3b are mostly connected without being interlocked. All of the connections have one or two directions in which they can be disassembled. Some of the halving joints need mechanical fasteners or adhesives to be connected securely.

Dovetail joints

Dovetail joints are applied to prevent members from being pulled apart. In figure 2.3c the arrows indicate in which direction the dovetail performs resistance against tensile forces. However dovetail joints are mostly used in shelf and cabinet units. They are not designed to resist great tensile forces.

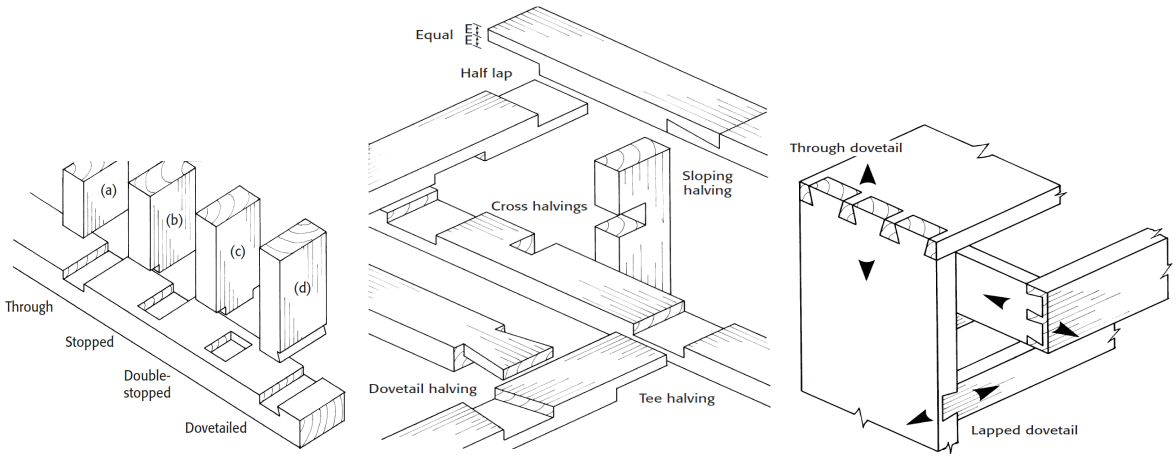

(a) Housing joints (b) Halving joints (c) Dovetail joints

Figure 2.3: Framing joints

2.1.3 Conclusion

The fundamental skill of the woodworker has been measured by his ability to join two pieces of wood securely and with elegance. Traditional wooden joints do no require mechanical fasteners, however the use of nails, screws and metal plates, such as gussets, do make the task easier. Making a strong joint of only wood requires more skills and expends more time. In the ancient world, wooden joints were often made without the use of glue, nails or other fasteners although all these aids were known back then. Many woodworkers today prefer to

incorporate nonwooden devices for joints. If robots are used for the execution of a joint, skills would not be necessary anymore and it would be less time consuming.

As mentioned before most timber joints are mainly used to transfer compressive forces. Some connections can transfer certain amounts of tensile forces, but are mostly not designed for it. When designing a new connection this should be taken into account. It is important to start with determining which eventual structure the joint will be part of. Afterwards it is possible to evaluate which forces can occur in this joint and the joint can be designed to particularly resist these forces.

2.2 Structural scheme

The rigid structure that the connection will be part of needs to be determined. Defining what it will be eventually might add extra boundary conditions. The designed joint will not only be used to connect two elements in the same direction. So it will not be part of a timber frame wall for example. As explained in the previous section timber connections are mostly used for transferring compressive forces. When looking at structures that only consist out of compression, the possibilities are very limited. The only option will be an arch (two-dimensional) or a dome (three-dimensional). To increase the amount of possibilities it is preferable to allow tensile forces as well. The best known structures without any bending moments are trusses.

2.2.1 Trusses

Trusses are in essence a collection of straight members that form a rigid structure. The joints are pinned connections and the loads are only applied on these joints. If not, bending moments will occur in the individual members. However, often gusset plates are used to connect the members of a truss. These connections are not hinged, but if the center lines of all the members intersect at the same point, it is reasonable to assume that the structure behaves like if it were pinned connections.

A distinction can be made between two-dimensional trusses and three-dimensional trusses. Two-dimensional trusses are member structures with all members and loads in a single plane. Within these trusses there are three main types that can be distinguished (Janssen, 2016). These are shown in figure 2.4. There are several essential differences between the trusses. Besides, as already is mentioned in the text next to the figure, having vertical members or not, the diagonals have a fixed task in the first two trusses when loaded with an uniformly divided static load. In the *Pratt* truss the diagonals are only in tension, in the *Howe* truss, the diagonals are for compressive forces only and in the *Warren* truss there is both tension and compression in the diagonals. Note that if the diagonal is in tension, the verticals are in compression, and vice versa. However, when a load is not static or uniformly divided, for example a moving car on a bridge, some members alternate between tension and compression and so will need to be designed accordingly.

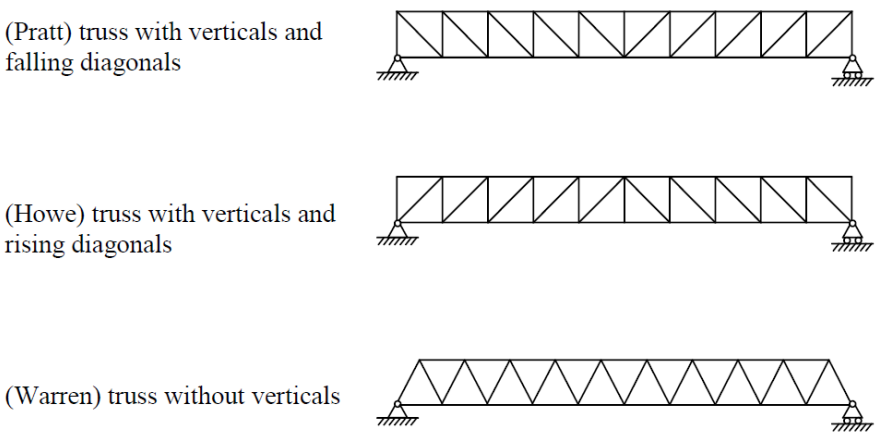

Figure 2.4: Three main types of trusses

The benefit from the trusses with verticals that beforehand it is already known in which members there is tension and in which there is compression only applies for static uniform loads. In theory every detail could be designed for either compression or tension. However, when a connection will be able to resist the tensile forces, it will most probably also resist the compressive forces. Members will be more vulnerable for tension as wood can transfer compressive forces easier in a connection. So the designed connection can presumably be used either in tension or compression. Moreover in case the load is not static or uniformly divided, tension might occur in the compression members, or contrariwise. So it would not be safe to design a connection only to resist one possible force flow.

Where a lot of members come together it will be hard to design a connection where everything can come together. For this reason the *Warren* truss will be more suitable, as there are maximally four members coming together, where in the other trusses five members come together.

Still it will be very difficult to join four different members in one node. First there has to be a splicing or lengthening joint in the horizontal members and then there have to be connecting or framing joints to join the diagonals. All of the members' center lines need to intersect at exactly the same point. Where members are in compression this could be possible, but when there is tension in the horizontal member, the reduced section will probably lead to failure. The effective area that can be used to transfer compressive forces will be similar, because all gaps are filled with the remaining members. Only, the gaps are filled with timber in a different angle, so it does decrease the resistance a little. Though, in tension these gaps do not contribute in the tensile strength. Therefore many connections in one point will significantly reduce the nodes strength in tension.

To reduce the effect of the described issue, a continuous member will be used in the horizontal members. Still the tension strength of the member will be reduced by the notches for the diagonals, but the remaining area can be used with the characteristic tensile strength of the timber elements itself, rather than the strength of the connection. Due to this modification the structure would not act as a truss perfectly. Now bending moments can occur in the horizontal members, although these will remain small in comparison with the tensile and compressive stresses. It is important to make sure the center lines come together in one

point.

2.2.2 Conclusion

Looking at structures where there is only compression and tension, trusses are the most common rigid structures. A combination of a *Warren* truss with continuous horizontal members will reduce the amount of elements coming together to a maximum of three members. With this amount, there is enough space to design a decent connection.

2.3 Conclusion

In the next chapter a connection will be designed with the explained boundaries. In essence, the goal is to design a connection where the diagonal meets the horizontal members. This connection should be designed in a way that it is able to design both compressive as tensile forces. Initially the design will focus mainly on the tensile capacity. These stresses will be governing as connections are more vulnerable for tensile stresses than compressive stresses.

Chapter 3

Design of new connection

3.1 Introduction

In this chapter the studied literature will be used to come to a new design of a timber connection. It is a way of form or shape finding to find an optimal shape for the connection. Form finding focuses more on finding an optimal shape of a structure that is in (or approximates) a state of static equilibrium. In this case, the focus lies on a part of a structure and not the structure as a whole.

The created designs will be analyzed and discussed, and the reasons to change a design will be elaborated. To get more insight in the stresses and strains in the connection, the designs are analyzed in *Abaqus*, this is a software program to make finite element analyses. All designs are generated in *Grasshopper*, in this way dimensions can be changed parametrically. This means that initially assumed dimensions can be adjusted later to increase strength or change the overall shape.

3.2 Sliding dovetail connection

The first design is based on the *Housed dovetail joint* in figure 2.2b. In this joint a dovetail is inserted in the larger opening of the mortise and then shifted sideways into the narrower slot which has the exact inverted shape. To ensure that the joint will not come apart easily, a wooden plug is inserted in the larger slot. The connection in the truss will not be perpendicular to the beams, so the connection is adjusted to the right angle. The modified dovetail connection is shown in figure 3.1a. Similar to the dovetail joint from figure 2.2b the connection is assembled by inserting it in the same way as explained. Once one diagonal is placed, the other diagonal can be inserted as well. This one is mirrored compared to the first one. Finally a wooden plug needs to be inserted between the diagonals.

The beams and diagonal will be milled from one piece of wood, square elements in this case. Therefore the corner of the dovetail (the right bottom in the figure) is missing. The connection has perfect sharp angles in the figure, however when milled these sharp angles cannot be realized. The milled connection would have more filleted corners.

The sliders shown in figure 3.1b are used to generate the connection and truss. All dimensions are in millimeters and the angle is in degrees. The height and width in this case is equal for the diagonals and beams. The extra length is added to keep the dovetail in place and resist the stresses at the end of the beam, this the length starting at the end of the mortise. The width of both the start and the end of the dovetail and the height of the dovetail have great effect on the strength of the connection, so should be adjustable to find the optimal

proportions. The sliders related to to the diagonal are used to change the parameters when for instance the span changes. The angle can only be changed between 30 and 60 degrees, other angles will decrease the strength of the truss tremendously.

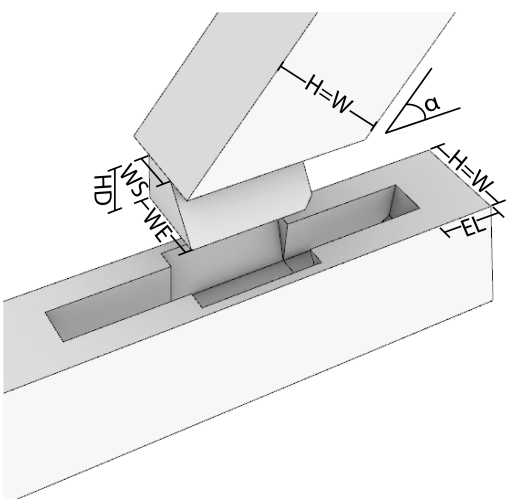

(a) Detail of sliding dovetail joint

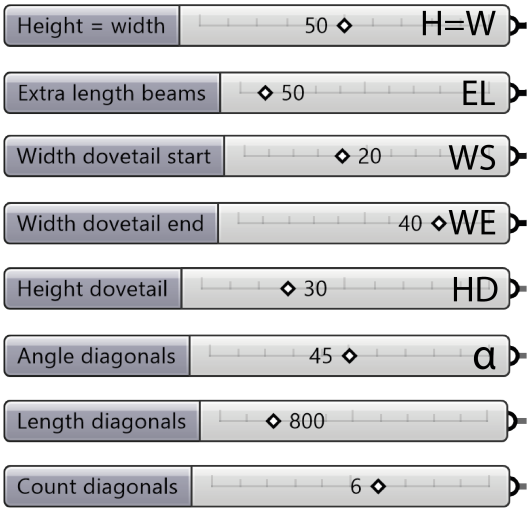

(b) Sliders in sliding dovetail joint

Figure 3.1: Sliding dovetail joint

For the complete assembly the steps are shown in figure 3.2. First the diagonals need to inserted in the top beam. One after another because there is only one larger opening. Then the bottom beam is moved upwards to the diagonals. Now the bottom bar can be shifted to secure the diagonals. Eventually a wooden plug is inserted in all the large openings. However, because the diagonals cannot be shifted once they are inserted in the top bar, the bottom bar needs as many large holes as there are diagonals. The diagonal 'couples' cannot make use of the same opening like in the first part of the assembly. So now the openings will be beneath all diagonals, they cannot be only between the diagonals. This makes this opening very hard to reach when inserting wooden plugs.

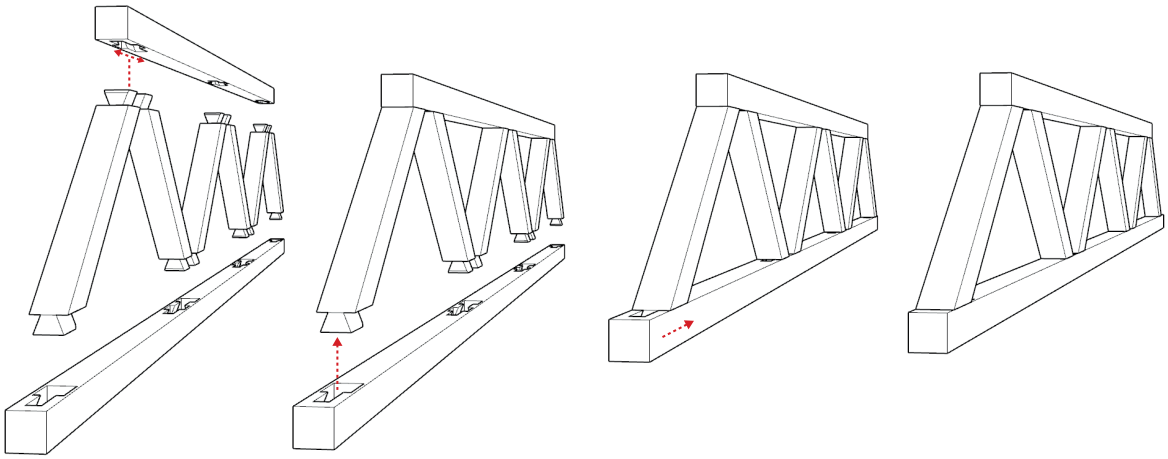

Figure 3.2: Assembly of sliding truss

3.2.1 Conclusions

The sliding dovetail connection has several disadvantages. First of all, the connection is turned with respect to the diagonal. This means that there will be stresses in directions that are not desired in timber. Secondly in the last step of the assembly the complete beam needs to be shifted, which could results in problems when the truss is large. Finally there will be a lot of openings that need to be filled with a wooden plug. This significantly decreases the cross section of the beams when it is in tension and makes the assembly a more difficult and time consuming step.

3.3 Rotating dovetail connection

To tackle the described problems, a rotating connection is explored. One of the great advantages from rotating the diagonals into the beams is that each diagonal can be inserted individually. No large elements need to be moved to assemble the rigid truss.

There are some restrictions that come with a rotating diagonal. First, the geometrical restrictions will be discussed. In figure 3.3 some of the restrictions are visualized. The angle of the diagonals with respect to the beams is limited. The left diagonal is inserted here first. To rotate the right diagonal into its mortise, the diagonal moves along the dotted circle. This will not be possible when the diagonals are placed in this angle. It is only possible if the angle between the diagonals is 90 degrees or larger. Assuming the structure is symmetrical, the connection is possible up to an angle of 45 degrees, like figure 3.3b. It could work when the diagonals are moved from each other, but the center lines will be further apart from each other in this case. The center lines have to cross each other for the most optimal functionality of the truss. When using equal sized beams and diagonals, this is only possible with angles smaller than 45 degrees. With an angle of 45 degrees, the beam height should be $\sqrt{2} \times 50 = 70.7$ mm to make sure the center lines intersect.

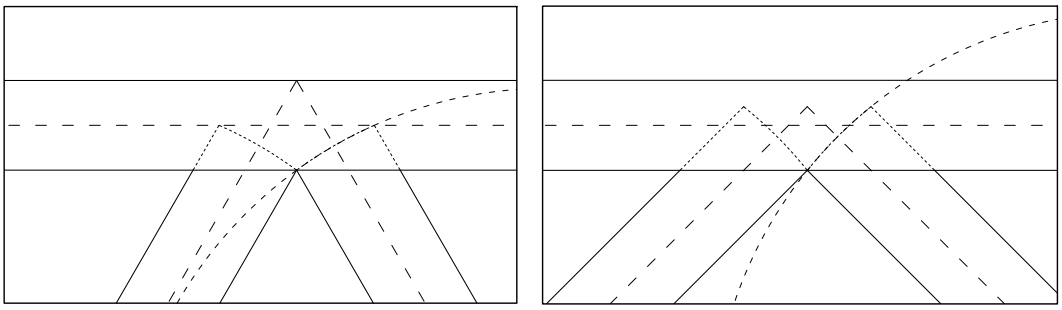

(a) Diagonals placed at 60°

(b) Diagonals placed at 45°

Figure 3.3: Restrictions rotating diagonals

Where in the previous connection the stresses in directions not parallel to the grain direction were in both the diagonals as the beams, in this connection it is mostly in the beam. Hence, this beam is made wider to resist more stresses. For convenience, the same width as the height is used.

Compared to the sliding dovetail, the rotating dovetail has some extra sliders. In figure 3.4 the connection and the sliders are shown. First the height and width of the diagonals and beams can be chosen individually. This has been done for the reason explained previously. Note that the dimensions of the beams are multiplied by $\sqrt{2}$ to make sure the center lines

cross. The remaining sliders are similar to the sliders of the sliding dovetail and have the same functions as explained there.

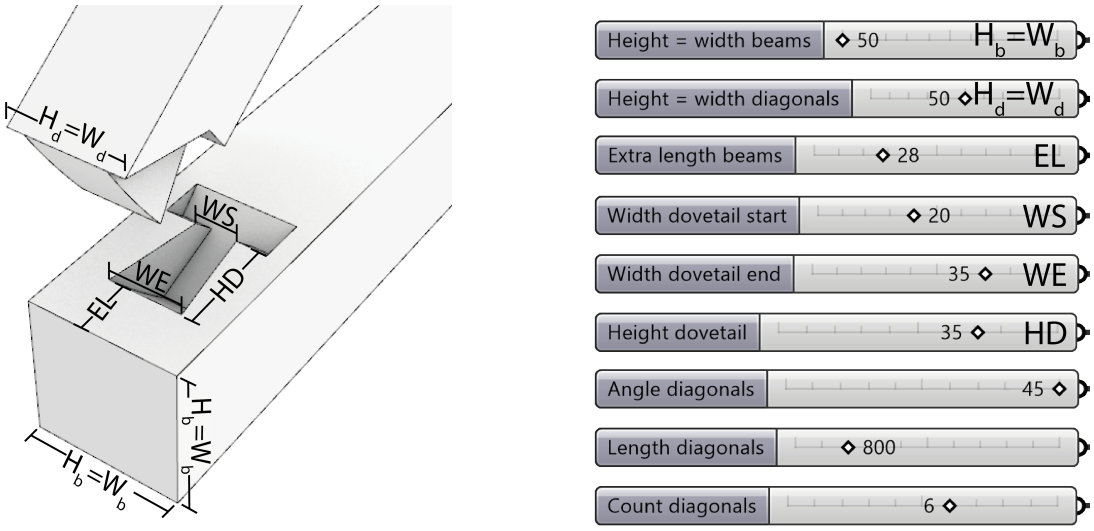

(a) Detail of rotating dovetail joint

(b) Sliders in rotating dovetail joint

Figure 3.4: Rotating dovetail joint

The assembly of the truss is more convenient than the sliding truss (figure 3.5). Every diagonal can be rotated in the right position. It is important to assemble one diagonal into its final position and then continue with the next one. It is not possible to put in two diagonals that are next to each other at the same time because the rotation path crosses.

Another great advantage of the rotating truss is that there are no empty openings that need to be filled afterwards. Ideally the tenon is inserted into the mortise with some resistance, so once pressed inside it will stay inside. Once a load is applied on the truss, the joint cannot come apart anymore because the stresses work perpendicular to the opening of the connection.

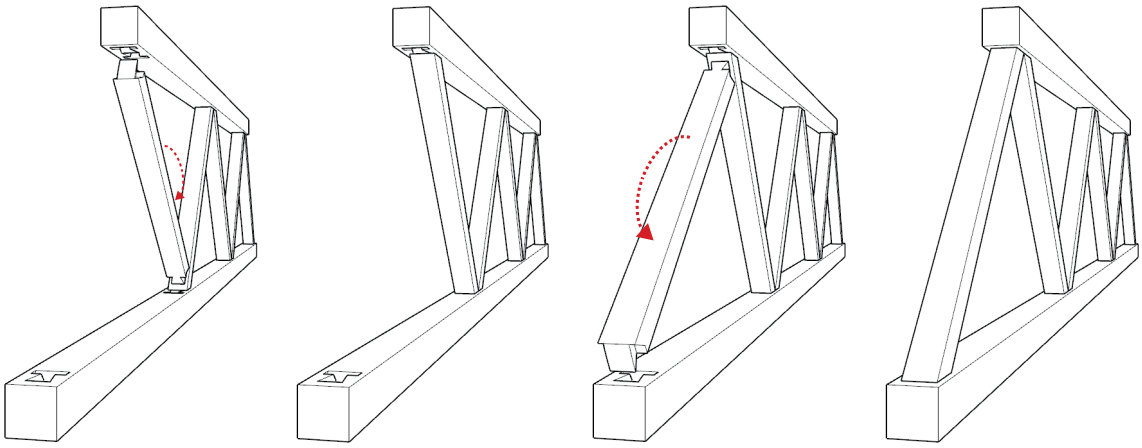

Figure 3.5: Assembly of rotating truss

To evaluate the weaknesses of the connection, a model has been generated in *Abaqus*. For the first calculation the material Western White has been chosen. This model is only for comparison between connections and the behaviour of timber in general. No exact results are taken from this model, so therefore the type of timber is less relevant. The material properties are shown in appendix A.1 and the input for the model in *Abaqus* is shown in appendix A.2. The connection is exactly the same as in figure 3.4a, but in this case two diagonals come together. The interaction is modeled as a hard contact interaction with a friction coefficient of 0.3. There is an extra boundary condition for the diagonal, displacements are only possible in the direction of the applied force, this has been done to prevent the diagonal from rotating. Otherwise the force makes the diagonal rotate out of the mortise. In a truss the next connection will prevent this rotation as well, so this approaches a truss better.

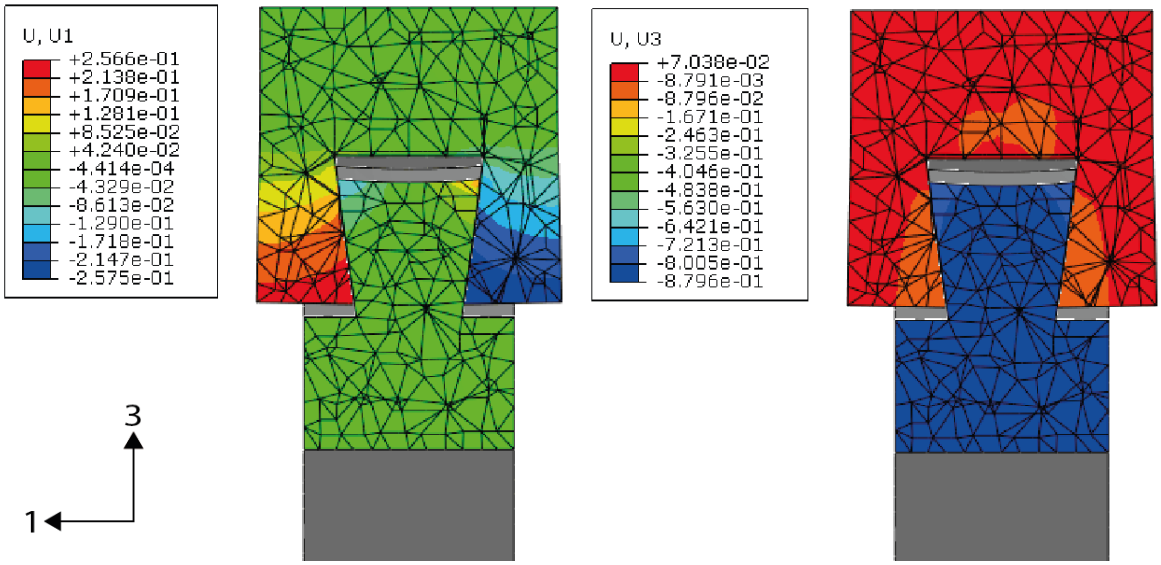

Figure 3.6: Deformations in dovetail connection (scale factor: 4)

To check the initial behaviour of the designed joint, first the displacements will be analyzed. In figure 3.6 the results of the displacements in the 1 and 3 axes are shown (complete output in appendix A.3). The directions of these axes are shown in the bottom left corner. Due to the fact that the mesh is cut at a certain point, the mesh looks chaotic. In the figure the tension that is applied is 5kN per diagonal. What immediately becomes clear is that the dovetail makes the beam tear apart. The result is that the diagonal is pulled out of the mortise, in this case almost 0.9mm, which is more than 1 percent of the beam height. Having this in a truss for every member in tension would give a large total deflection.

3.3.1 Conclusions

Making a rotating dovetail connection has several advantages compared to the sliding dovetail connection. Besides most stresses in the diagonals are parallel to the grain direction, there are no empty openings that need to be filled afterwards. Moreover it is easier to assemble as the diagonal can be inserted after each other without having to move the beams. Still, there are some disadvantages, the stresses in the beams make the mortise open which causes the

diagonal to being pulled out. To tackle this problem a new shape is investigated.

3.4 Rotating gooseneck connection

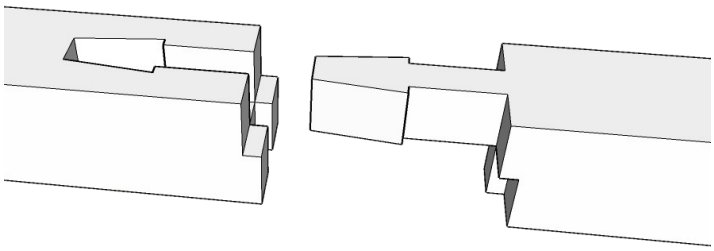

Figure 3.7: Stepped gooseneck splice

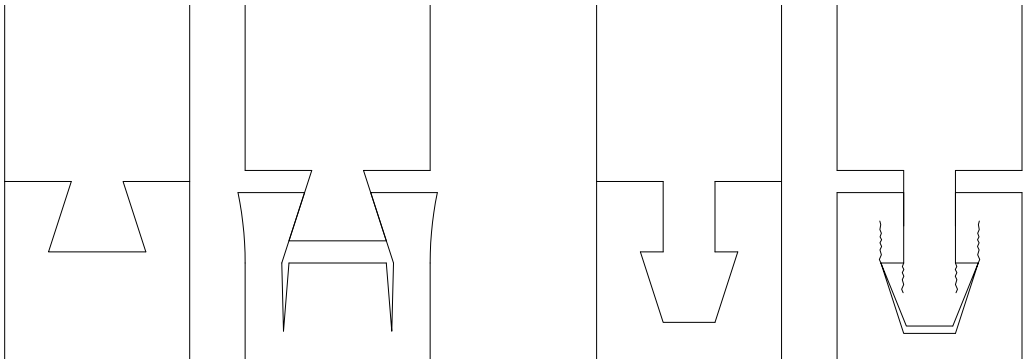

Figure 3.8: Probable failure modes

The biggest problem with the dovetail connection is that it pushes the beam apart. This will always be the case when the shape is tapering. To prevent this from happening another shape is investigated. In the book *Wood joints in classical Japanese architecture* (Sumiyoshi and Matsui, 1991) a *stepped gooseneck splice* (see figure 3.7, the figure is recreated because the quality of the figure in the book is very low) is discussed. In the book they do not use this connection, or something similar, as a connecting joint but only as a splicing joint. However when adjusted in the right way, the joint could be used to connect elements.

The biggest difference is that the load transfer of the dovetail joint is mostly via friction and in the gooseneck joint the load is transferred via shear. This distinction results in different failure modes. In the dovetail the tensile force in the direction of the element causes a tensile force perpendicular to this direction (see left illustration of figure 3.8). Timber has a low tensile strength perpendicular to the grain, so the connection will split relatively quickly. On the other hand, when a gooseneck connection is used (see right illustration of figure 3.8), the tension causes shear in both the mortise and the tenon. Despite that timber does not behave very well under shear, it is still considerably better than tension perpendicular to the grain.

Thus, the strength of a gooseneck joint will be higher than the strength of a dovetail joint.

With designing the gooseneck joint, some extra issues occur. In the dovetail connection the tapered part transfer both the stresses in the mortise as in the tenon. However, in the gooseneck joint, the height where the neck of the joint is located, is to transfer the stresses in the mortise. The 'head' of the joint has to have a certain height to transfer the stresses through the tenon. When placed in the same way as the dovetail joint, the areas to transfer the shear forces is small (see figure 3.9a). The red line on the tenon indicates where the force is applied. So the full head of the tenon cannot be used. The hatched part indicates where the shear force is transferred in the beam. Here the area to transfer the loads is also smaller because not the full height of the diagonal can be used. To increase the area where shear stresses can be transferred, the diagonal should be inserted deeper into the beams. In figure 3.9b this is shown. The full height of the diagonal can be used to transfer the shear loads as indicated by the red line. The 'triangle' to transfer the shear loads in the beam indicated by the hatched part is now similar to the dovetail connection.

To use both the shear areas in the beam and in the diagonal most effectively, it is necessary to match the start of the head of the gooseneck with the bottom of the beam. In other words, make sure the start of the red line in figure 3.9b matches with the bottom of the beam. In this way always the full triangle can be used in the beam, and the full head of the gooseneck can be used as shear area in the diagonal. The disadvantage from moving the diagonals is that the center lines of the members move as well. The intersection of the center lines would not be in one point if the diagonals are inserted deeper. Therefore the beam height has to be increased to solve this. In figure 3.9b this problem is solved. This means that the height of the beam is dependent on the height of the head of gooseneck. If the height of the head of the gooseneck increases, the diagonal has to be placed further into the beam, so the height of the beam has to be made larger to make sure the center lines intersect in one point.

The triangle between the diagonals will remain open afterwards. This has to be milled so the diagonal can be turned into the mortise. This results in a smaller area that can be used for compression in the beams, but because the height of the beam needs to be increased, this will not cause a significant decrease in strength.

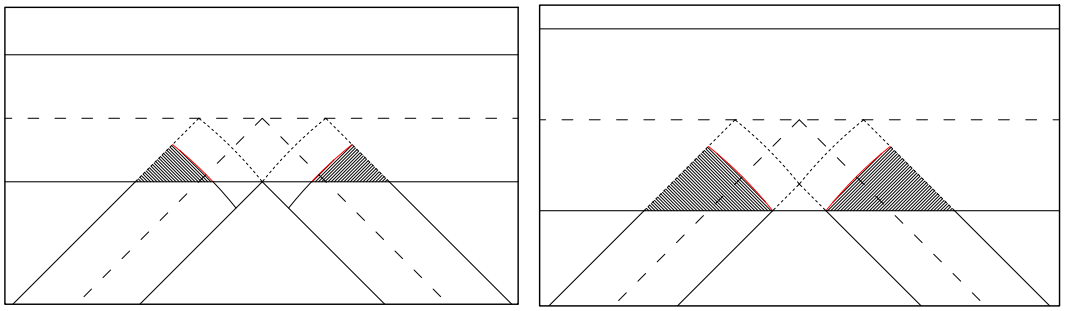

(a) Small shear area (b) Larger shear area

Figure 3.9: Shear area

In the gooseneck splice designed by the Japanese carpenters, the head of the gooseneck is tapering. The only reason for this is to make the connection aesthetically pleasing. For the connection of the truss this feature will not be visible as the diagonal is inserted into the beam. Making the end tapered only means that extra milling is needed to be done. Therefore

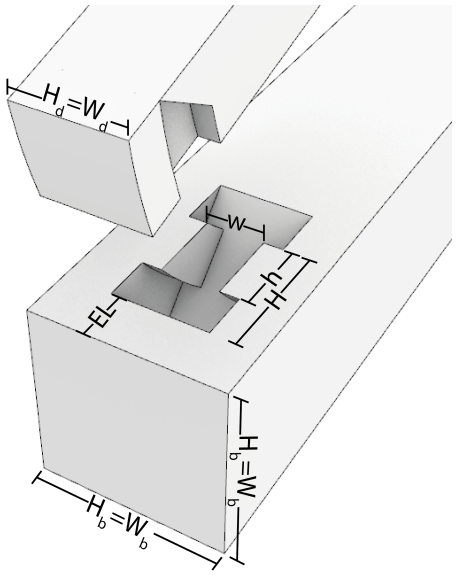

(a) Detail of rotating gooseneck joint

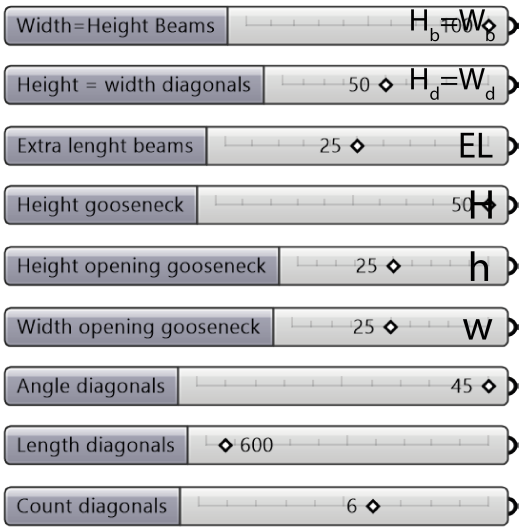

(b) Sliders in rotating gooseneck joint

Figure 3.10: Rotating gooseneck joint

the designed gooseneck joint has a straight head.

The newly designed connection is shown in figure 3.10a. Note that the corners are perfectly sharp, which will not be the case when the joint is milled. The sliders in figure 3.10b are similar to the sliders explained for the dovetail connection. However, there are a few differences. Firstly, the height of the gooseneck is the total height of the neck plus the head. Secondly the width of the opening (which is the neck) of the gooseneck can be adjusted. Finally the height of the opening of the gooseneck can be changed. The height of the head of the gooseneck always equals the height of the gooseneck minus the height of the opening of the gooseneck. These factors will have great effect on the strength of the connection so they should be able to be modified.

The gooseneck connection has been modelled in *Abaqus* as well. The material properties used are exactly the same as in the calculation for the dovetail joint. The loads and the boundary conditions are also identical. The visualisations are scaled with a factor of 50 (see figure 3.11), otherwise the deformations would not be visible clearly. Compared to the dovetail connection, the gooseneck stays in the mortise a lot better. The deformation is more than ten times smaller in vertical direction. With large loads the beam would be pushed apart a bit, which is visible in the image. However, the deformation here is increased by a factor of 50, so with the current load it is not teared apart so much. The deformation in the direction of the 1-axis is 3.7 times smaller than for the dovetail connection. The gooseneck connection behaves a lot better than dovetail connection under tension.

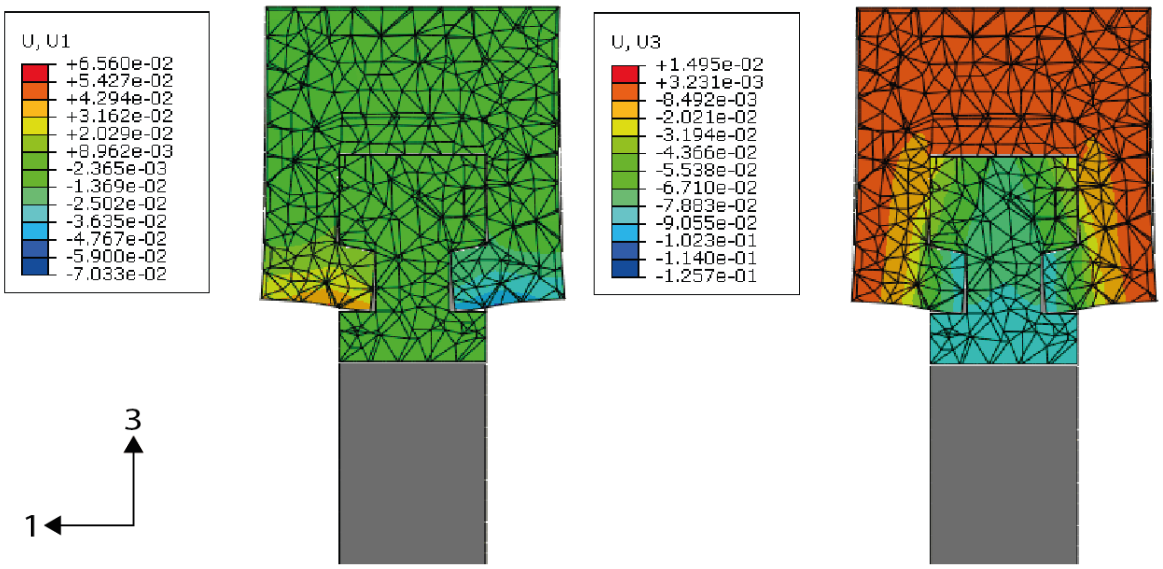

Figure 3.11: Deformations in gooseneck connection (scale factor: 50)

3.4.1 Conclusions

The rotating gooseneck connection solves a lot of the problems that were discovered in the dovetail connection. The stepped shape does not push the beam out of each other like the tapered shape. The shape relies more on the shear strength in stead of friction. Still, in the beam there are a lot of stresses which are not parallel to the grain direction. However, this is inevitable when designing a connection with only using timber. To optimize the connection, the geometrical proportions will be analyzed to acquire the strongest connection. Later on, the best timber material that can be used will be investigated as well to create a strong joint.

Chapter 4

Structural design

4.1 Introduction

In the previous chapter there already have been made some design choices based on structural aspects. Though, these aspect were analyzed globally to get more insight in the behaviour of the connection. It was used to compare different design options with each other and improve the shape of the connection. Geometric proportions were not discussed or analyzed yet.

In this chapter first the critical stresses will be located. Next, the most ideal materials for the designed connection will be discussed. It is necessary to determine the material properties, because the dimensions depend on the material properties in different directions. Afterwards the optimal dimensions are discussed. This will be done by first defining the altering parameters and the possible failure modes of the connection. Then the formulas for the stresses in the failure modes are summed up. Knowing the stresses and the strengths results in the unity checks. With altering the explained parameters an optimized joint can be found that fulfills all unity checks. The flow chart in figure 4.1 shows the order in which the optimization is executed. Afterwards results of the maximum allowable tensile force in the diagonal is shown for the different materials.

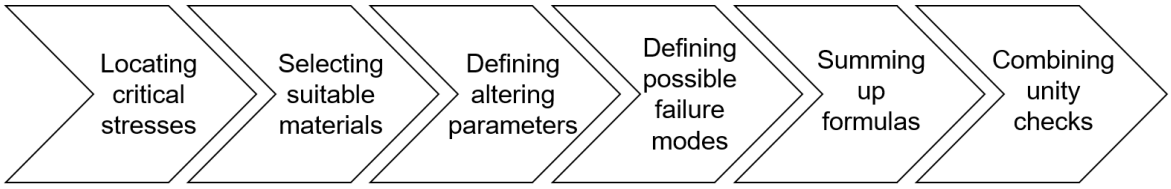

Figure 4.1: Flow chart of optimization process

Then the locking mechanism will be explained to make sure the elements are not separated. Eventually two different possible applications will be explained and two structural reports will be made to analyze the connection in a practical application. These structural reports will be added to the annex. The impact of changing the angle of the diagonals will be elaborated finally.

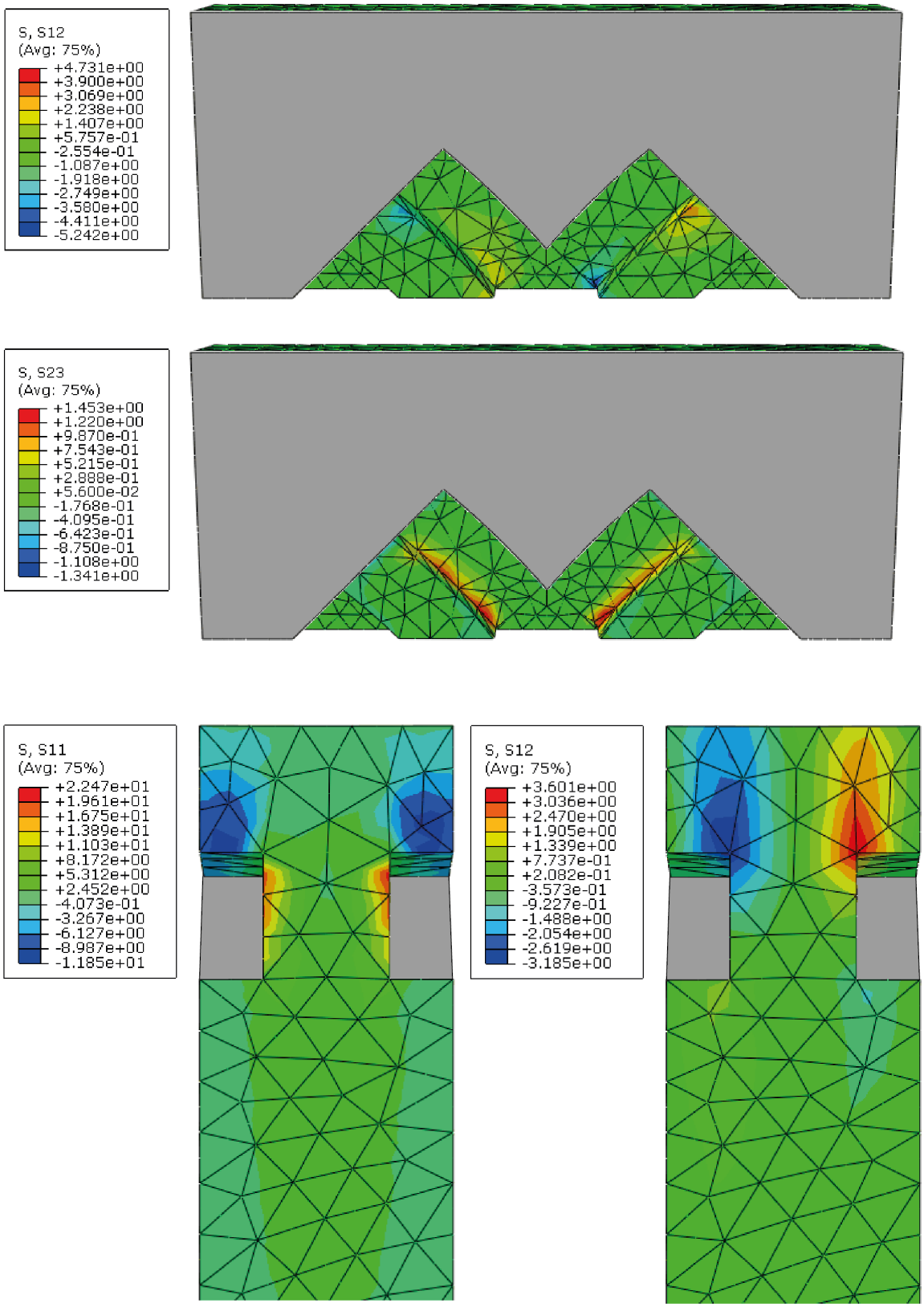

Figure 4.2: Deformations in gooseneck connection (scale factor: 1)

4.2 Material

To determine which material will behave best in the designed connection, it is important to check where the critical stresses will occur. With the critical stresses known, the failure mechanisms can be predicted. To examine these stresses the *Abaqus* model has been investigated to localize the positions with the highest stresses. In figure 4.2 the retrieved weak spots are shown. Note that these are not necessarily the places where the highest stresses occur, but the places where the stresses are most critical. Which means that timber in general is relatively weak for shear stresses and even more for stresses not parallel to the grain direction. Moreover, the retrieved numbers do not correspond with the actual stresses. This is due to high peak stresses in the narrow angles.

The critical stresses in both the beam and the diagonal come mostly from shear stresses. In the beam shear stresses in two directions are governing, this is because the diagonal applies force in angle of 45 degrees (see two top figures in figure 4.2). The force is then resolved into the horizontal and the vertical direction. S12 is shear in the horizontal direction, and S23 is shear in the vertical direction. So, in the beam there are shear stresses parallel and perpendicular to the grain.

In the diagonal the stresses are following the grain direction (see bottom figures in figure 4.2). The force is applied in the direction of the diagonal, so the stresses follow this direction as well. First, the highest stresses occur in the decreased section of the diagonal. These are tensile stresses in the grain direction (S11), the compressive stresses above are not very high so they will not cause failure. The other critical stresses in the diagonal are the shear stresses in the grain direction (S12). These might cause problems because timber is not very strong in shear. So, in the diagonal there are shear and tensile stresses in the direction of the grain.

Summing up all the critical stresses and stating the precondition that both the diagonal and the beam should be made out of the same material leads to the requirements for the material. It should be able to withstand shear stresses both parallel and perpendicular to the grain and it should resist tension stresses in the direction of the grain.

In general timber materials do not behave very well under stresses perpendicular to the grain. Normal timber elements will therefore not be suitable for the connection. A timber material with improved strength perpendicular to the grain is laminated veneer lumber (LVL). LVL is an engineered timber product that uses multiple layers of thin timber assembled with adhesives. Regular LVL is normally used because it is stronger, straighter and more uniform as it is produced in a factory under controlled specifications. This will not behave significantly better under perpendicular stresses. However, there are variations of LVL where one of every few layers is laid perpendicular compared to the others. This means it does decrease the overall strengths parallel to the grain, but it improves the strengths perpendicular to the grain. For that reason it has important benefits that makes the material suitable for the gooseneck joint.

In figure 4.3 three different types of LVL with cross layered veneers are compared. Structural timber C50 is added to the comparison to show the contrast with LVL. The stresses that are shown in the table correspond with the explained weak spots in the connection. Some values were not provided by the manufacturer because the material is too weak to use in this direction, those are substituted by 0 N/mm^2. The direction of the grain is always following the element, so the beam or the diagonal. Then, the timber can be used in two different orientations as is visualized in figure 4.4. For both orientations shear is shown in two directions, this represents the resolved stresses in horizontal en vertical direction. Note that

Beam								
	Steico LVL-X				*BauBuche Q*			
Tension	$f_{t,0,k}$	18.00 N/mm^2	$f_{t,0,d}$	9.75 N/mm^2	$f_{t,0,k}$	45.00 N/mm^2	$f_{t,0,d}$	30.00 N/mm^2
Shear								
Orientation 1	$f_{v,0,edge,k}$	4.50 N/mm^2	$f_{v,0,edge,d}$	2.44 N/mm^2	$f_{v,0,edge,k}$	7.80 N/mm^2	$f_{v,0,edge,d}$	5.20 N/mm^2
	$f_{v,90,edge,k}$	0.00 N/mm^2	$f_{v,90,edge,d}$	0.00 N/mm^2	$f_{v,90,edge,k}$	0.00 N/mm^2	$f_{v,90,edge,d}$	0.00 N/mm^2
Orientation 2	$f_{v,0,flat,k}$	1.10 N/mm^2	$f_{v,0,flat,d}$	0.60 N/mm^2	$f_{v,0,flat,k}$	3.80 N/mm^2	$f_{v,0,flat,d}$	2.53 N/mm^2
	$f_{v,90,flat,k}$	1.10 N/mm^2	$f_{v,90,flat,d}$	0.60 N/mm^2	$f_{v,90,flat,k}$	3.80 N/mm^2	$f_{v,90,flat,d}$	2.53 N/mm^2
Diagonal								
	Steico LVL-X				*BauBuche Q*			
Orientation 1	$f_{v,0,edge,k}$	4.50 N/mm^2	$f_{v,0,edge,d}$	2.44 N/mm^2	$f_{v,0,edge,k}$	7.80 N/mm^2	$f_{v,0,edge,d}$	5.20 N/mm^2
Orientation 2	$f_{v,0,flat,k}$	1.10 N/mm^2	$f_{v,0,flat,d}$	0.60 N/mm^2	$f_{v,0,flat,k}$	3.80 N/mm^2	$f_{v,0,flat,d}$	2.53 N/mm^2
Beam								
	Kerto-Q				*C50*			
Tension	$f_{t,0,k}$	19.00 N/mm^2	$f_{t,0,d}$	10.29 N/mm^2	$f_{t,0,k}$	33.50 N/mm^2	$f_{t,0,d}$	22.33 N/mm^2
Shear								
Orientation 1	$f_{v,0,edge,k}$	4.50 N/mm^2	$f_{v,0,edge,d}$	2.44 N/mm^2	$f_{v,k}$	4.00 N/mm^2	$f_{v,d}$	2.00 N/mm^2
	$f_{v,90,edge,k}$	0.00 N/mm^2	$f_{v,90,edge,d}$	0.00 N/mm^2	$f_{v,90,k}$*	0.80 N/mm^2	$f_{v,90,d}$	0.40 N/mm^2
Orientation 2	$f_{v,0,flat,k}$	1.30 N/mm^2	$f_{v,0,flat,d}$	0.70 N/mm^2	*Rolling shear strength is equal to twice the tension			
	$f_{v,90,flat,k}$	0.60 N/mm^2	$f_{v,90,flat,d}$	0.33 N/mm^2	perpendicular to the grain		$f_{t,90,k}$	0.40 N/mm^2
Diagonal								
	Kerto-Q				*C50*			
Orientation 1	$f_{v,0,edge,k}$	4.50 N/mm^2	$f_{v,0,edge,d}$	2.44 N/mm^2	$f_{v,k}$	4.00 N/mm^2	$f_{v,d}$	2.00 N/mm^2
Orientation 2	$f_{v,0,flat,k}$	1.30 N/mm^2	$f_{v,0,flat,d}$	0.70 N/mm^2				

Figure 4.3: Timber material properties for critical stresses
(Steico, 2017; Blaß and Streib, 2017; Mestäwood, 2017; NEN-EN 338:2016)

for structural timber C50 only one direction can be used, so for only one direction values are given.

Looking at the values shows that the second orientation is the only possible orientation for the beam as one of the strengths equals 0 for all kinds of LVL. The diagonal can be oriented in both ways, but for every kind of LVL the first orientation is stronger. Only looking at orientation 2 for the beam and orientation 1 for the diagonal gives us that BauBuche Q is the strongest timber for the designed joint.

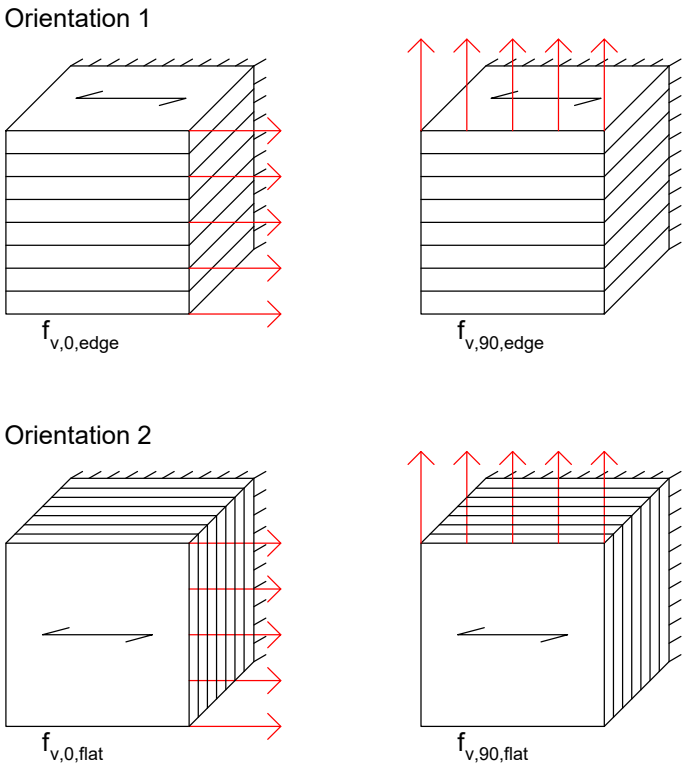

Figure 4.4: Orientation of LVL

4.3 Structural optimization

The current dimensions of the connection are not based on any structural conditions. Knowing the material properties an optimal form of the joint can be approached. To find this optimal shape, first the altering parameters that are used to define the shape have to be defined. The next step it is to find the governing failure modes that set the critical stresses in the joint. Finally using a combination of both can be used to optimize the geometrical dimensions of the joint.

4.3.1 Altering parameters

In figure 3.10b of the previous chapter all parameters that are used to determine the shape of the truss and the connection are shown. To optimize the joint only the parameters to define the dimensions of the joint are used.

Here the dimensions of the members do influence the strength of the joint, but not relatively. Increasing the width and height will increase the overall strength of truss and the connection but this does not increase the strength of the joint relative to the dimensions of the members. Therefore fixed sizes of the members are used to optimize only the joint.

The angle of the diagonals also affects the joint. If the angle is smaller than 45 degrees the shear area shown in figure 3.9b changes. However, this also changes the behaviour of the total truss. It is important to keep the tensile stresses in the diagonals as low as possible because the joint will fail in tension first. The greater the angle relative to the horizontal members, the smaller the stresses per diagonal. As explained earlier, in case of a symmetrical structure, the maximum angle is 45 degrees, otherwise the diagonal cannot be rotated inside

the mortise. So 45 degrees is the angle with the lowest tension stresses for a flat truss and will be used in the optimization first. Yet, when the shape of the truss is changed, angles smaller than 45 degrees might occur. For this reason a slider for the angle will be added so that the optimization can be performed for every individual connection.

Then three parameters with influence on the joint strength remain, the height of the gooseneck (H) and the width (w) and height (h) of the opening of the gooseneck (see figure 4.5). Here it is clear that the values of both w and h affect the strength of the connection. Value H of course also affects the strength of the connection, however only for the diagonal. Increasing H means the area that is used for the shear stresses in the diagonal increases. It does not increase the shear area of shear stresses in the beam, because only the part that fills the opening of the diagonal in the beam takes the shear stresses. And this area is not affected by H. Moreover increasing H means the diagonal will be inserted deeper into the beam, which decreases the overall strength of the beam. To avoid failure of the beam in tension, value H is set to a fixed number as well.

Of course the height of the head of the gooseneck influences the strength as well. Although, with H as a fixed number this height equals H minus h. Thus, this value does not have to be included as an extra parameter.

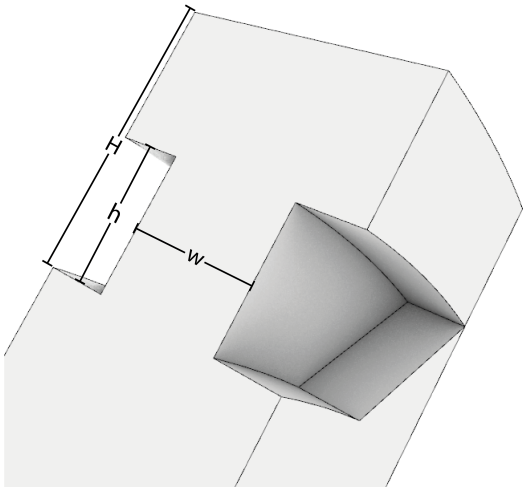

Figure 4.5: Different parameters shown on diagonal

4.3.2 Failure modes

To optimize the joint, it is important to check what the probable failure modes are. The dimensions need to be adjusted so that failure of the joint will be postponed. To find the failure modes it is necessary to keep the parameters in mind. Changing parameters will cause different failure modes to occur.

As already illustrated in figure 3.8 shear will be very important in the optimization. Timbers shear strength is significantly less than tension parallel to the grain. However, the failure mode illustrated in the figure is two-dimensional, which means the stresses are parallel to the grain. When used in three dimensions, the stresses in the diagonal are still similar to the ones in the two-dimensional representation. So shear will still be the most probable failure mode. Nonetheless, when changing the parameters an extra failure mode might occur. When w becomes smaller and h as well, the shear area increases (which is approximately H

minus h times the total height of the diagonal). Furthermore the area that takes the tension (which equals w times the height of the diagonal) becomes smaller. At a certain point tension in the diagonal become governing. Therefore, in the optimization both tension and shear of the diagonal have to be considered.

For the beam, the mortise of figure 3.8 does not quite represent the possible failure modes in the three-dimensional connection. There are two important differences compared to the designed joint. First of all the diagonal is inserted under an angle, so applied load has to be resolved in a vertical and horizontal direction. This gives a load perpendicular to the grain. This means that the shear area of the beam has to resist both the horizontal and vertical shear stresses. The second difference has to do with the tensile stresses. In the two-dimensional representation tension at the places where the sections area is smallest might cause failure. However, in the designed joint the mortise is not open, like in the two-dimensional representation. Before and after the joint the beam is completely solid, so this keeps the joint in place. Failure of tensile forces in the smallest section is therefore not likely to happen. For the optimization only shear in horizontal and vertical direction are considered. In table 4.1 the failure modes and their corresponding strengths and stresses are shown. The formulas for the stresses are the ones for pure tension or pure shear. This is the case because the joint is completely locked. There is no room for bending and the shown stresses will occur in their purest form.

Failure mode	Strength orientation 1	Strength orientation 2	Stress formula
Beam			
Shear X	$f_{v,0,edge}$	$f_{v,0,flat}$	F/A
Shear Y	$f_{v,90,edge}$	$f_{v,90,flat}$	F/A
Diagonal			
Shear X	$f_{v,0,edge}$	$f_{v,0,flat}$	F/A
Tension X	$f_{t,0}$	$f_{t,0}$	F/A

Table 4.1: Failure modes with corresponding strengths and stresses

4.3.3 Optimization

With the known parameters and the probable failure modes an optimization is executed in *Grasshopper*. In appendix B.2 an overview of this optimization is shown. In this section the optimization will be clarified an the found dimensions will be discussed. The important steps in the optimization will be elaborated.

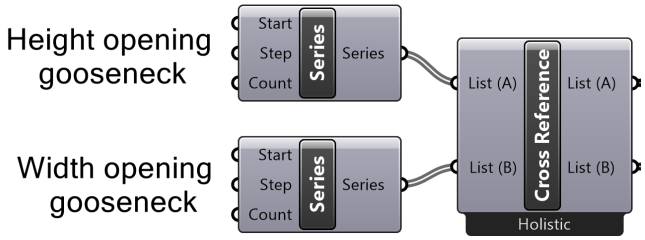

Figure 4.6: All options with parameters

First all possible combinations are generated. For the optimization the size of the diagonal is set to 100 times 100 millimeters. The series components in figure 4.6 resembles the values

of the height and the width of the opening in the gooseneck connection. The total height of the connection (H in figure 4.5) is set to 100 millimeters to avoid failure of the beam in tension. Making the total height larger means that more timber is taken away in the beam which reduces the effective section in tension. With these boundaries known all options for values h and w can be determined. The possible options inserted in the script are 1 to 99 millimeters for both the height and width of the opening. The numbers are integers because having decimal numbers will be hard to be fabricated so precisely eventually. In addition, this will not affect the strength much and increases the complexity of the optimization as one extra decimal will lead to 100 times as many possible combinations.

The cross reference component combines all the different heights and widths so all the possible combinations are found. The total number of combinations thus will be $99 \times 99 = 9801$ possibilities.

With all determined possible dimensions, the areas for the failure modes can be calculated. The script in appendix B.2 shows clusters. These clusters are separate scripts in which the critical areas are calculated with the altering heights and widths of the opening of the gooseneck. In figure 4.7a the critical shear areas in the beam are shown. With the input of the two parameters the areas are calculated. The h stands for the height of the opening of the gooseneck, the w for the width of the gooseneck and the α for the angle of the diagonal compared to the beam. The calculation of the shear areas in the beam can be found in equations 4.1 and 4.2.

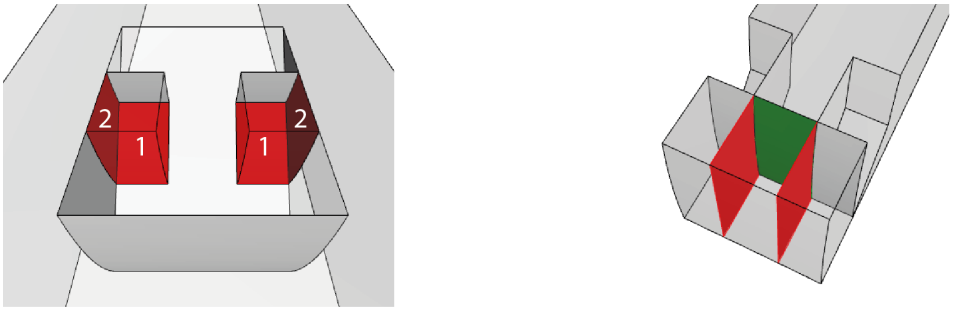

(a) Shear areas in beam

(b) Shear and tension areas in diagonal

Figure 4.7: Failure areas in beam and diagonal

Shear area 1:

$$2 \times (100 - w)/2 \times h \tag{4.1}$$

Shear area 2:

$$2 \times (\tan(\alpha) \times h^2/2) + (100 - \tan(\alpha) \times h) \times h \tag{4.2}$$

Both shear areas have been multiplied by two because the areas are twice in the joint. For the unity check for shear in the beam both shear areas added up to each other.

In the diagonal the two probable failure modes are shear (red) and tension (green) in figure 4.7b. The formula for the shear area in the diagonal can be found in equation 4.3 and the formula for the tension area in the diagonal in equation 4.4.

Shear area:

$$2 \times (100 - h) \times 100 \tag{4.3}$$

Tension area:

$$100 \times w \tag{4.4}$$

Then the forces in the elements are calculated. The input is the axial force in the diagonal. So, the tension and the shear force in the diagonal is equal to this force. For the force in the shear areas in the beam, the axial force needs to be resolved. There the axial force is multiplied by the cosine and the sine of the angle to calculate the resolved forces. For a diagonal with an angle of 45 degrees, both resolved forces are the same. However in other angles these are different so could effect the optimization.

In the next step the stresses can be calculated as all the areas and the forces in the members are known. The unity check is executed on all the found values afterwards. The characteristic or design strengths are taken from the table in figure 4.3. All values that are above 1 will be removed out of the list with possible combinations of the width and height of the opening. This is done in the last part of the script. All values for which all unity checks are below 1 are given in the panels at the most right of the script.

To find the optimal dimensions of the width and height of the opening, the slider which inputs the axial force of the diagonal can be changed. Increasing this value will reduce the amount of possible outcomes. At a certain point the outcomes are minimized, this will be the optimal dimensions.

The outcomes for the optimization of BauBuche Q gives two different solutions. This is because when increasing the axial force more, one of the options fails for another critical stress than the other. The two options therefore have more or less the same strength. The values that are taken are 56mm for the height and 16mm for the width. The diagonal with these dimensions will look like figure 4.8.

Figure 4.8: Diagonal with optimal dimensions in BauBuche Q

What stands out the most from the optimal diagonal is that the remaining section of the diagonal is small. This might look odd, but it resembles the strength of the material well. The tensile strength parallel to the grain is 6.5 times stronger than the shear strength in the diagonal and even more than 13 times stronger than the shear strength of the beam. So, the optimization meets the expectations for the dimensions.

Material	***h***		***w***		**Failure load**	
BauBuche Q	56	mm	16	mm	68.6	kN
Kerto Q	83	mm	8	mm	14.7	kN
Steico LVL-X	73	mm	14	mm	24.2	kN

Table 4.2: Size and failure load of joint in different types of LVL

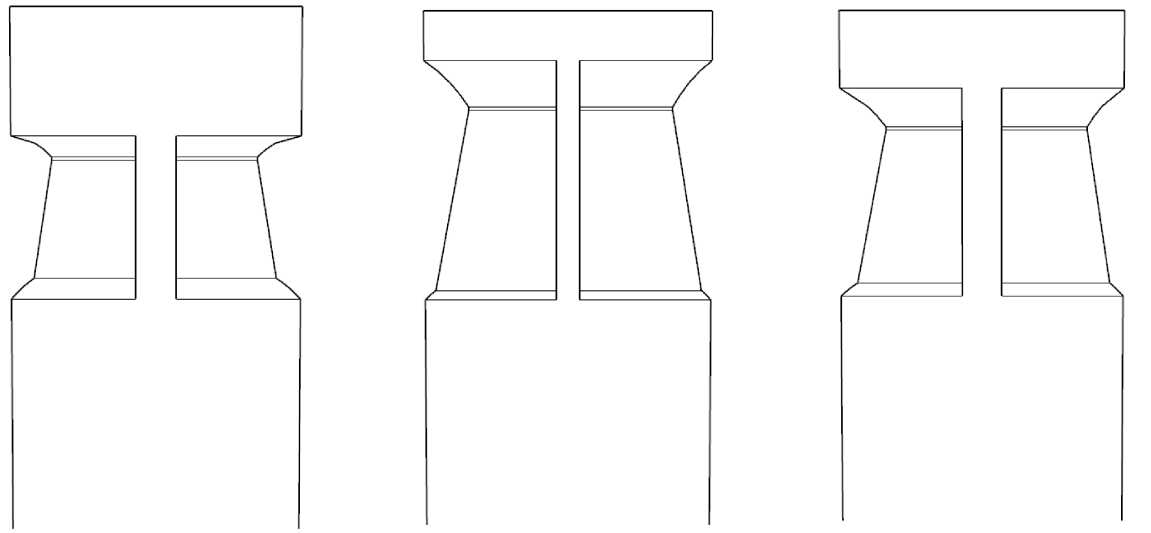

(a) Diagonal in BauBuche Q (b) Diagonal in Kerto Q (c) Diagonal in Steico LVL-X

Figure 4.9: Optimized diagonals in different types of LVL timber

In figure 4.9 the optimized diagonals for three different types of LVL timber are shown. In table 4.2 the values of the height (h) of the opening of the gooseneck, the width (w) and the critical failure load in the diagonal for each material. The h and w correspond with figure 4.5. Moreover, in table 4.3 the critical areas and the unity checks following from the stresses in these areas are shown. It is clear that for the different materials different geometrical proportions are optimal. The larger the total opening in the diagonal, the larger the total shear area in the beam. So, it is expected that Kerto-Q will have a large opening as the minimal shear strength is relatively low. This is mainly because Kerto-Q has two different strengths for the shear in the beam. That is why in table 4.3 only for shear in the X-direction in the beam of Kerto Q there is a relatively low U.C.. For all materials the tension area remains remarkably small. This also matches the expectations, because the tension strength parallel to the grain of all materials is a lot higher than the shear strengths. Another thing that stands out is the failure load. BauBuche Q is the strongest option, this is because it is made out of beech laminated veneer lumber. Kerto Q and Steico LVL-X are made out

of spruce or pine laminated veneer lumber. This is a softer and less strong material, which can be seen in the failure load. The difference between Kerto Q and Steico LVL-X is also reasonably big. Both products are made in a similar way, however in the specifications that are provided by both producers, the shear strength of Kerto Q in perpendicular direction is almost twice as weak as for Steico LVL-X. Therefore the failure load is lower.
From the figure and the tables it is clear that where the strength is lowest, the most material is placed. The beam is not shown, but has the inverse shape of the diagonal. So if the opening in the diagonal is larger, more material is placed at the shear areas in the beam. This can be read in table 4.3 as well.
As expected, the critical load is not as high as in a connection designed with mechanical fasteners or adhesives. If, for instance, a solid diagonal was placed in the beam in a similar way and a steel pin of 24mm would be inserted through the connection, the failure strength would be 82kN (according to NEN-EN 1995-1-1 equations 8.7 and 8.31 to 8.33). This is not even a strong joint design, so the difference is even bigger when an optimized bolted connection is used.

	Beam					**Diagonal**				
	Shear X			*Shear Y*		*Shear X*			*Tension X*	
Material	Area		U.C.	Area	U.C.	Area		U.C.	Area	U.C.
BauBuche Q	6384	mm^2	1.00	6384 mm^2	1.00	4400	mm^2	1.00	1600 mm^2	0.96
Kerto Q	8674	mm^2	0.46	8674 mm^2	1.00	1700	mm^2	0.96	800 mm^2	0.96
Steico LVL-X	7775	mm^2	1.00	7775 mm^2	1.00	2700	mm^2	1.00	1400 mm^2	0.96

Table 4.3: Critical areas and unity checks

4.4 Locking

When the diagonals are rotated in the beams, they can only be separated in one direction. Namely the same rotation as they are inserted. As mentioned, the force in the diagonals will be an axial force, so perpendicular to the rotation direction. This means that the structure is not likely to be separated when used in its final application. Though, during manufacturing, or when unexpected forces are applied to the structure, the diagonal might be pulled or vibrated out of the beams. If so, the structure will fail because the diagonals are essential.

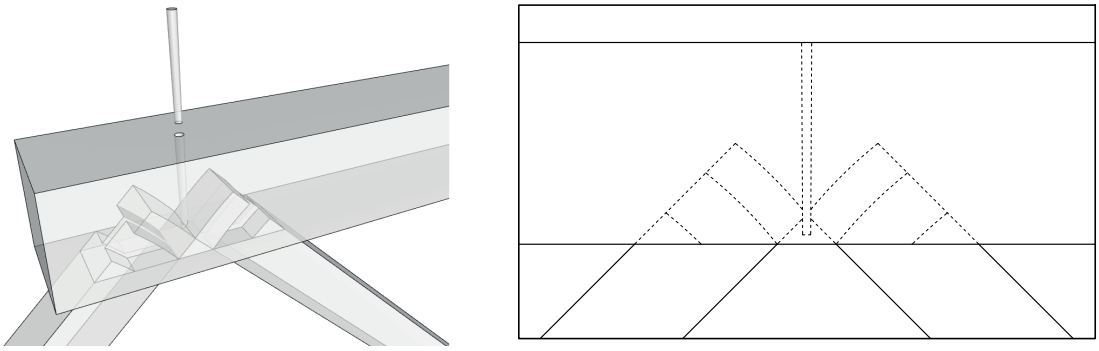

(a) Inserting locking pin

(b) Locking pin inserted

Figure 4.10: Locking the joint

To prevent this from happening it is important to lock the diagonals once they are inserted. The locking mechanism does not need to resist a lot of force, because structural force will not go through the mechanism. A recess will be milled in both the beams and diagonals at the place where two diagonals meet (see figure 4.10a). This can be done immediately after the elements are milled, so almost no extra time is needed for this. A dried wooden tapering pin can be inserted in the recess. Once the pin is exposed to the same humidity as the truss, the pin will expand so it is locked in the recess. In figure 4.10b the dotted lines show that the pin blocks the diagonals when being pulled out of the mortise. This can also be done at the bottom of the truss, although the pin should be inserted from the top as well, so the recess is mirrored compared to the recess in the top of the truss. The connection can easily be disassembled by removing the pin first and the diagonal afterwards.

4.5 Applications

In this section the possibilities with the connection are explained and two possible applications will be further analyzed in a case study. As mentioned the limit for the angle of the connection is 45 degrees compared to the bottom or top member if the structure is symmetrical. If a structure is not symmetrical, it might occur that the angle of one member is 60 degrees. The next member can be placed in an angle of 30 degrees with still fulfilling the requirements. Increasing the angle also decreases the shear area in the beam and thus the strength of the joint. Moreover an unsymmetrical structure will not be the strongest possible truss. Though it can be used, so it is a possible application.

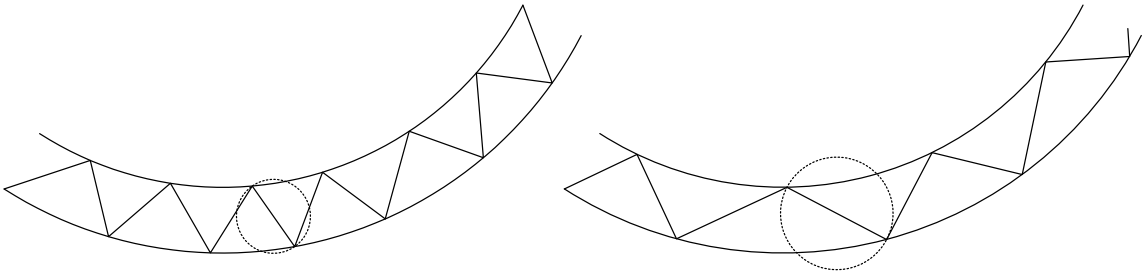

Figure 4.11: Solving impossible structures

With the explained information basically every possible shape can be turned into a truss. For instance an arched truss. The bottom and top members of an arched truss need to be continuous as well. For the connection an LVL material is required, so the structure will be made in LVL. As LVL consists out of several layers it is possible to make continuous curved elements. In figure 4.11 a random arch is shown. The arches are filled with diagonals to evaluate the possibilities. In the left figure one (and more others) diagonal cannot make the rotation to be inserted. The dotted line, which is the rotation path, crosses with the adjacent member. This problem can be solved be changing the angle of the neighbouring members. In the right figure, in which the outside members are exactly the same as in the left figure, this has been done. It results in longer and less members between the arches. With this workflow every possible shape can be made. Of course for certain shapes this results in extremely long members which is not beneficial for the strength of the truss. Therefore every different possible application should be investigated thoroughly before being applied.

In the next two sections two different application are calculated. First a flat truss will be used in a flat roof, in the other application a curved truss is used in a covering structure. Afterwards both variants will be compared to explain the differences in their behaviour.

4.5.1 Flat roof

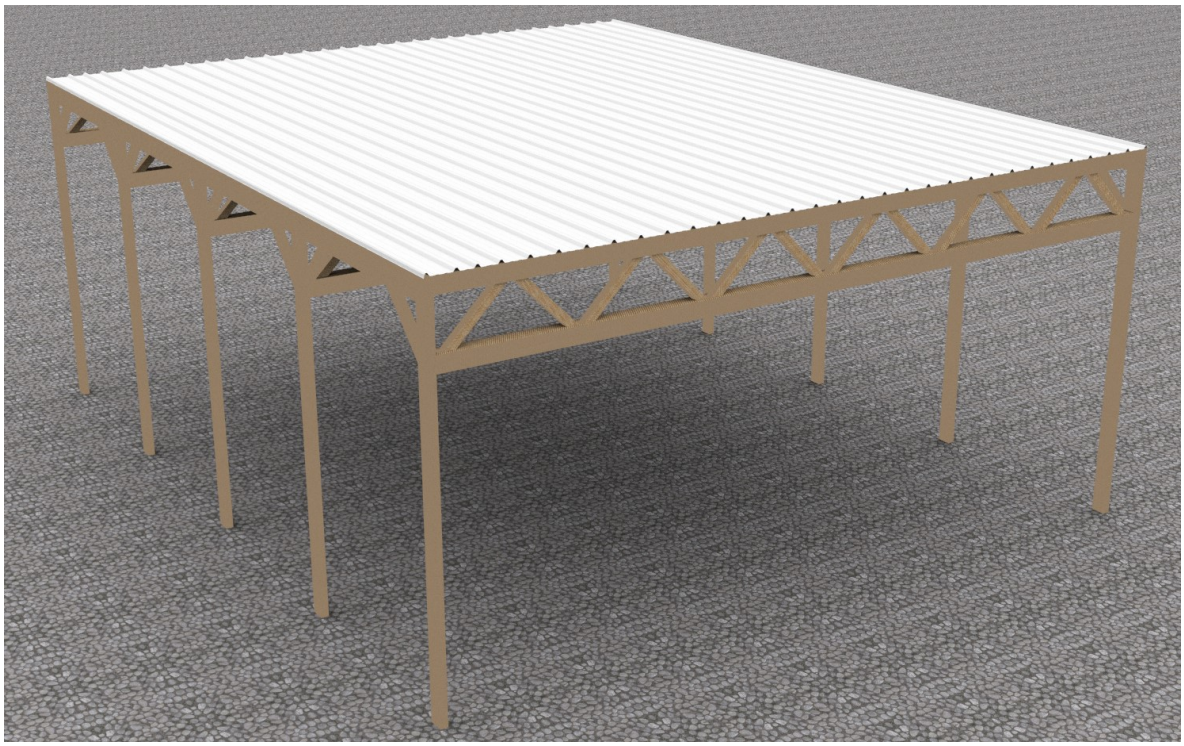

Figure 4.12: Application of truss in a roof

The most obvious application for the truss is a roof structure. In this example the trusses are used in a temporary covering structure (see figure 4.12). The span of the trusses is 10 meters and the height of the roof is 5 meters. The structural report focuses on the stresses in the elements of the truss, not the carrying structure. The material that is used in the calculated roof is BauBuche Q, as this is the strongest material for the connection. In annex I the structural report of this application can be found. The dimensions for the structure are $100 \times 100mm$ for the diagonals and $200 \times 200mm$ for the beams. The diagram that is fully calculated in the annex is shown in figure 4.13.

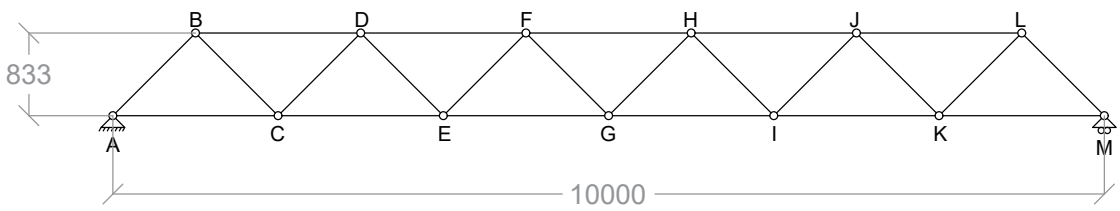

Figure 4.13: Mechanics diagram flat truss

Different loads are applied on the roof. Permanent, imposed, snow and wind loads are

projected on the structure. The values and calculations of these loads can be found in annex I.5. Then the load combinations are determined in the next section of the annex. All this data is implemented in a SCIA model. The data that has been input can be found in appendix D.2 and the resulting peak stresses in appendix D.3. The internal members of the structure are checked on tension, compression and bending stresses first. Then buckling is also checked. As expected the unity checks following are only very small. The detail of the joint is checked for compression following the Eurocode tooth joint calculations. Eventually the detail is also checked on tension on the possible failure modes. The unity checks in the joint were a lot higher, the maximal value is 0.86. As mentioned before the tensile strength of the joint will always be governing. An elaborate calculation of all the Ultimate Limit State checks can be found in annex I.7.1.

Finally the Serviceability Limit State is also checked. First maximal deflections in the middle of the span are determined. This is following from the permanent load plus the snow load (see annex I.7.2). The structure is seen as a fully hinged structure. With local equilibrium all the stresses, thus elongations of the elements can be determined. With the known elongations the deflection of the truss can be drawn. This results in a deflection of 2.98mm compared to 2.9mm which is found in SCIA. So changing the connection to hinged connections only affects the total deflection a little. This found deflection is without deflection of the joint. To determine this deflection, an Abaqus model has been made. It is found that in tension the total deflection of one element is multiplied by a factor of two. So, the members in tensions increase twice as much in length. Multiplying the elongation of all members in tension with a factor of two, give a newly found deflection that equals 3.25mm, which will not cause any problems.

4.5.2 Arched roof

In this example the connection is used in a curved truss which forms the structure of a covering roof. The covering structure is shown in figure 4.14. The span of the roof is 10 meters and the free height in the middle is 5.7 meters. In the structural report that can be found in annex II, the complete structure is calculated. The material that is used is BauBuche Q, as this is the strongest material for the connection. The dimensions for the structure are $100 \times 100mm$ for the diagonals and $200 \times 200mm$ for the beams. The diagram that is fully calculated in the annex is shown in figure 4.15. In this example two different connections are present. The diagonals have an angle of 45 degrees compared to the top member. So this connection is the same as in the previous example. Compared to the bottom member, the angle is 35.5 degrees. This means that the optimization must be executed for this connection as well. When changing the angle in the script to 35.5 degrees new optimal dimensions are found, the height h increases from 56 to $57mm$ and the width w decreases from 16 to $13mm$.

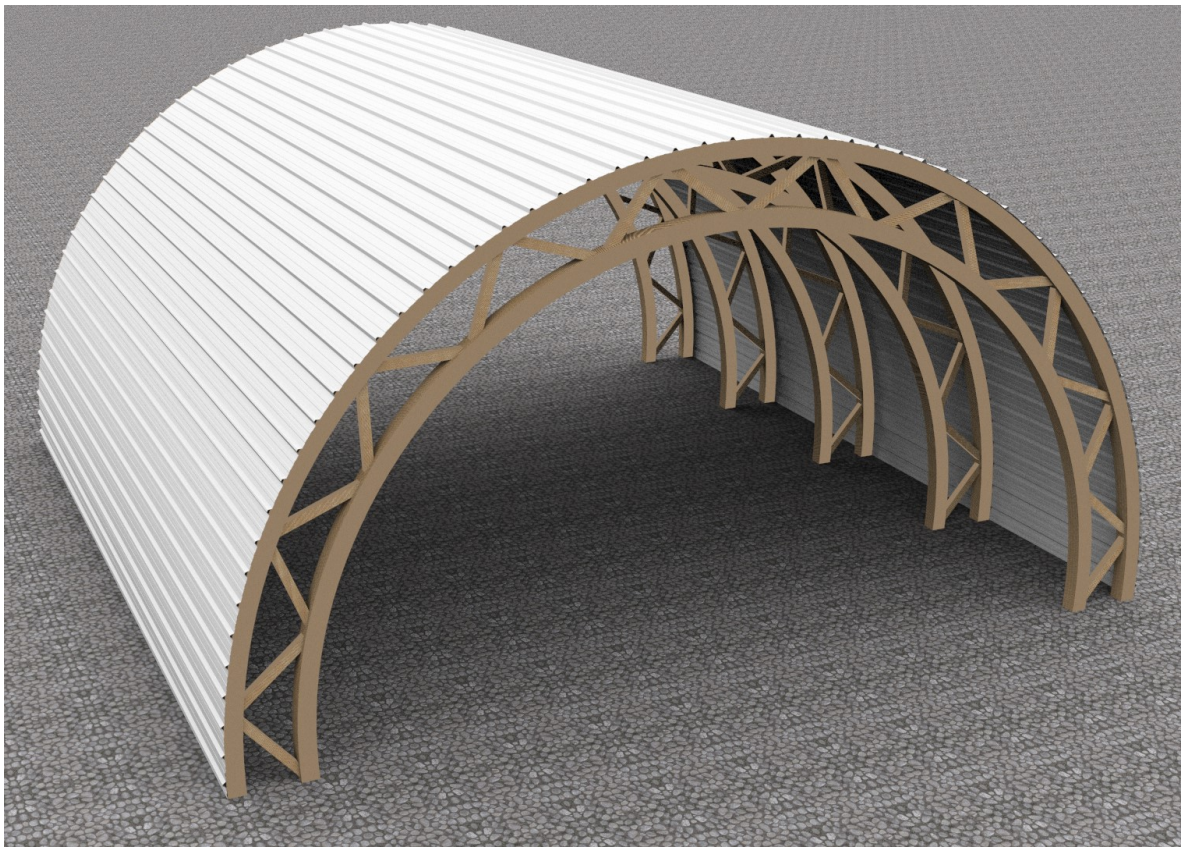

Figure 4.14: Application of an arched truss

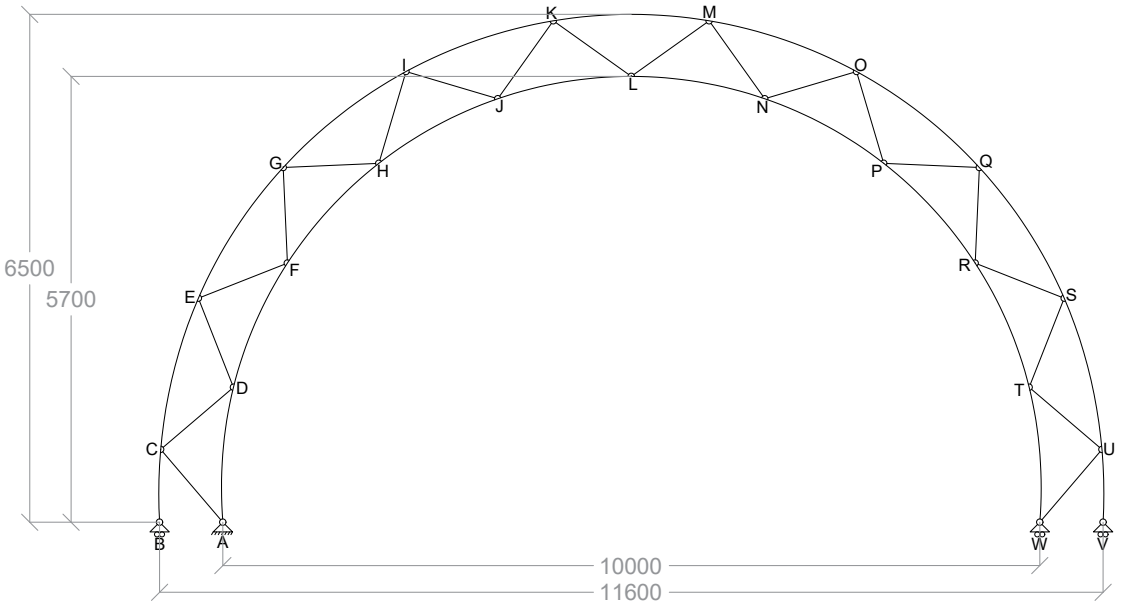

Figure 4.15: Mechanics diagram arched truss

Again, different loads are applied on the structure. Permanent, imposed, snow and wind

loads are projected on the truss. However, this time the truss also functions as a wall, so different snow and wind loads are applied. The calculated loads can be found in annex II.5. Afterwards the load combinations are determined. This data has been implemented in a SCIA model. The inputted data can be found in appendix D.5 and the resulting peak stresses in appendix D.6. For this case the internal members of the structure are checked on tension, compression and bending stresses as well. Buckling of the diagonals is checked afterwards. Similar to the flat truss the unity checks remain small. Then the detail of the joint is checked for compression following the Eurocode tooth joint calculations. This time the calculation is calculated twice, once for the 45 degree joint and once for the 35.5 degree joint. Hereafter also tension in both joints is checked. Again the unity checks in the joint were higher than in the elements, though the difference not as big as in the flat truss. The maximum unity check in the joint is 0.47. Still in this case the strength of the joint will always be governing. An elaborate calculation of all the Ultimate Limit State checks can be found in annex II.7.1.

Finally the Serviceability Limit State is checked. The found maximal deflection in vertical direction is $2.7mm$. This value is retrieved from SCIA, so the deflection of the joint is not included yet. The joint itself will deflect as well, so the total deflections will increase. In the previous calculated roof the increase due to this effect was less than 10 percent. The current diagonal has two different joints. However, the 35.5^{o} joint is stronger than the 45^{o} joint. Moreover, because of the arched shape there is less tension in the members. So the effect will be smaller than the previous calculated roof. Therefore it is assumed that the deflections in the roof will be tolerable.

4.5.3 Comparison of different structures

Not all diagonals in the arched truss have an angle of 45 degrees compared to the beams, this is impossible when making an arch. In this example the angles of the top beam compared to the diagonals are 45 degrees, but the angles of the bottom beam compared to the diagonals are 35.5 degrees. When changing the angle to 35.5 degrees new optimal dimensions are found, and the failure load changes as well. In table 4.4 the found optimized dimensions and maximal failure loads of the different materials are shown. This time for both a 45 degree angle and a 35.5 degree angle. For a smaller angle the failure load decreases for both BauBuche Q and Steico LVL-X. The shear area in the beam does increase but a smaller angle increases the force in X-direction (direction of the beam). The strength in both directions is the same so an increase in a force in one direction leads to a lower failure load. Kerto Q does increase in strength. This is because the shear strength in X-direction is higher than in Y-direction. So a smaller angle means that the resolved forces are higher in X-direction than in Y-direction.

Material	**Angle**		***h***		***w***		**Failure load**	
BauBuche Q	45.0	^{o}	56	mm	16	mm	68.6	kN
	35.5	^{o}	57	mm	13	mm	65.5	kN
Kerto Q	45.0	^{o}	83	mm	8	mm	14.7	kN
	35.5	^{o}	78	mm	8	mm	19.0	kN
Steico LVL-X	45.0	^{o}	73	mm	14	mm	24.2	kN
	35.5	^{o}	74	mm	14	mm	23.4	kN

Table 4.4: Size and failure load of joint in different types of LVL with different angles

Both elaborated structures meet all the Eurocode requirements, so are possible applications. In table 4.5 the highest tensile and compressive forces in the diagonal are shown. The most critical unity checks, which are for both cases tension in the detail, are shown as well. As expected, the tensile forces in a flat truss are higher, where in a curved truss there is more compression. That is also the reason why the unity check is more critical in the flat truss. The difference in failure load is less than five percent for the joint in 35.5 or 45 degrees. So the gap between the highest unity check is mainly because of the difference in tension in the diagonal.

	Flat truss		**Curved truss**	
Max. tension	39.4	kN	20.7	kN
Max. compression	25.9	kN	35.9	kN
Highest unity check	0.86		0.47	

Table 4.5: Extreme values different applications

The detail of the 35.5 degree joint looks a bit different. Firstly the shear area in the beam is larger because of the rotation. In figure 4.16 the shear areas are shown. In the right figure the area is slightly bigger because of the rotation. Furthermore the distance between the elements increases if the angle decreases. In figure 4.16b the corners of the elements do not touch each other where in figure 4.16a they do. This is because the center lines have to cross each other for an optimal force flow. Decreasing the angle means that the center lines of the diagonals intersect below the center line of the beam. To solve this, the diagonals are placed a bit apart from each other. Another solution would be to decrease the beam's height. The center line would be lower, so intersecting with the center lines of the diagonal. In the case of the arch truss this is a possible solution, as the unity checks in the beams only remain very small. A (small) decrease in size would not result in failure. Though, the bottom and top beam would have different dimensions in this case. For production reasons this might not be the best solution.

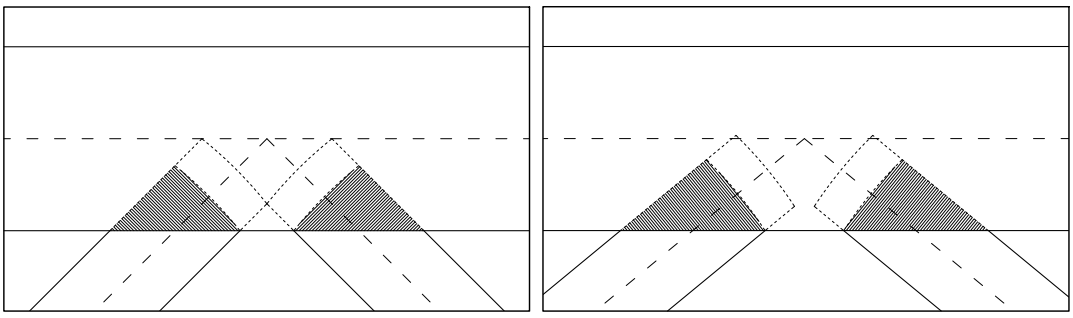

(a) Detail 45 degree joint (b) Detail 35.5 degree joint

Figure 4.16: Detail of both joints

Chapter 5

Fabrication

5.1 Introduction

In this chapter the fabrication of the truss will be discussed. The structure will be made by an ABB IRB 1200-5/0.9 robotic arm (ABB, 2020b). First the theoretical fabrication will be elaborated. The elements that have to be made will be analyzed. Knowing the elements will set some boundary conditions for the end effector. Then, an end effector that meets all the conditions will be designed. Once the end effector and the elements are known the robotic movements to mill the elements will be discussed. Once all the elements have been made the assembly can take place. For this part another end effector is needed, which will be explained first. Afterwards the robot movements to assemble the elements are discussed.
Once the theoretical fabrication is explained, the execution of the complete process is reviewed. Issues that have not come to sight in the theoretical part will be discussed and (temporary) solutions are explained. Finally recommendations for a better fabrication are considered.

5.2 Milling

5.2.1 Elements

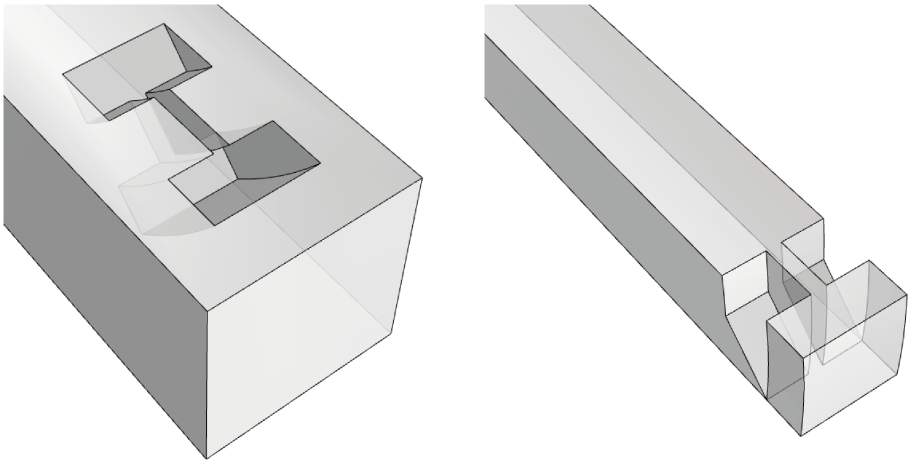

(a) Beam (b) Diagonal

Figure 5.1: Elements to be milled

The elements that will be milled are the beams and diagonals found in the structural optimization for BauBuche Q. These can be found in figure 5.1. To make the elements producible the size has been changed. Compared to the calculated applications the size of the elements is decreased with a factor 2. This means the beam is $100 \times 100mm$ and the diagonal is $50 \times 50mm$.

Looking at the elements immediately shows that milling the diagonal will be easier. The openings can be reached from the top and the sides (in the figure) and are not so deep. From the side to the middle the opening is maximal $21.25mm$ deep.

For the beam it is harder to reach the deepest part in the mortise. Calculated from the deepest point to the top surface it is almost $70mm$. Milling this point also means the mill has to be inserted in a slanted direction, so there has to be some space for the end-effector to rotate near the surface of the beam.

5.2.2 End effector

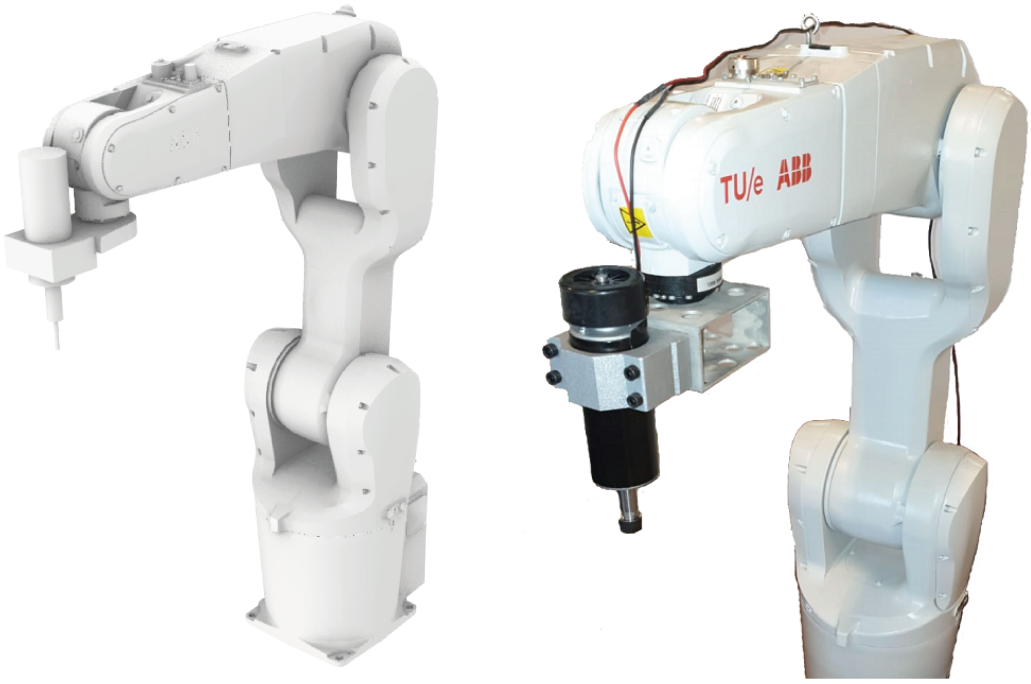

(a) End effector used in the scripts

(b) End effector mounted to the robot

Figure 5.2: End effector for milling

The end effector that is used for milling consists out of two parts. First of all there is a motor that is needed for the rotation of the mill. Secondly there is the mill. The mill can be changed if needed.
In figure 5.2 the end effector is shown in both the scripts and the real life robot. Note that in figure 5.2a the mill is already mounted to the end effector and in figure 5.2b it is still missing. The motor can be changed in height compared to the robot. The higher the motor is mounted, the closer the tip of the mill is to the attachment plane of the robot. When the distance is shorter the accuracy will be higher, because the lever arm is shorter. However, when the motor is mounted higher, it decreases the rotational freedom of the robot. Some

movements cannot be made then. To find the optimal height of the motor the complete script is ran in Grasshopper to check whether the end effector collides with the robot.

For the mill several conditions are important. The smaller the diameter of the mill, the 'sharper' the corners can be milled. Having a high diameter means the designed shape will be approached less accurately. However, the smaller the diameter of the mill, the more the mill will vibrate in perpendicular direction. This decreases the precision as well. For the length of the mill the same applies. When a mill is longer, it is more likely to vibrate in perpendicular direction. Nevertheless the mill still needs to be long enough to make the elements. As mentioned the maximum depth is $70mm$ without extra space for the end effector to rotate. To make sure the end effector does not come into collision with the element a length of $100mm$ is set as a minimum length for the mill.

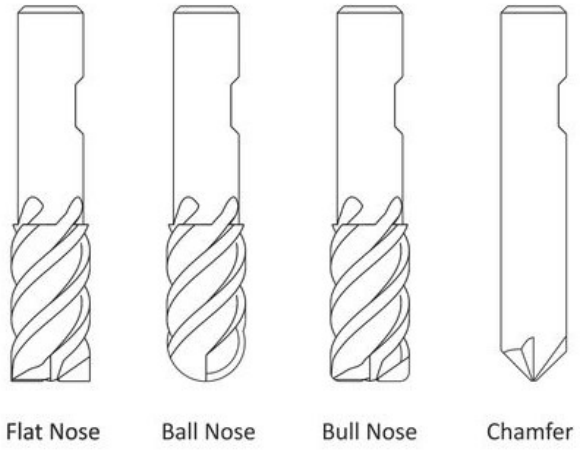

Figure 5.3: Mill ends

Another important property of the mill is the mill end. In figure 5.3 the most common mill ends are shown. For milling flat surfaces, a flat nose or a bull nose end will result in a smooth and clean surface. The difference is that the bull nose has a radius corner, so it is used for creating a fillet at the bottom. A ball nose end will, depending on the space between the milling lines, give an undulating end result. However, the flat and clean end result can only be accomplished if the mill is used perpendicular to the surface. This will not be possible in the designed elements. When using the mill under an angle towards the surface it is better to use a ball nose end or the chamfer end. However the chamfer end can only be used to cut angles. In the designed elements both cutting under an angle and making surfaces are important for the mill. Thus, the ball nose end will be chosen as the mill.

5.2.3 Robot movements

Currently there is software available to generate milling paths for CNC milling machines. In this software the program generates a path in X, Y and Z direction but does not include rotations. Milling paths for complex geometries, such as the designed connection, cannot be automatically generated. Therefore the path has been generated manually in Grasshopper. The path is a line that follows a number of planes. All the planes are retrieved from the designed model, so that the rotation of the end effector is always right. Of course, this is

not completely manual, but still time consuming and far from automatic. This section briefly explains how the path has been generated.

Milling path beam

The milling of the beam is divided in multiple steps. The steps are visualized and explained hereafter. The green lines in the figure always indicate the milling path. The end effector of the robot is also shown so that the direction of the mill is visible. Only the path where the mill is actually milling is shown, in between there are paths to get from one step to the other.

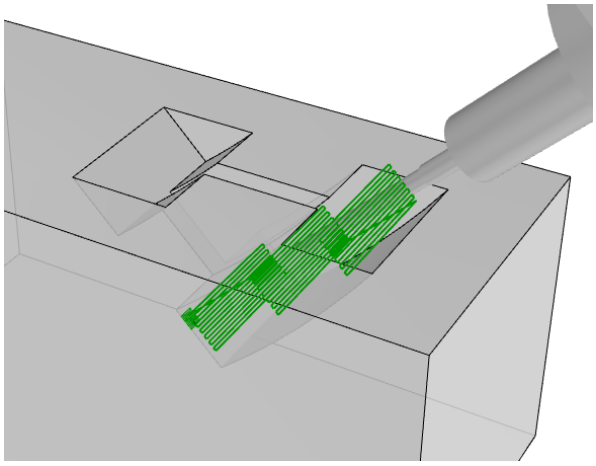

Figure 5.4: Step 1

First the material in the middle of the opening is removed. In figure 5.4 this is done in three times. The distance between the paths can be adjusted according to the height that the mill is able to mill in one go.

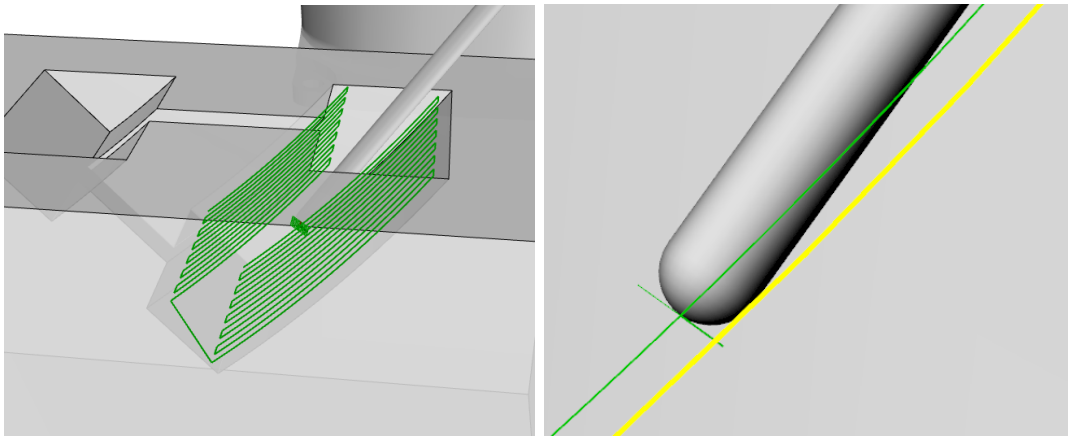

(a) Step 2 (b) Step 2 detail

Figure 5.5: Step 2

The next step is to finish the opening. The path in figure 5.5a shows that the mill moves in the length direction of the beam. This is done so the wavy pattern that is caused by the ball nose mill can be milled inverted on the diagonal. This saves milling time, as otherwise

the mill should make a lot of lines close to each other to get a clean end result.
In figure 5.5b a section of the mill is shown. Again the green line indicates the milling path, but here the yellow line shows the curved side that has to be milled. With the tip of the mill on the green line and the right rotation the side of the mill touches the yellow line. This rotation is needed because the mill cannot reach this surface in another way.

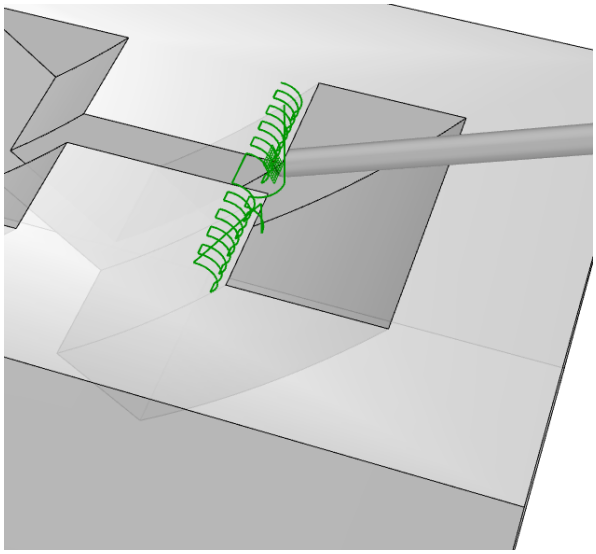

Figure 5.6: Step 3

In the next step the edges of the joint are filleted. This step is needed so that the diagonal can slide into the beam. Sharp angles cannot be made with the mill, so everywhere where there is a sharp corner it has to be filleted. Note that the inverse of the fillet is obtained automatically because the mill cannot reach the internal corners.

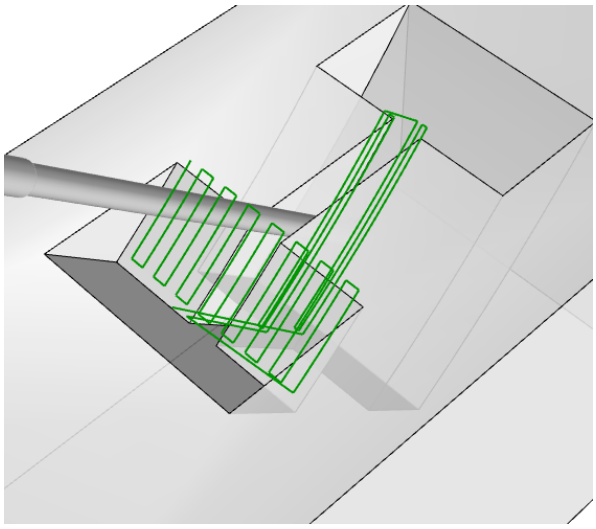

Figure 5.7: Step 4

Then step 1 is executed at the other side. In the middle there are only two lines because

the opening is small.

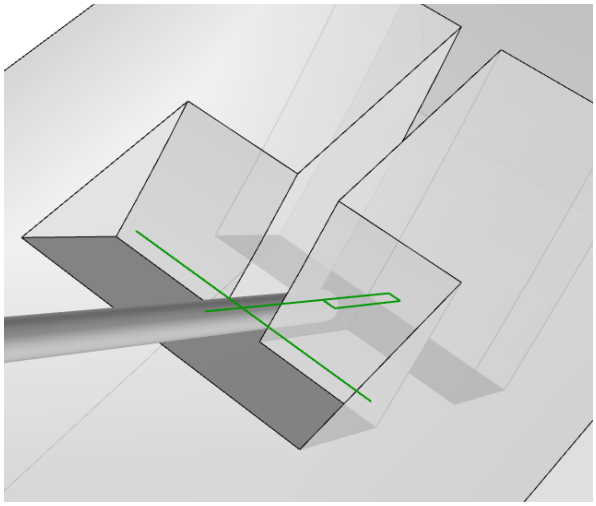

Figure 5.8: Step 5

In the next step the same as in step 2 is done. The opening is finished so the eventual shape is made. However this side is not curved, so now the edge of the mill (which is flat) can be used to make the surface. Only a few milling lines are needed here because the height of the mill can be used.

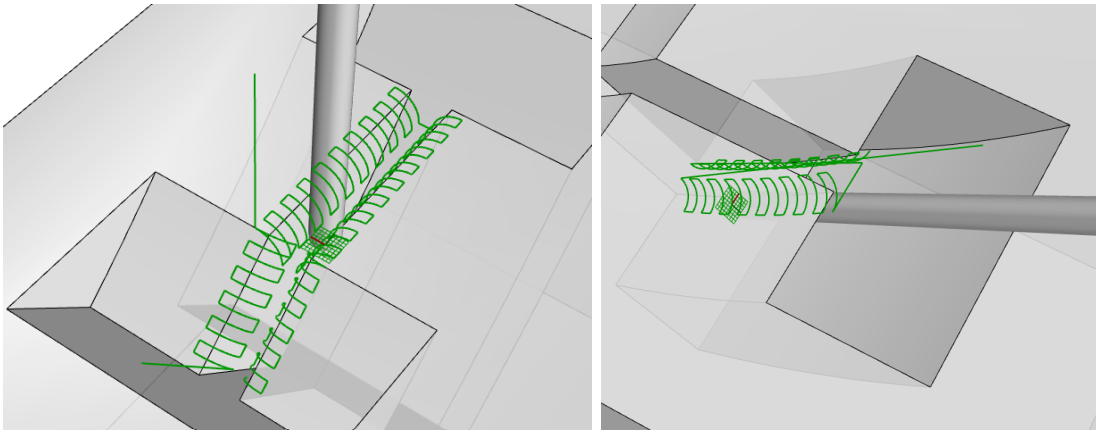

(a) Step 6 (b) Step 7

Figure 5.9: Step 6 and 7

Step 6 and 7 are needed again to fillet the corners. The milling paths in both figures look identical, however the orientation is different. In figure 5.9a the top of the mill is used, where in figure 5.9b the side of the mill is used. Step 7 is in the opening that was milled first, though the fillet could not have been made then as first the material on the other side needed to be removed. It is important to notice that the distance between the paths can be changed. It needs to be tested which maximal distance still gives a smooth result.

The different approaches to mill the surfaces indicates why it has to be generated manually. Some milling path are almost identical, but to make it possible to reach the path without colliding with the element different rotations are needed.

Milling path diagonal

The milling of the diagonal is again divided in steps. In this case the parts of the members are easier to be reached by the mill. However rotation around the diagonal causes more difficult situations for the robot to move from one to another point.

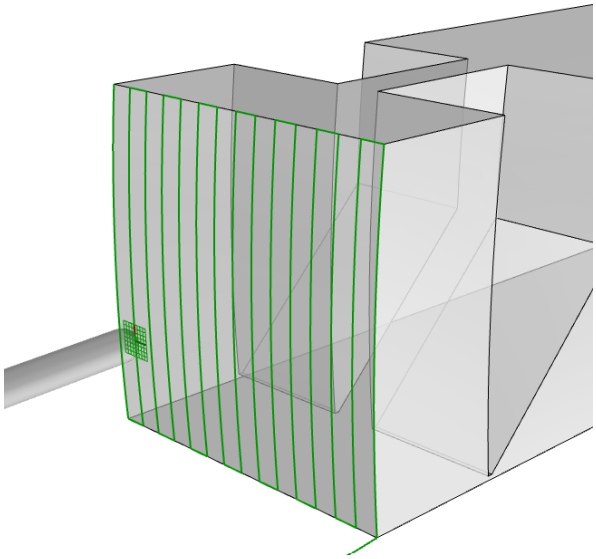

Figure 5.10: Step 1

First the top of the diagonal need to be milled. The surface is flat and needs to have the

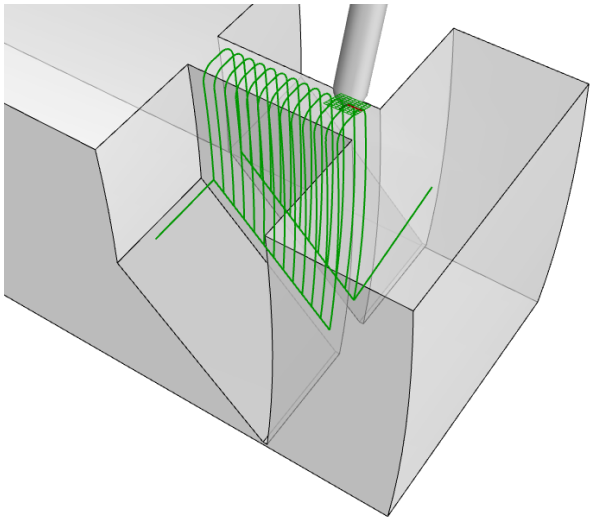

Figure 5.11: Step 2

same curvature as the opening in the beam. The milling path is in the same direction as the milling path of the beam. The distance between the paths is also the same, only here the lines jump half the distance between the lines. With this adjustment the wave pattern in the diagonal fits perfectly in the wave pattern of the beam.

In the next step the opening is milled. In figure 5.11 this is done with one milling line. However, depending on how much the mill can mill at once this can be adjusted.

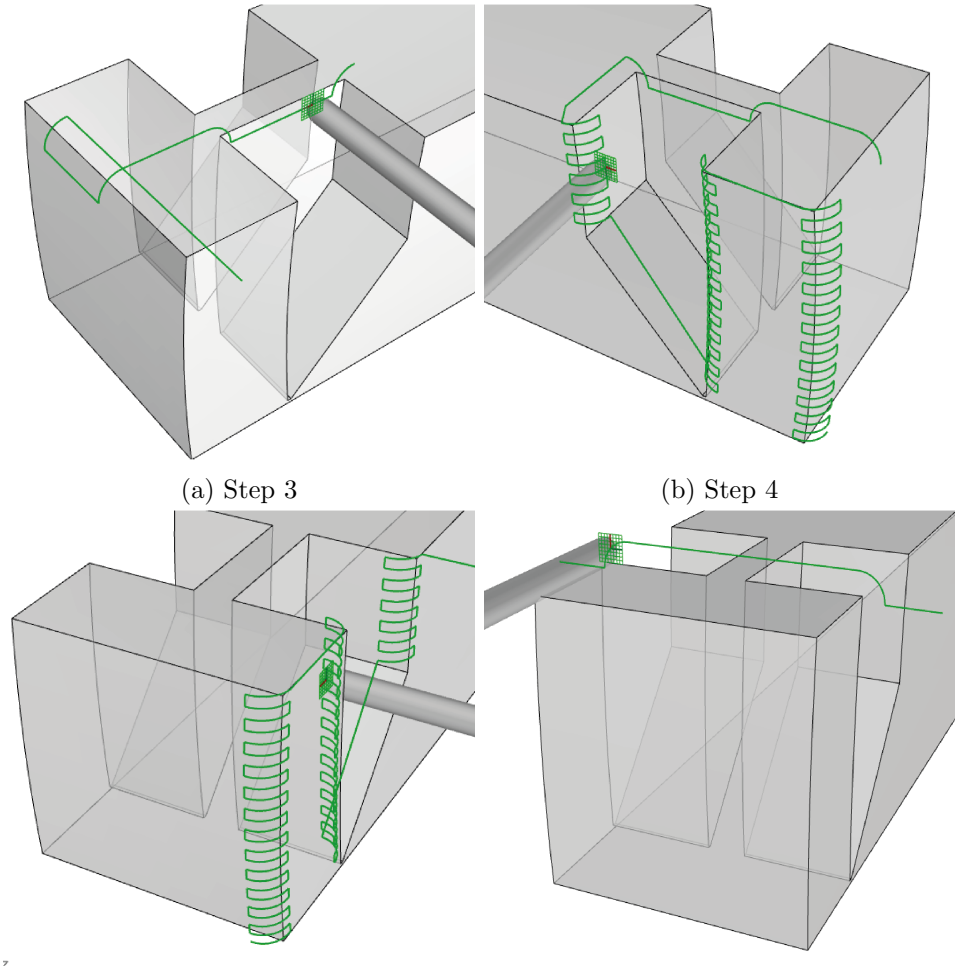

(a) Step 3

(b) Step 4

(c) Step 5

(d) Step 6

Figure 5.12: Step 3 until 6

Step 3 until 6 are all steps considering filleting the element. The edges that are not filleted, such as the slanting edge, are in contact with the beam at a place where it is not milled. So the sharp angle comes from the original shape of the beam.

Looking at all the milling paths that are needed to make the diagonal and the beam it becomes clear that a large part is to fillet edges. Compared to Japanese joinery this is an extra step to fabricate the elements. Though, only one end effector is needed to make this joint, so a lot of production time is saved.

The process to generate the milling path is now reasonably time consuming. For the designed connection the milling path is parametric. Changing the dimensions of the connections will change the milling path as well. However with new designs the milling path needs to be generated manually again. Software to automatically generate these paths is currently only available for simple geometries.

Still, the robot path is not suitable yet. Sometimes the robot cannot find a way to move from plane A to plane B. Singularities can occur, which is a configuration in which the robot end-effector becomes blocked in certain directions (Bonev, n.d.). To evaluate whether these singularities occur, the robot movements can be displayed in Rhino with the plugin *Robot Components*. The end effector can be moved over the complete trajectory to check if it is possible. When the robot makes a movement that is not possible, the robot becomes red. Whenever this happens, planes have to be added in between so that the robot finds a way to get to the next point.

Even now, it is still not sure that the robot can make all the generated movements. The plugin that is used is an 'experimental' tool that gives an idea how the robot movement will look. To check whether everything is possible the rapid code, both main and base, have to be exported to Robot Studio (ABB, 2020a). Robot Studio is the program that supplies the code to the actual robot. A simulation can be run in robot studio to see the movements. If something is not possible, the robot stops and an error message is shown. Once all the errors are fixed, the complete execution can be ran in Robot Studio. It can also be displayed in Rhino, which is useful to check whether the end effector will collide with the robot itself or the elements. Once everything runs well now, the script is ready to be executed by the robot.

5.3 Assembly

For the assembly of the elements another end effector is needed. The end effector needs to be able to pick up elements and place them in the right location. The idea is that one robot holds the beam and another robot rotates the element into the mortise. However for this fabrication only one robot is used. Therefore the beams are placed on their side and fixed to a table. The robot rotates all the elements into the beams.

A hydraulic clamp will be used to pick up the elements. With this clamp the robot can hold the elements tight enough to force them into the mortise. In figure 5.13 the assembly of the diagonals is illustrated. The robot has to hold the diagonal exactly in the middle, otherwise it is not possible to rotate the diagonals in both the top and bottom beam. Once the element is hold in the right place, the robot can move the element to the right location as is shown in the left figure. Yet the element is still rotated 45 degrees so it does not collide with anything. Once in place, only one axis of the robot needs to rotate 45 degrees to put the element into place.

Once the complete truss has been assembled the dried wooden tapering pins can be inserted in the connections. The robot can use the clamp for this as well. For this operation no force needs to be applied to insert the pin. When the pin gets to the same level of humidity as the other elements it will expand and tighten itself.

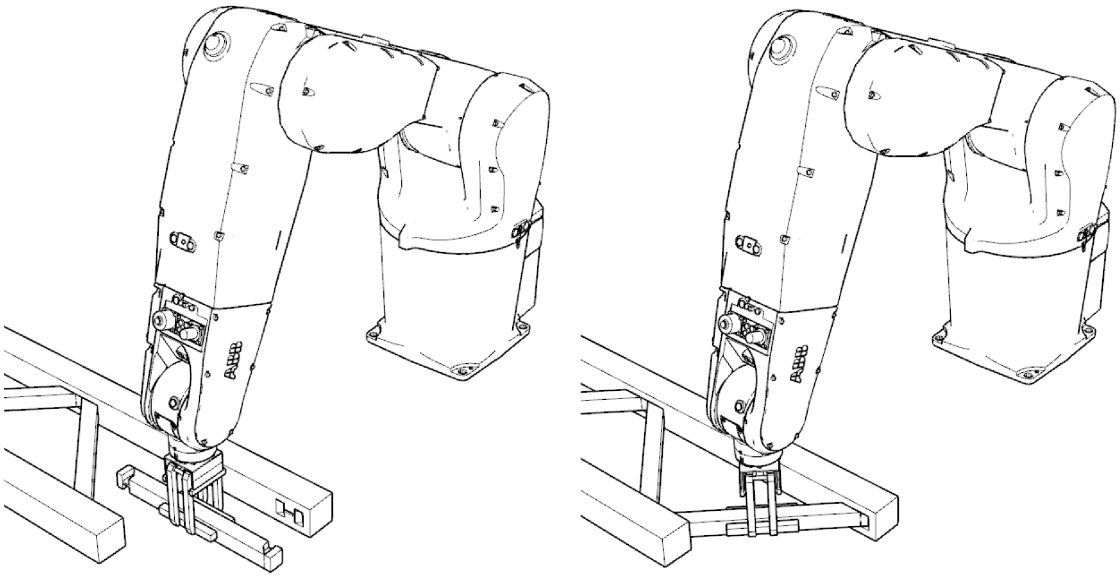

Figure 5.13: Assembly of elements

5.4 Execution

To see if the theoretical fabrication can be executed, first simple tests are performed to analyze the different parameters of the end effector. The three most important parameters are the displacement speed, the rotation speed and the milling depth. Furthermore in case of milling a surface the distance between the paths is important as well.

5.4.1 Test setup

The motor that is used is a $500W$ mini-spindle motor with a maximum rotation speed of $12000RPM$. The mills that can be mounted to the motor have a diameter of $1-7mm$ where the mill is mounted (Mysweety, n.d.).
For the first test the mill that is used is a mill that was available in the laboratory. It is a flat nose mill, the *Phantom 33.520.0500* (Deventer, n.d.). The diameter of the mill is $6mm$ where the mill is mounted and $5mm$ for the milling part. Furthermore the total length of the mill is $68mm$ and the length of the milling part is $24mm$. The company of the mill told that with the maximum rotation speed of the motor, hard materials could not be milled. Styrodur foam and MDF should be possible. The rotation speed should always be at the limit, and for the displacement speed of the mill $10mm/s$ should be a good speed to start with. If the mill is filled with material, the displacement speed should be decreased. If the foam starts to melt, the displacement speed should be increased. Furthermore the rotation should be positive and if possible the milling method should be climb milling. Climb milling is generally the best way to machine parts today since it reduces the load from the cutting edge, leaves a better surface finish, and improves tool life (Harvey, n.d.).

In figure 5.14 the test setup is shown. A base plate is mounted to the base table on which the robot is mounted. This base plate is shown in figure 5.15. The specimens can be placed over the cylinders that come out of the base plate. Afterwards they can be secured with four bolts. With this setup the specimens are always placed at the exact same place, which is

useful for defining the coordinates of the planes that have to be milled. A vacuum cleaner is placed behind the robot with the end of the hose placed close to the specimen. The fine dust will immediately be sucked into the vacuum cleaner, so no fine dust stays in the air.
The control panel of the robot is visible in the right bottom of the figure. Here the robot can be played, paused or stopped during the process. The motor is connected to a rotary knob which is placed outside the fence. In this way the robot can be controlled completely from outside the fence, which is necessary for safety reasons.

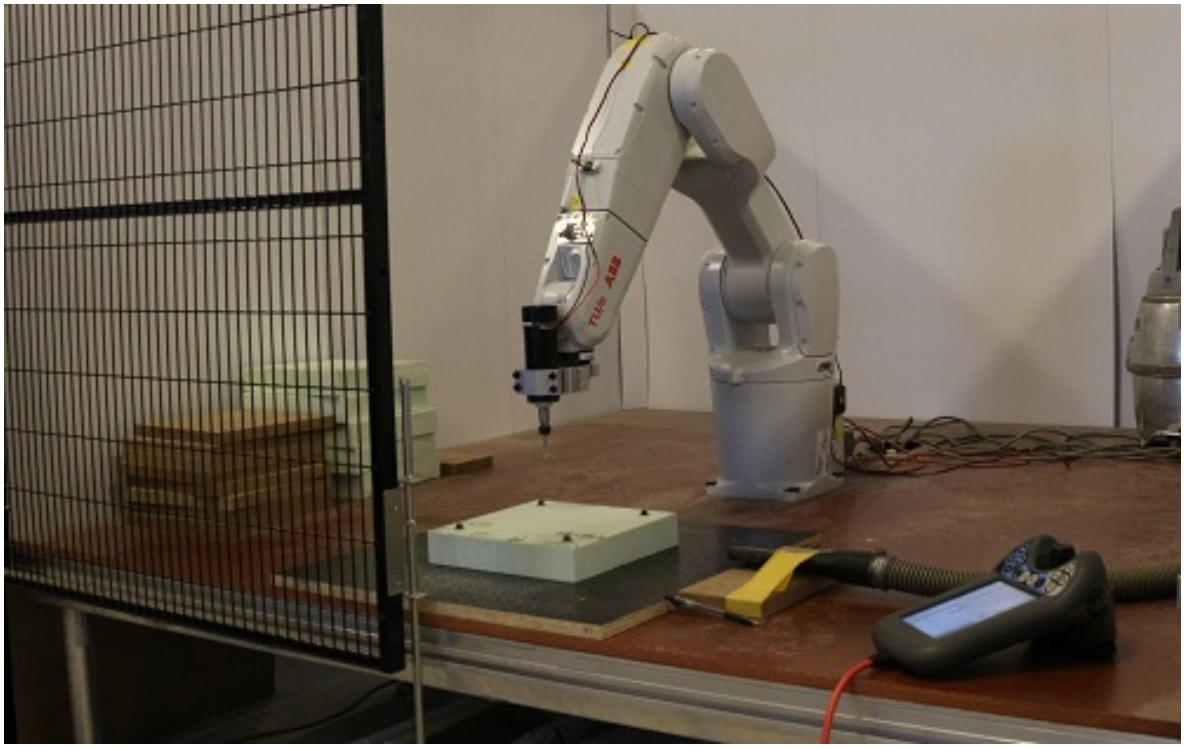

Figure 5.14: Test setup milling with robot

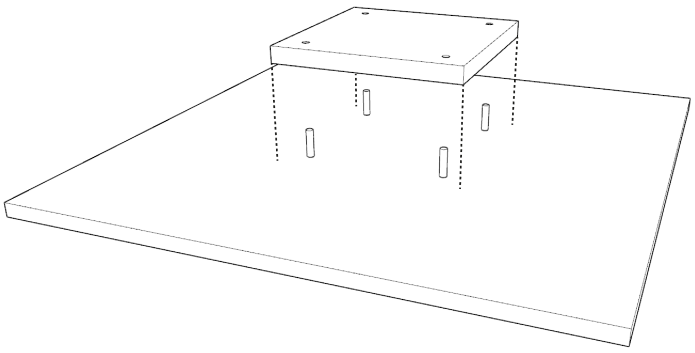

Figure 5.15: Mounting specimens

5.4.2 Performing tests

Now the elements can be milled. The tests that are conducted are gradually increased in complexity. All tests are proceedings that are used in a similar way for milling the final model. First all tests are performed on styrodur foam, if this does not cause any problems they can be executed on MDF as well. The process and the result of all tests can be found in appendix C. The variables for each test are shown in a table as well.

In specimen 1 straight lines are milled. The milling speed was perfect, no material was gathering in the opening and the foam was not melting either. The movement speed seemed to be a bit fast. When the arm was moved to a certain point and stopped there, the table to which the robot is attached to vibrated. To prevent inaccuracies due to this circumstance, the moving speed is decreased to $50mm/s$ in the next specimen. The lines were milled perfectly and the movements in between were flawless. The only remark is that the lines were not milled parallel to the side of the specimen. This means that the base plate is rotated towards the start position of the robot. Moreover the lines are not centered perfectly. For the next specimen the center of the specimen is moved and turned in comparison to the robot.

In the second specimen curved lines were milled. As mentioned before the lines are inserted as a collection of planes. A curved line in this case is a curved line divided into points (planes). For these curved lines they are divided in 50 points. The results show a smooth curve, so the division is good. Having it divided in less points might result in a polyline. The robot executed all the curves perfectly. The decrease of the moving speed worked out well, the table is not shaking anymore.

Specimen 3 and 4 are almost identical. In both tests a flat surface is being milled. In specimen 3 the lines are $4.5mm$ apart from each other and in specimen 4 this is $4mm$. The depths are respectively 5 and $10mm$. The results show that for both specimens the output is a smooth surface. The distance of $4.5mm$ is good for creating smooth surfaces with a $5mm$ mill. Along the top and the bottom side in figure C.3 and C.4 it is visible that a straight line was milled. On the other sides this was not the case, which causes a more coarse side.

In specimen 5 a curved surface is milled. The script was not completed because the end effector came close to a collision with the robot. The rotational freedom with the end effector is very limited. The already finished part show a smooth curved surface, so the movements there are possible and the end result is good.

The next specimens are made from MDF. The tests are similar to specimen 1 until 4. Only the milling depths and milling speeds are altered. In specimen 6 again five lines are milled. During milling the first line the mill got stuck near the end of the line. First the mill seemed to be broken, but after checking what happened it was visible that the line became deeper towards the end of the line. What happened was that the mill was not tightened well enough to the motor. This caused the mill to fall deeper during milling until in eventually reached the bottom plate and stopped. To prevent this from happening again the mill was tightened very securely, the milling depth was adjusted and the milling speed was reduced as well. With the adjusted depths and speeds everything went good. Although the mill made a lot of noise, so a careful procedure was necessary.

In specimen 7 curved lines are milled in MDF. These lines were milled quite flawless despite the noise, so the milling depth was gradually increased again. All the lines were performed perfectly, so the reason the first line of specimen 6 failed was only because of the loose connection of the mill.

For specimen 8 and 9 again two flat surfaces were milled, but this time in MDF. The distance between the lines stayed $4.5mm$ because this resulted in a smooth surface in the previous tests. The milling depth was increased to $7.5mm$ when the mill started to make even more noise. It seemed to be the limit of the milling depth at once. Furthermore, in specimen 9 extra lines were added to smoothen the sides of the surface. The difference in figure C.9 compared to figure C.8 is clear.

Conclusions

The milling itself worked out perfectly in styrodur foam. The end results were smooth and the robot was very accurate. In MDF the milling made a lot of noise, this is probably due to the fact the the number of rotations per minute of the spindle motor is too low for milling harder materials. It is still possible if the milling speed and depth is limited.

Reducing the moving speed of the robot solved the problem of a vibrating table. It is important to keep this speed as a maximum speed to make sure the end results stay good.

The working table is not perfectly straight in comparison to the robot. Not only is it a bit rotated, it also is not completely horizontal. For the executed tests this was not a problem, however when making a diagonal that has to be perfect to fit into the beam this will be a problem. For the tests where more accuracy is needed, first all four corners of the specimen are inserted into the robot path model. This will be done by jogging the end effector to every corner point and read out the X-,Y- and Z-coordinates. When all four corners are implemented in the design it will certainly be straight in every direction.

The way the end effector is mounted to the robot limits the rotational freedom a lot. If the target plane has a small rotation compared to the plane of the base of the robot, the distance between the end effector and the robot starts to become narrow.

5.4.3 Making designed connection

In the designed connection the end effector needs to be able to rotate a lot. With the current design of the end effector this would not be possible. To still execute the designed joint the fabrication has been changed. The diagonal can still be milled, however not at once. Compared to figure 5.1b the diagonal is turned 90 degrees. First one side can be milled, than the diagonal is flipped over and the other side can be milled. In case of the beam this is not possible. Therefore the beam has been cut in two parts. In figure 5.16 the cut beam is shown. With both adjustments the mill only has to be held in vertical direction. No rotations are needed, so milling will be possible with the current setup. As explained before, now before every test the corners of the specimen are referenced in the design model. With this approach the model will always be accurate and even inaccuracies in the material will not affect the end result. After the elements are milled they can be glued together. The created elements are almost identical to the designed elements.

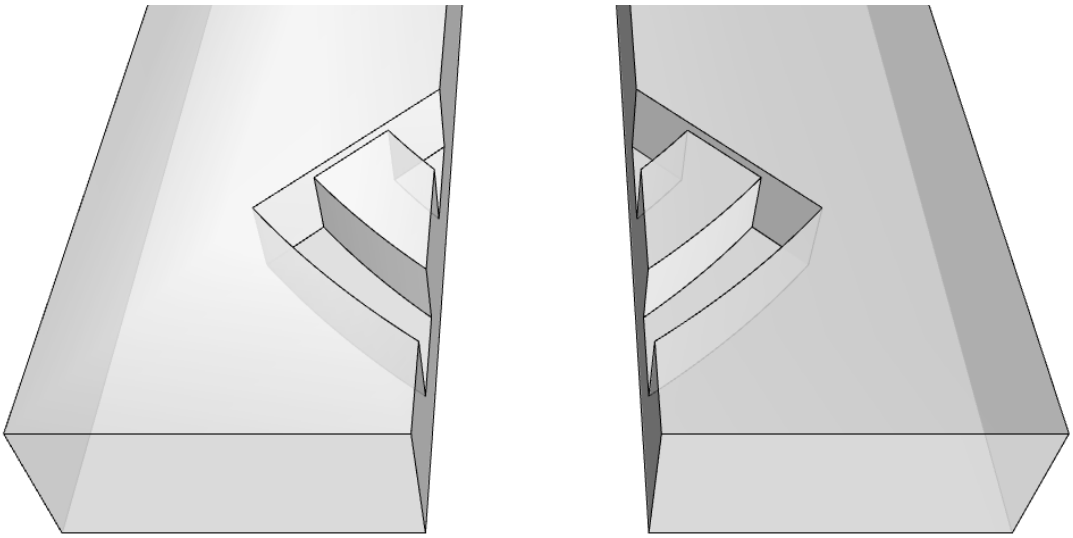

Figure 5.16: Beam element cut in two parts

In appendix C.2 the pictures of the milling of the beam and diagonal are shown. The milling speed was set to $10mm/s$ and the distance between the paths was $4.5mm$. These values gave the best results during milling the test specimens. The end result was smooth a clean, and the elements fitted perfectly into each other. Figure 5.17 shows the assembly of the elements.

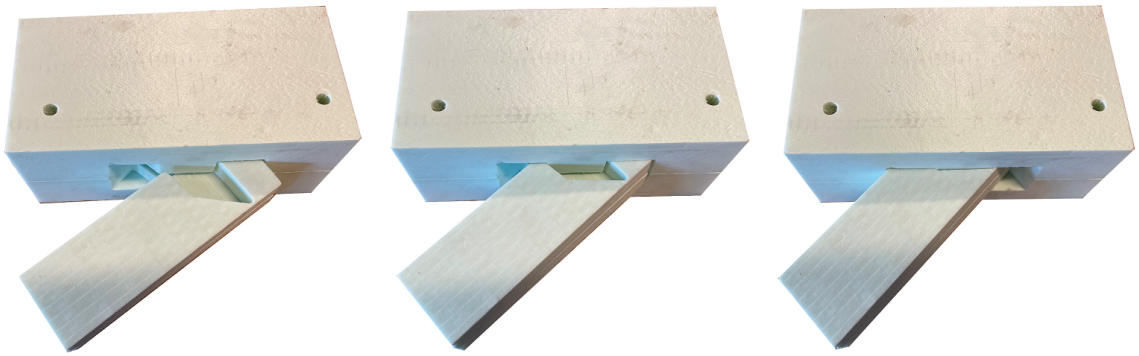

Figure 5.17: Assembly of foam model

Chapter 6

Laboratory test

6.1 Introduction

In this chapter a laboratory test will be explained and executed for the designed connection. Initially the laboratory tests had to be done simultaneously with the found results from the numerical and theoretical research. However due to the COVID-19 pandemic the laboratory of the Built Environment department at the TU/e was closed for some time. Therefore the designed connection is found with the help of theoretical and numerical research. To check whether the found optimal design behaves like it is calculated, a laboratory test will be conducted. Anyhow, in stead of testing the connection independently on the different failure modes, the complete connection is tested at once.

6.2 Material

In the calculated examples BauBuche Q is used as the LVL material because it results in the highest strength. However, BauBuche Q is made of beech laminated veneer lumber (Blaß and Streib, 2017) which is a hard material. This also gives the highest strengths compared to other LVL materials. With the available equipment in the laboratory at the TU/e it is hard to process this material to the eventual shape. Milling the material would need a motor with a high number of rotations per minute to mill precisely. Since the main reason of the test is to see how the joint behaves, not the maximal capacity, it is chosen to use a different LVL material. The results found in another material can be assumed to be similar to BauBuche Q, though with lower strengths. Most LVL is commonly produced from softwood, in Europe mainly spruce (*Picea Abies*) and pine (*Pinus sylvestris)* are used (Hakkarainen et al., 2020). These softwoods are easier to process, so for the fabrication in the laboratory more suitable as specimen material. Kerto Q is made out of spruce veneers with, similar to BauBuche Q, one of the five layers placed in perpendicular direction. The behaviour of the material is close to BauBuche Q, only it is weaker. Moreover the ratios between tension and different shear strengths are not the same.

The optimized joint in Kerto Q from table 4.2 is taken. The angle that will be used in the laboratory test will be 45 degrees. The found dimensions are 83mm for the height of the opening of the gooseneck, and 8mm of the width of the gooseneck (see figure 6.1). However, this is the case if the size of the diagonal is 100mm. The available material has a thickness of 68mm, so the found dimensions are multiplied by 0.68. In table 6.1 the characteristic

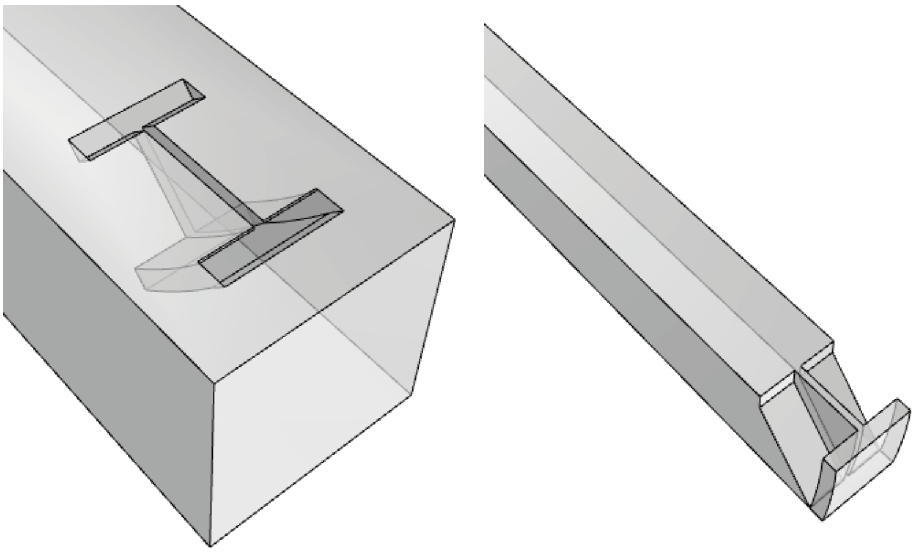

(a) Beam (b) Diagonal

Figure 6.1: Elements to be tested

strengths for the failure modes can be found. Moreover the failure load for the joint with the adjusted dimensions is shown. What immediately becomes clear is that especially the flatwise shear strength is a lot lower for Kerto Q. The flatwise shear is the shear that takes place in the beam in (local) X and Y direction. Therefore the shear area in the beam is dimensioned bigger than in the diagonal. Also the tension area in the diagonal seems very thin, this is because the tensile strength is a lot higher than the shear strength. Overall the differences in characteristic strengths lead to a large difference in failure load. The joint in Kerto Q is almost 5 times as weak as in BauBuche Q.

Characteristic strengths	BauBuche Q	Kerto Q	
$f_{t,0,k}$	45	19	N/mm^2
$f_{v,0,edge,k}$	7.8	4.5	N/mm^2
$f_{v,0,flat,k}$	3.8	1.3	N/mm^2
$f_{v,90,flat,k}$	3.8	0.6	N/mm^2
Failure load	BauBuche Q	Kerto Q	
F_{cr}	31.8	6.8	kN

Table 6.1: Characteristic strengths and failure load Baubuche Q and Kerto Q

6.3 Production of specimens

As explained in the previous chapter, the motor that is used for milling with the robot is not powerful enough. Milling soft materials is possible, but already with milling MDF it seemed to be struggling. Kerto Q is made out of layers of spruce veneers glued together. The veneers are compressed by 10 percent to achieve higher strengths and stiffnesses (Metsäwood, 2016). The combination of compressed veneers and glue makes the material harder to process. To make sure the specimens are made accurately, a CNC-machine in the structural laboratory will be

used. The specimen can move in X-, Y-, and Z-direction according to a manually defined path. The approach is similar to how the foam model was fabricated. Again, the beam is cut in two halves that are milled separately and then glued together. For the diagonal, one side is milled, then the specimen is turned and then the other side is milled. However, as the path is entered manually into a computer connected to the CNC-machine, it is chosen to leave out the curvature. This curvature was normally needed to rotate the diagonal into the beam. Though, for the test a connection where the diagonal slides into the beam also works. The rotation is only necessary when there is an interlocking joint at both the start and the end of the diagonal. Furthermore, this adjustment hardly affects the behaviour of the joint. The shear areas change with less than 1 percent. Leaving out the curvature will reduce the risk of fabrication errors.

Figure 6.2: Milled beam

Figure 6.3: Milled diagonal

In figure 6.2 and 6.3 the milled elements are shown. The beam halves will be glued together with the same glue that is used for laminating the veneers. The glue process has

been executed following the application guidelines (Technik, 2015).

6.4 Test setup

The test that will be performed on the joint is a tensile test. As mentioned before, the joint is weaker in tension than in compression. The difference is so big that, when applied in a truss, the members in tension are always governing. An illustration of the test setup is shown in figure 6.4. The diagonal will be connected to a base with a hinged connection. The beam will also be connected with a hinge to the part where the force is applied on. The center of this connection lies in the extended center line of the diagonal. This is done to make sure the force is always applied exactly in the direction of diagonal and no eccentricities can occur.

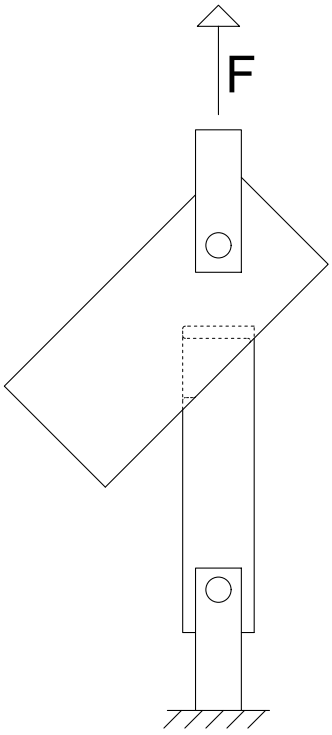

Figure 6.4: Test setup

To make sure the gooseneck connection will be governing, it is important that the bolted connections are stronger. In appendix B.1 the strengths of these bolted connections are calculated. The bolted connection in the diagonal has a strength of 24.4kN, where the bolted connection in the beam has a strength of 36.7kN. As mentioned, the estimated failure strength of the joint lies a bit below 7kN. So it is safe to assume that the test will fail in the designed joint.

As mentioned earlier, the complete connection will be tested at once. As the connection is not visible from the outside, it is hard to tell what happens exactly inside the joint. To try to analyze the behaviour in the best way possible, an additional measuring instrument is used to monitor the behaviour. A strain gauge will be glued to the tension area in the diagonal. Unfortunately it is not possible to apply strain gauges for the shear areas. In figure 6.5 the

strain gauge on the diagonal is shown. Since the diagonal fits into the beam perfectly, there is no 'extra' space for the strain gauge. The two options were making a cavity in the diagonal, in which the strain gauge is placed, or making a cavity in the beam. As one of the possible failure mechanisms is tension in the diagonal, taking away material there would mean the joint is reduced in strength. So the cavity has been made in the beam, here no critical forces are transferred, so it does not affect the strength of the joint. It is essential that the cavity is big enough for the strain gauge. If the beam touches the strain gauge it might influence the outcome.

As the strain gauge is very thin and vulnerable, it is chosen to put the diagonal into the beam before gluing the beam. Because the diagonal fits into the beam perfectly, there is no extra space, thus quite a lot of friction when inserting. This means a force needs to be applied to insert the diagonal. It is expected that this might cause the strain gauge to break. So first the diagonal is placed in half the beam, then it is glued and the other halve is placed on top. To prevent glue going into the connection some space around the joint is not glued. Unfortunately during drying, still some of the glue managed to get into the joint. This might influence the results, so it should be taken into account when analyzing the results.

The test will be performed in a displacement controlled way. This means the force that is applied will move with a constant speed upwards. It is important that the test resembles a real application. So the test speed should not be too high, this will result in a unrealistic high resistance. Moreover, it is hard to see what happens inside the joint, so for this reason it is also better to perform the test slowly. The failure mechanism can be analyzed better if it happens slowly in stead of breaking very fast. With these two reasons in mind the test speed is set to $0.5mm/min$.

While setting up the test, it became clear that there are many places where initial displacements might occur before the force is applied on the joint. This occurs mainly in the steel bolt connections. To calculate the deflection of the joint only, a Linear Variable Differential Transformer (LVDT) is added (see figure 6.6). The LVDT is attached to the diagonal,

(a) Strain gauge on diagonal

(b) Cavity in beam

Figure 6.5: Strain gauge

and the top touches a horizontal plate glued to the beam. Furthermore the cable that comes from the strain gauge is visible as well.

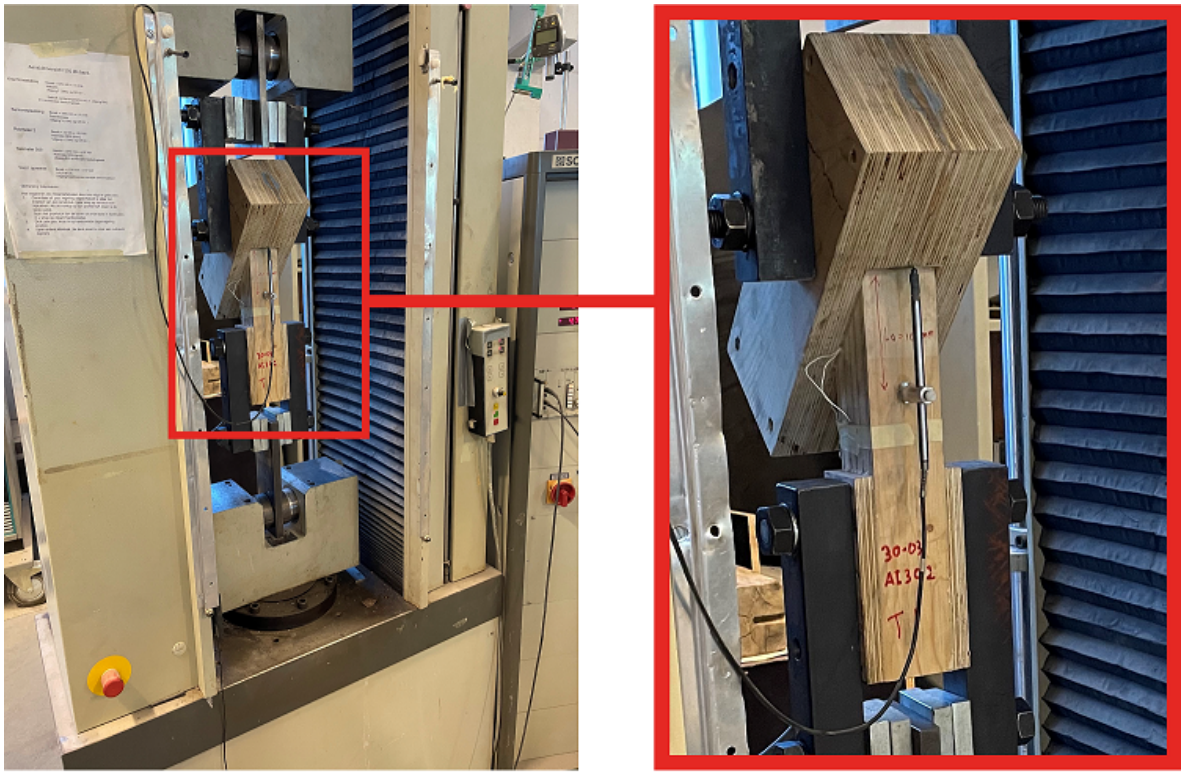

Figure 6.6: Test setup with LVDT

6.5 Results

The first thing that is visible when analyzing the force-displacement graph of figure 6.7 is that the connection looks like a 'safe' connection. After reaching the peak force, the joint is still able to resist more than half the peak force for a reasonably long time. However, the designed joint consists out of three probable failure modes that are all brittle. The only remaining strength after the joint fails in one of the failure modes is the friction of the timber. This friction is not able to resist more than half the peak force, so it is assumed that the glue that went into the joint provides extra strength after failure.

The joints strength is calculated to resist 6.8kN. In the graph for both tests a change in direction is visible around 6.2kN. This might indicate that failure in the timber occurs here, and in the next phase the glue takes over the force. Unfortunately it is hard to draw conclusions from these numbers as it is unknown how much the glue contributes in the total strength. What is also possible, is that here the crossed laid veneers broke. In figure 6.9 and 6.10 there are notches visible where the diagonal broke. These notches are at the places where the veneer is laid in the other direction. So possibly they broke before the complete section broke, and this could be the change of direction in the graph.

In both graphs the lines are almost identical until 6.2kN. Only in the beginning the lines of test 2 are odd. This is because the camera ran out of battery and test was started over

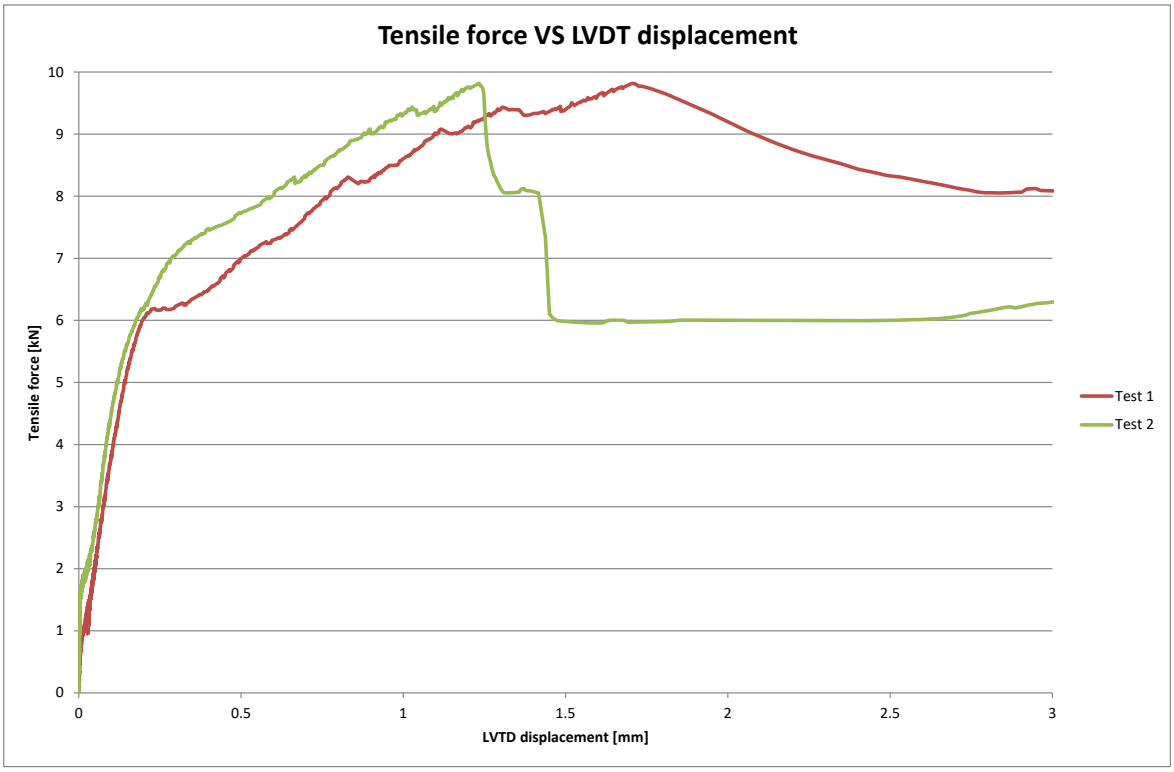

Figure 6.7: Graph tensile force VS LVDT displacement

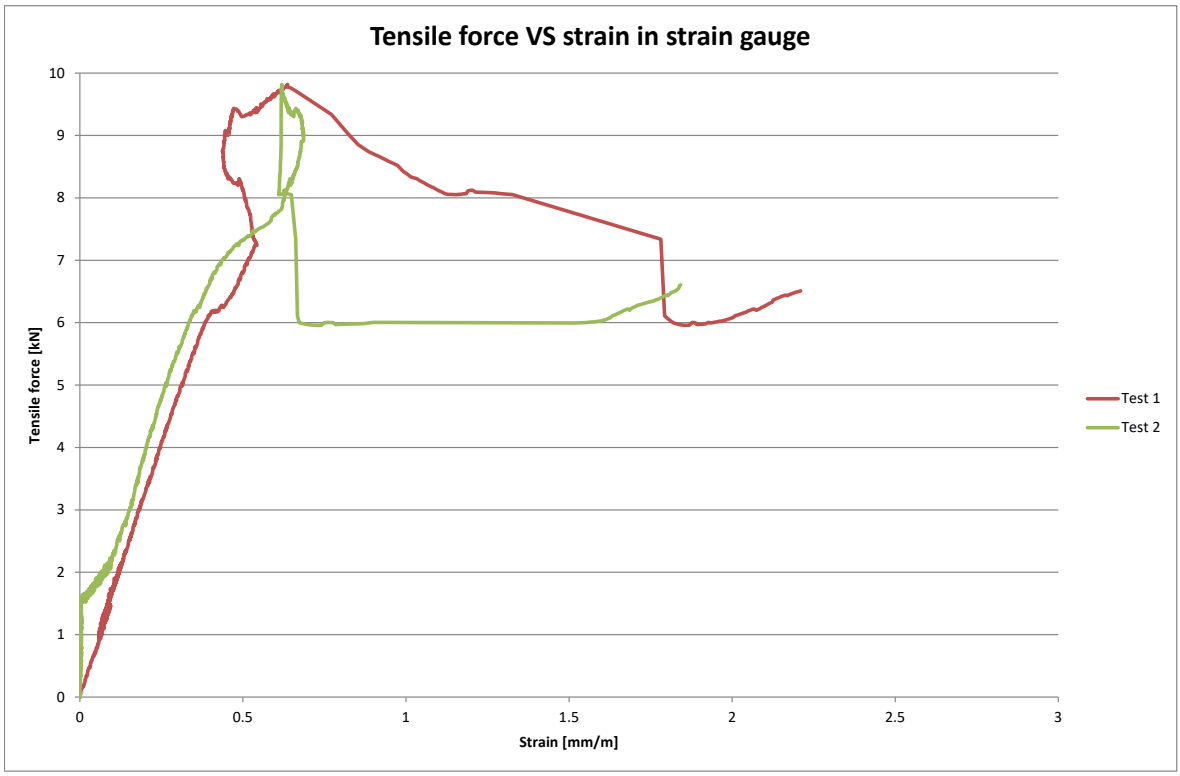

Figure 6.8: Graph tensile force VS strain in strain gauge

Figure 6.9: Failed connection test 1

Figure 6.10: Failed connection test 2

after a few minutes. When it was started again the tension was released a bit, so from the start the line gradually gets to the same steepness as test 1. Having two almost identical lines firstly indicates that the joints are comparable in the elastic part. Though, the glue that got into the joint was completely random. This is also visible in the pictures, the glue was not at the same places for both joints. Therefore it is assumed that the glue does not contribute in strength in the first elastic part of the test. So after 6.2kN either the complete tension area broke and the glue took over, or the crossed laid veneers broke and the resistance was still without extra strength provided by the glue. Either ways, the joints strength reached 6.2kN, which is close to the calculated 6.8kN. Nevertheless, the joint itself might be stronger if only crossed laid veneers broke. Unfortunately no hard conclusions can be drawn from this information.

Looking at the strain in the strain gauge shows that for test 1 after 7.3kN, and for test 2 after 9kN, the strain decreases a bit. This probably happened after the tension area broke. As is visible in both figure 6.9 and 6.10, the strain gauge is not at the place where the diagonal failed. If this would be the case, the strain would have increased tremendously after failure. In this case, after failure some of the stress in the part where the strain gauge is placed, is released. This leads to a decrease in strain. The strain is not released completely, as there is still tension in the section due to friction. So this is what happened in the graph in figure 6.8.

6.6 Conclusions

The results from the test are not sufficient to draw conclusions. Ideally first all failure modes should be tested individually. The results out of these tests can be used to adjust the geometrical proportions accordingly. Eventually as similar test as the executed one can be used to check whether the joint behaves the same in the eventual application. Now, due to skipping the first steps and also due to the fabrication accidents the results are not completely trustworthy. Although it is plausible that the joints strength is similar to the calculated strength.

Chapter 7

Conclusions and recommendations

7.1 Introduction

In this final chapter conclusions from the different chapters will be summarized and the main goal of this research will be discussed. The drawn conclusions will result in recommendations for future work that will be initiated afterwards.

7.2 Conclusions

7.2.1 Preliminary study

A robot could replace the skills that are needed for woodworkers to make complex joints. Also, it would be less time consuming to realize such a connection. These complex joints are mostly designed to transfer compressive forces, and in some occasions also some tension. Moreover, the nodes where members come together become very weak if too many members are connected in the same node. To set a realistic goal for the joint to be made, a structural scheme is determined. With the found restrictions a *Warren* truss is most suitable for the to be designed joint. The top and bottom member of the truss can be continuous, so that only three elements come together in one node.

7.2.2 Design of new connection

The connection will be most vulnerable for tension. So, the design focuses on the tensile strength of the joint. First a sliding dovetail joint is designed, then the join is adjusted to a joint that rotates into its mortise to improve the flexibility. Only the diagonals need to be rotated, so larger structures can be made. To limit the deflection perpendicular to the grain the gooseneck joint is chosen. Though, still a lot of stresses perpendicular to the grain are present. This is inevitable when designing a timber joint using only timber. If two members come together in an angle towards each other, there will always be stresses not parallel to the grain. Normally mechanical fasteners or adhesives can transfer these stresses to the grain direction, however in this case the timber has to transfer them.

7.2.3 Structural design

The material that is used for the joint is an LVL material. Due to the stresses perpendicular to the grain it is essential that the material also has strength in an angle to the grain. An optimized joint is found by analyzing the failure modes. These are shear in two different areas in the beam, and tension and shear in the diagonal. For the different types of LVL, a different optimized joint is found. A dried wooden pin will be inserted in the joint to

prevent disassembly when no forces are applied. The joint can be used in a real application, the structural calculations of two examples can be found in annex I and II. An arched truss behaves better than the flat truss, due to higher tensile forces in a flat truss. Designing a joint without using mechanical fasteners or adhesives results in a weaker connection, though some structural applications are possible. Adding for instance a steel pin of 24mm would already increase the strength by 20 percent. Optimizing the joint for a bolted connection would increase the strength even more. Therefore it should not be seen as an alternative joint design in a real application, because a joint with mechanical fasteners or adhesives will always be stronger.

7.2.4 Fabrication

In theory, a complete truss can be fully fabricated and assembled by a robot. In practice two important issues occurred. First of all the motor showed difficulties with milling in MDF, which is one of the softest timber materials. For safety reasons no other timber materials were milled. Milling in foam went smooth, however, milling under an angle was restricted due to the design of the end effector. The robot would collide with the end effector when milling angled surfaces. Milling the designed connection is therefore impossible in the current setup. With a changed fabrication method it was still possible to make the joint, however not without human interfering.

7.2.5 Laboratory test

For production reasons Kerto Q is chosen as the material for the tensile test. As the joint is not visible from the outside an strain gauge has been placed in the joint to get more insight in the behaviour. Moreover a LVTD is placed to calculate the deflection of the connection only. Due to production issues, some of the glue went inside the joint. In the test results, this is visible as the graph shows a safe structure even though the failure modes are brittle. The joint seems to have a similar strength to the calculated strength, although it is hard to draw conclusions as the influence of the glue is not known exactly.

7.2.6 Research goal

The research goal that is introduced in the introduction is partially met:

"Design and develop a timber connection, fabricated and assembled by a robot, without using mechanical fasteners or adhesives."

A timber connection without mechanical fasteners or adhesives is designed and developed. In theory, the fabrication and assembly is completely possible by the robot. Though, the real fabrication is until a certain level done by the robot, however it is not made in timber and human interference is required. Furthermore the assembly of the elements have not been tested by the robot, so a full robotic fabrication and assembly have not been reached. With the gained knowledge, it is found out that the individual proceedings are possible. With the right resources, such as a more powerful motor and a new end effector design, the designed connection could be made completely by the robot.

7.3 Recommendations

7.3.1 Timber

Currently theoretical strengths have been used for the optimization of the joint. Some strengths were not provided, so it is assumed that material cannot be stressed in this direc-

tion. However, there will always be some strength. For future research it would be good to test all in individual failure modes to verify the given strengths and find the missing ones. With the strengths known in all directions, a different shape might be stronger. Due to the COVID-19 pandemic the laboratory was closed for a long time, so only the end result is tested unfortunately. This does not give sufficient knowledge about the separate failure modes.

7.3.2 Structural design

For similar reasons as mentioned in the previous paragraph the structural design is based on theoretical values. In future research it would be important to check each step with practical tests. In the design part a real model would give more insight in the behaviour and functionality of the joint. Moreover, when optimizing the joint each individual failure mode should be tested. It is hard to predict how a material like timber behaves when it is used in a real application. Different designs are now compared in a theoretical or numerical way, to verify these results laboratory tests would give more insight. Also, from the way a joint can break, a lot can be learned. In theory this is not a visible aspect. Furthermore the goal of the research should be thought about. If the goal is to design a stronger connection it is recommended to implement fasteners in the design. An alternative would be to create a joint where a metal fasteners is hidden inside the joint, so the joint looks the same. Without fasteners a very strong joint cannot be designed.

7.3.3 Design

The design of the timber joint is done in a parametric way. With this approach the design can be optimized later on. For determining the robot path, the designed shape is taken, and manually the path is made for that joint. This is still done parametrically, so it is adjustable. However, if the shape changes a lot the robot path has to be made all over again. To improve this workflow, the robot path can be integrated earlier. For instance, the design can be designed in a similar way as the robot would make the design. So, material is taken away at certain parts. If this is modelled individually, the step to making a robot path is less time consuming and the whole process is more automated.

7.3.4 Laboratory test

Of course, as mentioned, the laboratory test is now conducted to finalize the research. The disadvantage is not only that the found results cannot be used to improve the design, but also that alternative tests cannot be examined. Now, to make sure the strain gauge did not break, an approach is followed that lead to glue in the joint. A more safe approach would have been to first glue the beam only, and make the cavity for the strain gauge big enough so the gauge would not break during assembly. Unfortunately now no material was left to check this approach. Would the laboratory test have been executed earlier in the process, more different methods could have been tested.

Bibliography

ABB. (2020a). *Operating manual robotstudio.*

ABB. (2020b). *Product specification irb 1200* (tech. rep.).

Blaß, H. J. & Streib, J. (2017). *Baubuche beech laminated veneer lumber design assistance for drafting and calculation in accordance with eurocode 5* (tech. rep.). Karlsruhe, BauBuche.

Bonev, I. (n.d.). *What are singularities in a six-axis robot arm?* https://www.mecademic.com/en/what-are-singularities-in-a-six-axis-robot-arm (accessed: 25.02.2021)

Deventer, A. T. (n.d.). *Hsse-co uni.frezen lang 5mm weldon.* https://www.atd.nl/hsse-co-unifrezen-lang-5-mm-weldon-215071/ (accessed: 25.02.2021)

Green, D. W., Winandy, J. E. & Kretschmann, D. E. (1999). *Wood handbook - wood as an engineering material.* Forest Products Laboratory.

Hakkarainen, J., Linkosalmi, L., Huovinen, A., Vares, S., Häkkinen, T., Hakkarainen, J. & Veikkola, M. (2020). *Lvl handbook europe.* Helsinki, Federation of the Finnish Woodworking Industries.

Harvey. (n.d.). *Climb milling vs. conventional milling.* https://www.harveyperformance.com/in-the-loupe/conventional-vs-climb-milling/ (accessed: 25.02.2021)

Hayashi, T., Harada, M., Karube, M. & Ukyo, S. (n.d.). *Strain analysis of traditional japanese timber joints under tensile loading.*

Heesterman, M. & Sweet, K. (2018). *Robotic connections: Customisable joints for timber construction.*

Janssen, H. (2016). *Statics of structures - part: Equilibrium of structures.*

Locher, M. (2010). *Traditional japanese architecture an exploration of elements and forms.*

Mestäwood. (2017). *Kerto manual, mechanical properties* (tech. rep.).

Metsäwood. (2016). *Kerto slim bouwen met hout.* Apeldoorn, Metsä Wood Holland.

Mysweety. (n.d.). *500 w luchtgekoelde 0,5 kw mini-spindle motor + 220 v mach3 snelheid power converter + 52 mm klem + 13 stuks er11 collet voor cnc-graveermachine.* https://www.amazon.nl/luchtgekoelde-spindle-snelheid-converter-graveren/dp/B01LNBOCDA/ref=sr_1_1?__mk_nl_NL (accessed: 25.02.2021)

Porter, B. & Tooke, C. (2001). *Carpentry and joinery 1* (3^{d}, Vol. 1). Oxford, Routhledge.

Steico. (2017). *Steico bausystem furnierschichtholz lvl* (tech. rep.).

Sumiyoshi, T. & Matsui, G. (1991). *Wood joints in classical japanese architecture* (F. Kovacs, Trans.). Japan, Kajima Institute Publishing Co.,Ltd.

Technik, H. (2015). *Single-component polyurethane adhesive for the manufacture of engineered wood products.*

List of figures

All other figures are own work.

Annex I

Structural report flat roof

I.1 Structural design

In this example a possible situation in which the trusses can be utilized is analyzed. The trusses will be used to carry the roof of a temporary covering structure. The structural report focuses on the load carrying capacity of the trusses as they will be used as roof carrying beams. The trusses will carry a roof and will transfer the loads to the walls or columns where they are placed onto. A mechanical representation is shown in figure I.1.
The dimensions of the the trusses are assumed to be 100 × 100 mm for the diagonals and 200 × 200 mm for the bottom and top beam. In this example the trusses will carry a floor of 10 × 12 meter. The span will be 10 meters and they will be placed in a grid with a center to center distance of 3 meters. The height of the roof will be 5 meters. In the structural report, first the members will be checked by the internal forces. Then the detail where the diagonals are connected to the beams will be checked. Finally the displacements will be checked as well.

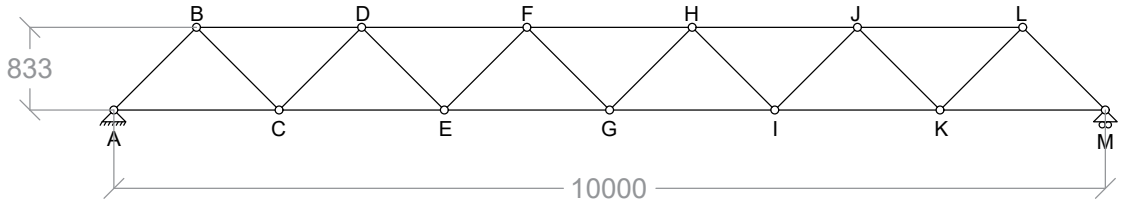

Figure I.1: Mechanical diagram of truss [dimensions in mm]

I.2 Standards and regulations

The following European codes with Dutch appendices may have been used for the structural calculations of the given parts:

- Eurocode 0:
  - NEN-EN 1990 Grondslagen van het constructief ontwerp;
- Eurocode 1:
  - NEN-EN 1991-1-1 Algemene belastingen: Volumieke gewichten, eigen gewicht en opgelegde belasting voor gebouwen;

- NEN-EN 1991-1-3 Algemene belasting: sneeuwbelasting;
- NEN-EN 1991-1-4 Algemene belasting: windbelasting;

- Eurocode 5:
  - NEN-EN 1995 Ontwerp en berekening van houtconstructies.

I.3 Assumptions structural calculations

Building indication:	Roof	
Design lifespan:	Class 1, 10 years	(NEN-EN 1990 NB table 2.1)
Safety class:	Consequence class: CC1	(NEN-EN 1990 NB table B1)
Reliability class:	RC1, (KFI factor = 0,9)	(NEN-EN 1990 table B3)
Usage class:	Class H (Roofs)	(NEN-EN 1990 tabel A1.1)
	$\psi_0 = 0, \psi_1 = 0, \psi_2 = 0$	
Wind area:	III	(NEN-EN 1991-1-4 figure NB.1)
Terrain category:	II, No buildings	(NEN-EN 1991-1-4 table 4.1)

I.4 Assumptions materials

Timber type:	Board BauBuche Q
Material properties	See appendix D.1

I.5 Assumed loads

I.5.1 Permanent loads

Roof

qG_k; Roofing	$0.24kN/m^2$
qG_k; Underlayment	$0.10kN/m^2$
qG_k; Ceiling	$0.10kN/m^2$
qG_k	$0.44kN/m^2$

I.5.2 Imposed loads

Roof class H (conform NEN-EN 1991-1-1)
The imposed loads is a point load of $1.5kN$ on the middle of the roof.

I.5.3 Snow load

Equation I.1 calculates the snow load per square meter conform NEN-EN 1991-1-3 expression 5.1.

$$s = \mu_i \times C_e \times C_t \times s_k = 0.56kN/m^2 \tag{I.1}$$

$\mu_i = 0.8$ for flat roofs
$C_e = 1.0$
$C_t = 1.0$
$s_k = 0.7kN/m^2$

q_s; Flat roof	$0.56kN/m^2$

I.5.4 Wind load

Wind pressure

Equations I.2 until I.8 are all conform NEN-EN 1991-1-4 for wind loads.

$$v_b = c_{dir} \times c_{season} \times v_{b,0} = 24.5 m/s \tag{I.2}$$

$c_{dir} = 1.0$
$c_{season} = 1.0$
$v_{b,0} = 24.5 m/s$

$$k_r = 0.19 \times \frac{z_0}{z_{0,II}}^{0.07} = 0.21 \tag{I.3}$$

$z_0 = 0.2$
$z_{0,II} = 0.05$

$$c_r = k_r \times ln(\frac{z}{z_0}) = 0.82 \tag{I.4}$$

$z = 10m$
$z_0 = 0.2$

$$v_m = c_r \times c_o \times v_b = 20.07 m/s \tag{I.5}$$

$c_o = 1.0$

$$I_v = \frac{k_l}{c_0 \times ln(\frac{z}{z_0})} = 0.26 \tag{I.6}$$

$k_l = 1.0$

$$q_p = (1 + 7 \times I_v) \times \frac{1}{2} \times \rho \times v_m^2 = 0.70 N/mm^2 \tag{I.7}$$

$\rho = 1.25 kg/m^3$

$$w_e = q_p \times c_{pe,10} \tag{I.8}$$

$c_{pe,10} = Zone : F = -1.8, \quad G = -1.2, \quad H = -0.7, \quad I = +/- 0.2$

w_e is given in table I.1 and I.2 as the pressure per area.

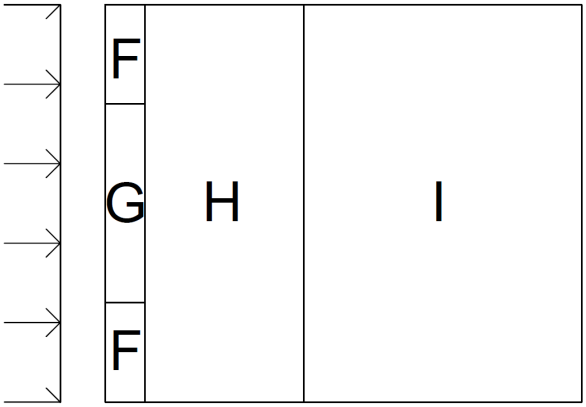

Figure I.2: Wind load side 1 conform NEN-EN 1995-1-4 figure 7.6 (*plan view*)

Zone	F	G	H	I
Length (x) $[m]$	1	1	4	7
Width (y) $[m]$	2.5	5	10	10
Surface $[m^2]$	2.5	5	40	70
Pressure $[kN/m^2]$	-1.26	-0.84	-0.49	$+/-0.14$

Table I.1: Wind load side 1

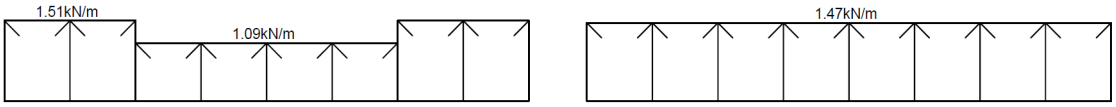

Figure I.3: Load distribution side 1. Left: 1^{st} truss, Right: 2^{d} truss

If the wind is in the direction of figure I.2, the trusses run from the top to the bottom. The trusses that will be affected by the wind load maximally is either the most left one, or the one next to that one. The first one will be loaded by: $1 \times -1.26 + 0.5 \times -0.84 = 1.51kN/m$ for the first 2.5 meters and $1 \times -0.84 + 0.5 \times -0.49 = -1.09kN/m$ in the middle 5 meters. The second truss will be loaded by: $3 \times -0.49 = -1.47kN/m$ over the whole length.

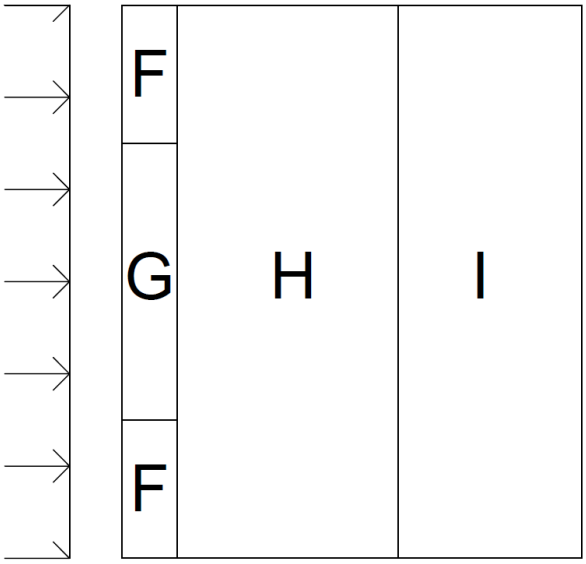

Figure I.4: Wind load side 2 conform NEN-EN 1995-1-4 figure 7.6 (*plan view*)

Zone	F	G	H	I
Length (x) $[m]$	1.2	1.2	4.8	4
Width (y) $[m]$	3	6	12	12
Surface $[m^2]$	3.6	7.2	57.6	48
Pressure $[kN/m^2]$	-1.26	-0.84	-0.49	$+/-0.14$

Table I.2: Wind load side 2

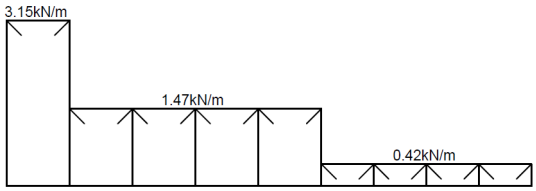

Figure I.5: Load distribution side 2

If the wind is in the direction of figure I.4, the trusses run from the left to the right. The trusses that will be affected by the wind load maximally are the second and the second-last one. The loads per meter are calculated as follows:

0 to 1.2 meters $1.5 \times -1.26 + 1.5 \times -0.84 = -3.15 kN/m$
1.2 to 6 meters $3 \times -0.49 = -1.47 kN/m$
0 to 1.2 meters $3 \times -0.14 = -0.42 kN/m$

The load distributions are shown in figure I.5.

Internal pressure

For the calculation of the internal wind pressure the values for a flat covering structure are taken. It is assumed the roof structure will be filled maximally by half the height. This means

that value $\psi = 0.5$ for the determination of the internal pressure. In table I.3 and I.4 the found loads by internal pressure are shown.

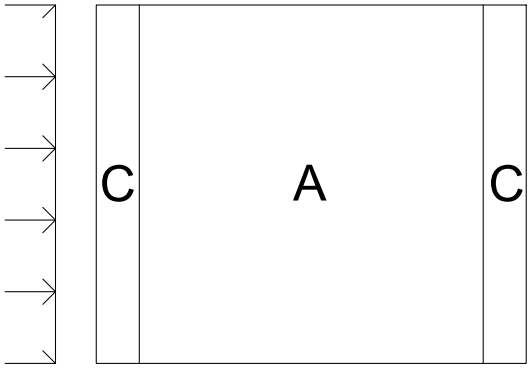

Figure I.6: Internal pressure side 1 conform NEN-EN 1995-1-4 table 7.6 (*plan view*)

Zone	A	C
Length (x) $[m]$	9.6	1.2
Pressure $[kN/m^2]$	-0.74	-1.26
Load $[kN/m]$	-2.21	-3.78

Table I.3: Internal pressure side 1

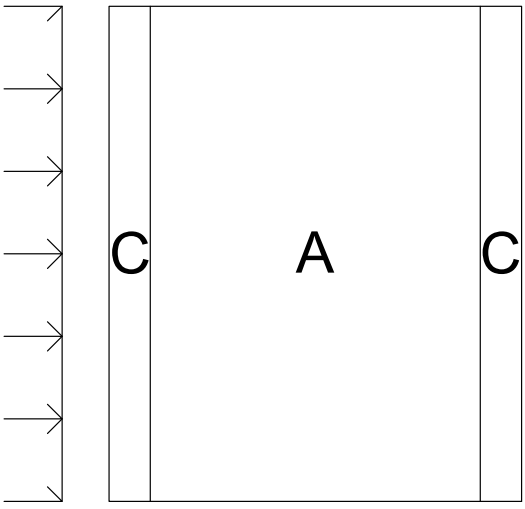

Figure I.7: Internal pressure side 2 conform NEN-EN 1995-1-4 table 7.6 (*plan view*)

Zone	A	C
Length (x) $[m]$	8	1
Pressure $[kN/m^2]$	-0.74	-1.26
Load $[kN/m]$	-2.21	-3.78

Table I.4: Internal pressure side 2

I.6 Load combinations

The load combinations are conform *NEN-EN 1990 NB table A1.2 (B)*. ψ_0=0 for snow, wind and imposed loads.

Ultimate Limit State:
Equation 6.10a shown in equation I.9:

$$1.20 \times G + (1.35 \times 0 \times q_r + 1.35 \times 0 \times q_s + 0.9 \times 0 \times q_{we} + 0.9 \times 0 \times q_{wi}) = 1.20G \quad \text{(I.9)}$$

Equation 6.10b shown in equations I.10 until I.13:

$$1.10 \times G + 1.35 \times q_r + (1.35 \times 0 \times q_s + 0.9 \times 0 \times q_{we} + 0.9 \times 0 \times q_{wi}) = 1.10G + 1.35q_r \quad \text{(I.10)}$$

$$1.10 \times G + 1.35 \times q_s + (0.9 \times 0 \times q_{we} + 0.9 \times 0 \times q_{wi} + 1.35 \times 0 \times q_r) = 1.10G + 1.35q_s \quad \text{(I.11)}$$

$$0.9 \times G + 1.35 \times q_{we}(i) + 1.35 \times q_{wi}(i) + (1.35 \times 0 \times q_r + 1.35 \times 0 \times q_s) = 0.9G + 1.35q_{we}(i) + 1.35q_{wi}(i) \quad \text{(I.12)}$$

$$0.9 \times G + 1.35 \times q_{we}(ii) + 1.35 \times q_{wi}(ii) + (1.35 \times 0 \times q_r + 1.35 \times 0 \times q_s) = 0.9G + 1.35q_{we}(ii) + 1.35q_{wi}(ii) \quad \text{(I.13)}$$

Serviceability Limit State:
Load combination conform table A2.6 shown in equations I.14 until I.17

$$1.0 \times G + 1.0 \times q_r + (1.0 \times 0 \times q_s + 1.0 \times 0 \times q_{we} + 1.0 \times 0 \times q_{wi}) = 1.0G + 1.0q_r \quad \text{(I.14)}$$

$$1.0 \times G + 1.0 \times q_s + (1.0 \times 0 \times q_{we} + 1.0 \times 0 \times q_{wi} + 1.0 \times 0 \times q_r) = 1.0G + 1.0q_s \quad \text{(I.15)}$$

$$1.0 \times G + 1.0 \times q_{we}(i) + 1.0 \times q_{wi}(i) + (1.0 \times 0 \times q_r + 1.0 \times 0 \times q_s) = 1.0G + 1.0q_{we}(i) + 1.0q_{wi}(i) \quad \text{(I.16)}$$

$$1.0 \times G + 1.0 \times q_{we}(ii) + 1.0 \times q_{wi}(ii) + (1.0 \times 0 \times q_r + 1.0 \times 0 \times q_s) = 1.0G + 1.0q_{we}(ii) + 1.0q_{wi}(ii) \quad \text{(I.17)}$$

I.7 Calculation truss

I.7.1 Ultimate Limit State

Internal forces

All load cases have been implemented in a SCIA model. In appendix D.2 these inputs can be found. In the visualisations the other structural data is shown as well. First of all, the supports are both hinged connections. One of the two is a sliding support. The beams are continuous members, and all the diagonals are connected in a hinged way in between. The dimensions of the model are the same as in figure I.1. The loads are applied as point loads on the nodes. This is done because the loads on the roof are transferred via the underlayment to the nodes.
All the ULS and SLS load combinations, I.9 until I.17, are inserted in the SCIA model. The SLS load combinations will be discussed later in the report.
Now that all the input is known, the structural model is calculated. The extreme stresses found in the members are shown in appendix D.3. For the diagonals only the members with

the highest (tensile) and the lowest (compressive) stresses are shown. The beams are continuous, so here the peak stresses (both positive and negative) are shown.

Diagonals
First, the diagonals are checked on tension and compression.
The design tensile strength is:

$$k_{mod} \times \frac{f_{t,0,k}}{\gamma_m} = f_{t,0,d} = 36.04 N/mm^2 \tag{I.18}$$

where $f_{t,0,k}$ is multiplied with factor k_l (see appendix D.1).
The design compressive strength is:

$$k_{mod} \times \frac{f_{c,0,k}}{\gamma_m} = f_{c,0,d} = 35.53 N/mm^2 \tag{I.19}$$

$$\eta = \frac{\sigma_{t,0,max}}{f_{t,0,d}} = \frac{3.94}{36.04} = 0.11 \leq 1.0 \tag{I.20}$$

$$\eta = \frac{\sigma_{c,0,max}}{f_{c,0,d}} = \frac{2.59}{35.53} = 0.07 \leq 1.0 \tag{I.21}$$

Both tensile as compression forces in the diagonals will not lead to failure of the truss.

The diagonals are connected by hinges, so only axial forces are conducted through the elements.

Beams
First, the beams are checked on the maximal tension and compression. The design strengths are the same as in the diagonals, because the orientation of the elements does not affect the tensile and compressive strengths.

$$\eta = \frac{\sigma_{t,0,max}}{f_{t,0,d}} = \frac{2.38}{36.04} = 0.07 \leq 1.0 \tag{I.22}$$

$$\eta = \frac{\sigma_{c,0,max}}{f_{c,0,d}} = \frac{2.41}{35.53} = 0.07 \leq 1.0 \tag{I.23}$$

Both tensile as compression forces in the beams will not lead to failure of the truss.

Then the shear and bending stresses will be checked. The most extreme value (positive or negative) out of the values in appendix D.3 are taken. The material used is orthotropic, so has a plane of symmetry in the middle of the section. So if the most extreme stress meets the requirement, the other will as well. The found stresses are really small, which comes because the truss will behave more or less like a fully hinged truss. In a fully hinged truss only axial forces occur, now some bending and shear stresses occur, but they are very small.

The design shear strength is:

$$k_{mod} \times \frac{f_{v,k}}{\gamma_m} = f_{v,d} = 5.20 N/mm^2 \tag{I.24}$$

The design bending strength is:

$$k_{mod} \times \frac{f_{m,0,k}}{\gamma_m} = f_{m,0,d} = 40.00 N/mm^2 \tag{I.25}$$

$$\eta = \frac{\sigma_{v,max}}{f_{v,d}} = \frac{0.11}{5.20} = 0.02 \leq 1.0 \tag{I.26}$$

$$\eta = \frac{\sigma_{m,0,max}}{f_{m,0,d}} = \frac{0.59}{40.00} = 0.01 \leq 1.0 \tag{I.27}$$

The shear forces and bending moments will not lead to failure of the truss.

Buckling

The last check for internal forces is the buckling check of the diagonals.

$$\lambda = L \times \sqrt{\frac{A}{I}} = 40.8 \tag{I.28}$$

$L = 1178.5mm$
$A = 10000mm^2$
$I = 8.3 \times 10^6 mm^4$

Equation I.29 is conform NEN-EN 1995-1-1 expression 6.21:

$$\lambda_{rel} = \frac{\lambda}{\pi} \times \sqrt{\frac{f_{c,0,k}}{E_{0,05}}} = 0.86 \tag{I.29}$$

$f_{c,o,k} = 53.3 N/mm^2$
$E_{0.05} = 12200 N/mm^2$

Equation I.30 is conform NEN-EN 1995-1-1 expression 6.27:

$$k = 0.5 \times (1 + \beta_c \times (\lambda_{rel} - 0.3) + \lambda_{rel}^2) = 0.90 \tag{I.30}$$

$\beta_c = 0.1$

Equation I.31 is conform NEN-EN 1995-1-1 expression 6.25:

$$k_c = \frac{1}{k + \sqrt{k^2 - \lambda_{rel}^2}} = 0.86 \tag{I.31}$$

Equations I.32 and I.33 are confrom NEN-EN 1995-1-1 expressions 6.23 abd 6.24:

$$\frac{\sigma_{c,0,d}}{k_c \times f_{c,0,d}} + \frac{\sigma_{m,y,d}}{f_{m,y,d}} + k_m \times \frac{\sigma_{m,z,d}}{f_{m,z,d}} \leq 1 \tag{I.32}$$

$$\frac{\sigma_{c,0,d}}{k_c \times f_{c,0,d}} + k_m \times \frac{\sigma_{m,y,d}}{f_{m,y,d}} + \frac{\sigma_{m,z,d}}{f_{m,z,d}} \leq 1 \tag{I.33}$$

$\sigma_{m,y,d}$ and $\sigma_{m,z,d} = 0N/mm^2$ so:

$$\frac{\sigma_{c,0,d}}{k_c \times f_{c,0,d}} \leq 1 \tag{I.34}$$

$\sigma_{c,0,d} = 3.94N/mm^2$
$f_{c,0,d} = 35.53N/mm^2$

$$\frac{\sigma_{c,0,d}}{k_c \times f_{c,0,d}} = 0.12 \leq 1 \tag{I.35}$$

Buckling will not cause failure of the structure.

Detail

In this section the connection of the diagonal members to the bottom and top member will be checked. First the connection will be checked for the maximal compression, then it will be checked for tension.

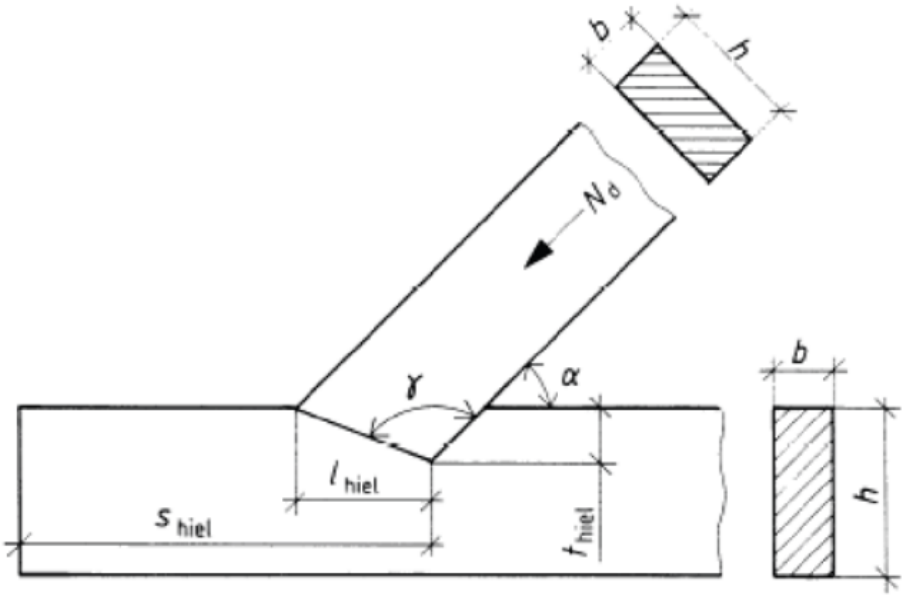

Figure I.8: Tooth joint conform NEN-EN 1995-1-1 figure NB.4

In figure I.8 the *hiel* is replaced by *amb* in the formulas below.
$N_{c,d} = \sigma_{c,0,d} \times A = 39400N$

$b = 100mm$
$s_{amb} = 152mm$
$t_{amb} = \frac{100}{\sqrt{2}}mm$
$l_{amb} = \frac{100}{\sqrt{2}}mm$
$\alpha = 45^{\circ}$

Equations I.36 until I.38 are conform NEN-EN 1995-1-1 expressions NB.8.4, NB.8.5 and NB.8.6.

$$\begin{aligned} &\sigma_{c,0,d} \leq f_{c,0,d} \\ &\sigma_{c,0,d} = \frac{N_{c,d} \times \cos\alpha}{t_{amb} \times b} = 3.94N/mm^2 \end{aligned} \tag{I.36}$$

$$\begin{aligned} &\sigma_{c,90,d} \leq f_{c,90,d} \\ &\sigma_{c,90,d} = \frac{N_{c,d} \times \sin\alpha}{l_{amb} \times b} = 3.94N/mm^2 \end{aligned} \tag{I.37}$$

$$\begin{aligned} &\sigma_{v,d} \leq f_{v,d} \\ &\sigma_{v,d} = \frac{N_{c,d} \times \cos\alpha}{s_{amb} \times b} = 1.83N/mm^2 \end{aligned} \tag{I.38}$$

$$f_{c,0,d} = k_{mod} \times \frac{f_{c,0,k}}{\gamma_m} = 35.53N/mm^2 \tag{I.39}$$

$$f_{c,90,d} = k_{mod} \times \frac{f_{c,90,k}}{\gamma_m} = 12.67N/mm^2 \tag{I.40}$$

$$f_{v,d} = k_{mod} \times \frac{f_{v,k}}{\gamma_m} = 5.20N/mm^2 \tag{I.41}$$

$$\eta = \frac{\sigma_{c,0,d}}{f_{c,0,d}} = \frac{3.94}{35.53} = 0.11 \leq 1.0 \tag{I.42}$$

$$\eta = \frac{\sigma_{c,90,d}}{f_{c,90,d}} = \frac{3.94}{12.67} = 0.31 \leq 1.0 \tag{I.43}$$

$$\eta = \frac{\sigma_{v,d}}{f_{v,d}} = \frac{1.83}{5.20} = 0.35 \leq 1.0 \tag{I.44}$$

For compression the connection meets all requirements.

For tension in a tooth joint no ULS-checks are provided by the Eurocode. The most probable failure mechanisms will therefore be analyzed in both the diagonals and edge beams details. First the diagonals are checked.

In the diagonal the two most probable failure modes are tension in the reduced section ($\sigma_{t,0,d}$) and shear of the 'teeth' ($\tau_{v,d}$). In figure I.9 these failure modes are shown in the left part. Due to the fact that the detail is 'sandwiched' in the beam, no other deformations can occur. So there will be pure shear in the detail. Note that the representation is 2D but the calculation is three-dimensional. Equations I.45 until I.50 check whether the diagonal resists the stresses.

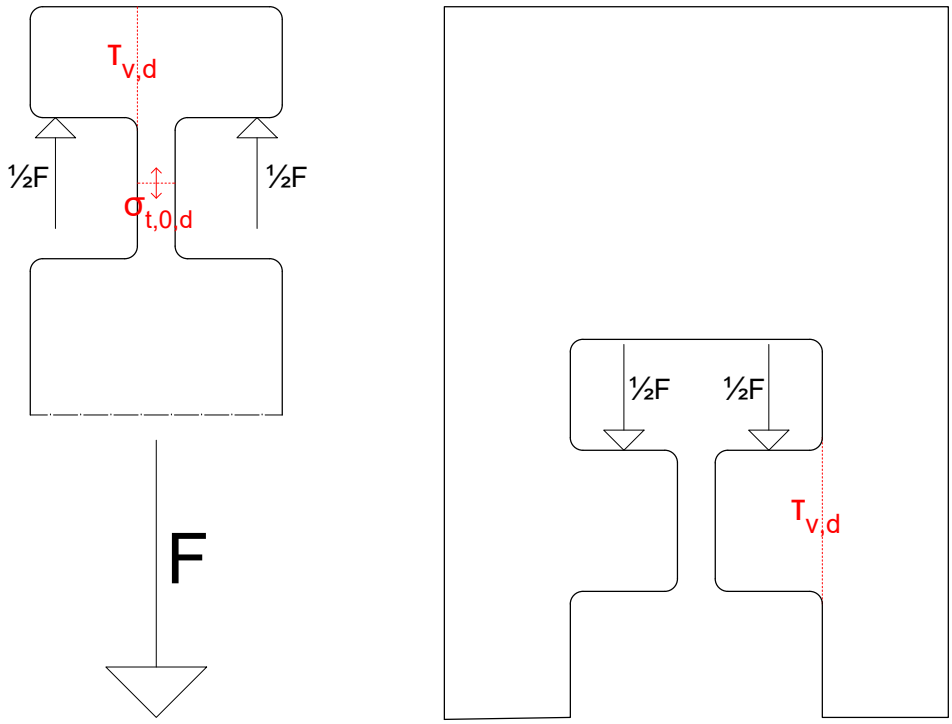

Figure I.9: 2D representation of detail with probable failure modes

$$\begin{aligned} \sigma_{t,0,d} &\leq f_{t,0,d} \\ \sigma_{t,0,d} &= \frac{F}{A} = 24.63 N/mm^2 \end{aligned} \tag{I.45}$$

$F = \sigma_{t,0,d} \times A = 39400N$
$A = 16 \times 100 = 1600mm^2$

$$f_{t,0,d} = k_{mod} \times \frac{f_{t,0,k}}{\gamma_m} = 34.00 N/mm^2 \tag{I.46}$$

$$\begin{aligned} \tau_{v,d} &\leq f_{v,d} \\ \tau_{v,d} &= \frac{V}{A} = 4.48 N/mm^2 \end{aligned} \tag{I.47}$$

$V = F/2 = 19700N$
$A = 44 \times 100 = 4400mm^2$

$$f_{v,d} = k_{mod} \times \frac{f_{v,k}}{\gamma_m} = 5.20 \quad N/mm^2 \tag{I.48}$$

$$\eta = \frac{\sigma_{t,0,d}}{f_{t,0,d}} = \frac{24.63}{34.00} = 0.72 \leq 1.0 \tag{I.49}$$

$$\eta = \frac{\tau_{v,d}}{f_{v,d}} = \frac{4.48}{5.20} = 0.86 \leq 1.0 \tag{I.50}$$

Tension in the detail of the diagonal will not lead to failure of the structure.

For the calculation of the beam it is important to notice that the section shown in figure I.9 on the right is cut in an angle of 45 degrees. This means that the forces do not act in the direction of the beam, but slanted compared towards the grain direction. To calculate whether the beam meets the requirements, the forces are resolved in both x (parallel to the grain) and y (perpendicular to the grain) direction. Looking at the figure, it might be expected that tension in the narrowest parts of the beam might also lead to great stresses. However, the beam is only this narrow where the section is made. Right next to the connection the full beam's area is able to resist stresses. Therefore this will not be one of the possible failure modes. For the shear force both the x and the y direction are considered. In case of a force in the y direction this causes a rolling shear. Equations I.51 until I.54 check whether the beam resists the stresses.

$$\begin{aligned} \tau_{v,d} &\leq f_{v,d} \\ \tau_{vR,d} &\leq f_{vR,d} \\ \tau_{v,d}, \tau_{vR,d} &= \frac{V}{A} = 2.17 N/mm^2 \end{aligned} \tag{I.51}$$

$V = \frac{1}{2}F/\sqrt{2} = 13930N$
$A = 6412mm^2$

$$\begin{aligned} f_{v,d} &= k_{mod} \times \frac{f_{v,k}}{\gamma_m} = 2.53 N/mm^2 \\ f_{vR,d} &= k_{mod} \times \frac{f_{vR,k}}{\gamma_m} = 2.53 N/mm^2 \end{aligned} \tag{I.52}$$

$$\eta = \frac{\tau_{v,d}}{f_{v,d}} = \frac{2.17}{2.53} = 0.86 \leq 1.0 \tag{I.53}$$

$$\eta = \frac{\tau_{vR,d}}{f_{vR,d}} = \frac{2.17}{2.53} = 0.86 \leq 1.0 \tag{I.54}$$

Tension in the detail of the beam will not lead to failure of the structure.

I.7.2 Serviceability Limit State

Load combination SLS	Deflection middle of roof					
	U_x		U_z		U_{total}	
A.14	0.2	mm	1.5	mm	1.5	mm
A.15	0.3	mm	2.9	mm	2.9	mm
A.16	-0.2	mm	-2.3	mm	-2.3	mm
A.17	-0.2	mm	-2.1	mm	-2.1	mm

Table I.5: Deflections due to load combinations

In table I.5 the calculated deflections found in the middle of the roof are shown. Note that the X-direction is horizontal and the Z-direction is vertical. The span of the roof is 10 meters, so the found deflections are acceptable.

To incorporate the deflections of the joint in the total deflection the structure is seen as a fully hinged structure. The difference in the deflection with this adjustment is less than 10 percent.
The deflection is biggest for load case A.15, which is the permanent plus snow loads. The force F that is acting on the structure in SLS is: $5kN$ for this load combination. With local equilibrium all internal forces in the members can be calculated. In appendix D.4 these axial forces can be found in the table. With the stress caused by these axial forces the elongation is calculated. The length of the deformed members can be determined now.
The structure is symmetrical, which means that both halves deform in the exact same way. It also means member FH remains straight in the deformed situation. With two nodes known, the next node can be placed by drawing the circles where the diameter equals the new length. So node G is found by drawing the circles with the diameters equal to the new length of FG and GH. This process can be continued until all nodes are found. To automate this process a Grasshopper script has been generated to calculate the deformed structure. The elongations are being retrieved from an Excel file where everything is calculated. An additional advantage is that is also possible to add extra elongations for imperfection of the connection or a factor for translation stiffness in the connection. Without any imperfections the deflection in the middle of the truss equals: $w_{max} = 2.98mm$. This value is almost identical to the found value from the SCIA calculations.

The found deflection will only be the case if the joint does not deflect at all. In compression it may be assumed that this will be the case. However, in tension the connection will deflect. To measure the deflection of the joint in tension, an Abaqus model has been generated. The deflection of the connection in the direction of the diagonal is found to be almost half the deflection due to the axial force. With two joints (begin and end) per diagonal, this means that the deflection in the joints is almost equal to the previous calculated deflection. Only diagonals BC, DE, IJ and KL are in tension, so the elongations of these diagonals have been multiplied by two. With the newly found elongation the script calculated a deflection in the middle of the truss $w_{max} = 3.25mm$. With a span of 10 meters this deflection will not cause any problems.

Annex II

Structural report arched roof

II.1 Structural design

In this example a possible situation in which the trusses can be utilized is analyzed. The arched trusses will be used to carry a temporary covering structure. The structural report focuses on the load carrying capacity of the trusses as they will be used for both roof and walls of a structure. The trusses will carry a roof or wall and the forces will be transferred through the trusses to the foundation. In figure II.1 a mechanical representation is shown. The dimensions of the the trusses are assumed to be 100 × 100 mm for the diagonals and 200 × 200 mm for the bottom and top beam. In this example the trusses will carry a floor of 10 × 12 meter. The span will be 10 meters and they will be placed in a grid with a center to center distance of 3 meters. The height in the middle of the roof will be 6.5 meters. In the structural report, first the members will be checked by the internal forces. Then the detail where the diagonals are connected to the beams will be checked. Finally the displacements will be checked as well.

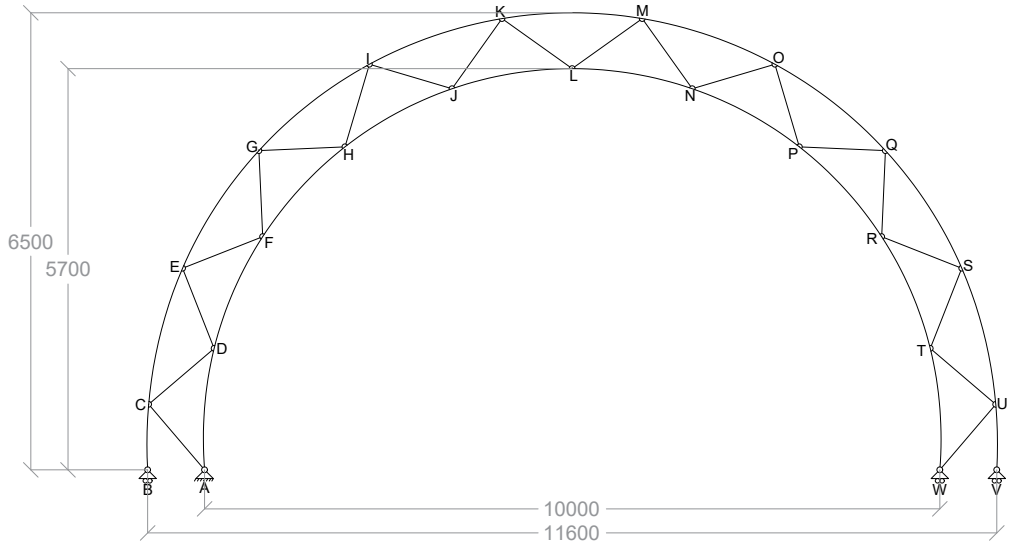

Figure II.1: Mechanical diagram of arched truss [dimensions in mm]

II.2 Standards and regulations

The following European codes with Dutch appendices may have been used for the structural calculations of the given parts:

- Eurocode 0:
  - NEN-EN 1990 Grondslagen van het constructief ontwerp;
- Eurocode 1:
  - NEN-EN 1991-1-1 Algemene belastingen: Volumieke gewichten, eigen gewicht en opgelegde belasting voor gebouwen;
  - NEN-EN 1991-1-3 Algemene belasting: sneeuwbelasting;
  - NEN-EN 1991-1-4 Algemene belasting: windbelasting;
- Eurocode 5:
  - NEN-EN 1995 Ontwerp en berekening van houtconstructies.

II.3 Assumptions structural calculations

Building indication:	Roof	
Design lifespan:	Class 1, 10 years	(NEN-EN 1990 NB table 2.1)
Safety class:	Consequence class: CC1	(NEN-EN 1990 NB table B1)
Reliability class:	RC1, (KFI factor = 0,9)	(NEN-EN 1990 table B3)
Usage class:	Class H (Roofs)	(NEN-EN 1990 tabel A1.1)
	$\psi_0 = 0, \psi_1 = 0, \psi_2 = 0$	
Wind area:	III	(NEN-EN 1991-1-4 figure NB.1)
Terrain category:	II, No buildings	(NEN-EN 1991-1-4 table 4.1)

II.4 Assumptions materials

Timber type:	Board BauBuche Q
Material properties	See appendix D.1

II.5 Assumed loads

II.5.1 Permanent loads

Roof

qG_k; Roofing	$0.24 kN/m^2$
qG_k; Underlayment	$0.10 kN/m^2$
qG_k; Ceiling	$0.10 kN/m^2$
qG_k	$0.44 kN/m^2$

II.5.2 Imposed loads

Roof class H (conform NEN-EN 1991-1-1)
The imposed loads is a point load of $1.5 kN$ on the middle of the roof.

II.5.3 Snow load

For cylindrical shaped roofs the Eurocode provides a distribution of the snow load as is shown in figure II.2. Angles larger than 60 degrees are not included in the loads. Therefore for members BC, UV, CE, SU: $\mu_3 = 0$. In the other members the maximum value has to be chosen which is $\mu_3 = 2.0$

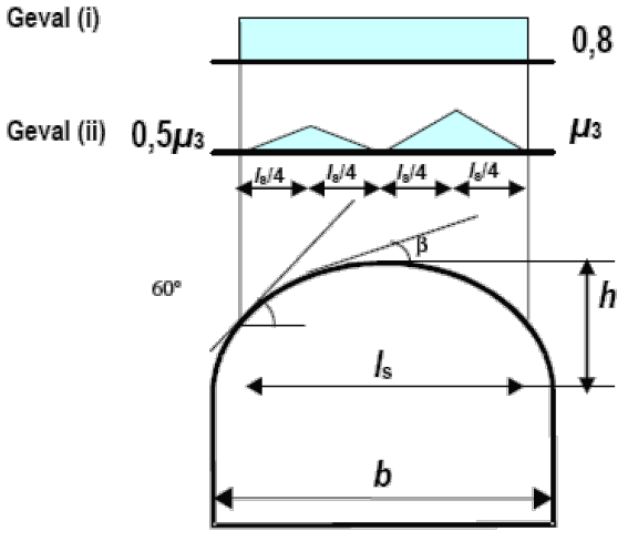

Figure II.2: Snow load on cylindrical roofs conform NEN-EN 1991-1-3 figure 5.6

Equation II.1 calculates the snow load per square meter conform NEN-EN 1991-1-3 expression 5.1.

$$s = \mu_i \times C_e \times C_t \times s_k = 0.56kN/m^2 \tag{II.1}$$

$\mu_i = 0.8$ for case (i)
$\mu_3 = 2.0$ for case (ii)
$C_e = 1.0$
$C_t = 1.0$
$s_k = 0.7kN/m^2$

q_s; Cylindrical roof	$0.56kN/m^2$	for case (i)
q_s; Cylindrical roof	$1.40kN/m^2$	for case (ii)

The maximum snow load on truss will be: $3 \times 0.56 = 1.68kN/m$ for case (i) and $3 \times 1.40 = 4.20kN/m$ for case (ii).
Note that in case (ii) the load must also be projected on the structure as illustrated in figure II.2.

II.5.4 Wind load

Wind pressure

Equations II.2 until II.8 are all conform NEN-EN 1991-1-4 for wind loads.

$$v_b = c_{dir} \times c_{season} \times v_{b,0} = 24.5m/s \tag{II.2}$$

$c_{dir} = 1.0$
$c_{season} = 1.0$
$v_{b,0} = 24.5m/s$

$$k_r = 0.19 \times \frac{z_0}{z_{0,II}}^{0.07} = 0.21 \tag{II.3}$$

$z_0 = 0.2$
$z_{0,II} = 0.05$

$$c_r = k_r \times ln(\frac{z}{z_0}) = 0.66 \tag{II.4}$$

$z = 6.5m$
$z_0 = 0.2$

$$v_m = c_r \times c_o \times v_b = 16.17m/s \tag{II.5}$$

$c_o = 1.0$

$$I_v = \frac{k_l}{c_0 \times ln(\frac{z}{z_0})} = 0.29 \tag{II.6}$$

$k_l = 1.0$

$$q_p = (1 + 7 \times I_v) \times \frac{1}{2} \times \rho \times v_m^2 = 0.50N/mm^2 \tag{II.7}$$

$\rho = 1.25kg/m^3$

$$w_e = q_p \times c_{pe,10} \tag{II.8}$$

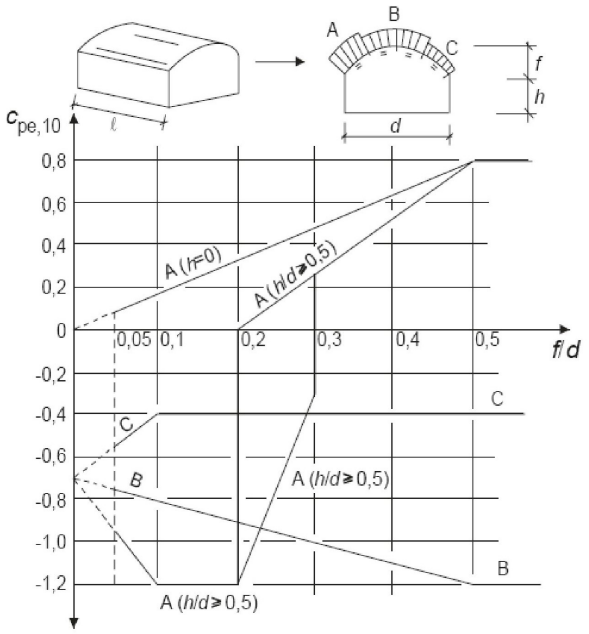

Figure II.3: Wind load on cylindrical roofs conform NEN-EN 1991-1-4 figure 7.11

The $c_{pe,10}$ values are retrieved from figure II.3.
$c_{pe,10} = Zone : A = +0.8, \quad B = -1.2, \quad C = -0.4$

w_e is given in table II.1 as the pressure per area, the load per meter is given in the last row.

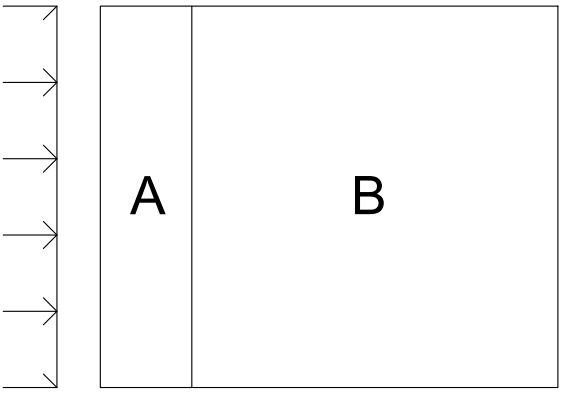

Figure II.4: Wind load on cylindrical roofs conform NEN-EN 1995-1-4 figure 7.5 (*plan view*)

Zone	A	B
Length (x) $[m]$	2.4	9.2
Pressure $[kN/m^2]$	0.40	−0.60
Load $[kN/m]$	1.20	−1.80

Table II.1: Wind load on arched truss

Internal pressure

For the calculation of the internal wind pressure the roof is interpreted as a double-sided slanted roof. It is assumed the roof structure will be filled maximally by half the height. This means that value $\psi = 0.5$ for the determination of the internal pressure.

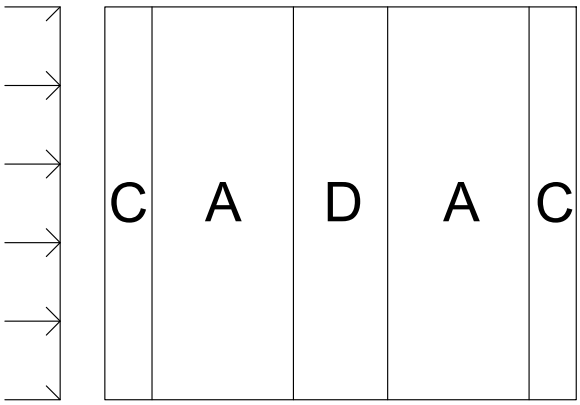

Figure II.5: Internal pressure conform NEN-EN 1995-1-4 table 7.7 (*plan view*)

Zone	C	A	D
Length (x) $[m]$	1.2	3.6	2.4
Pressure $[kN/m^2]$	0.70	−0.70	−1.00
Load $[kN/m]$	−2.10	−2.10	−3.00

Table II.2: Internal pressure on arched truss

II.6 Load combinations

The load combinations are conform *NEN-EN 1990 NB table A1.2 (B)*. ψ_0=0 for snow, wind and imposed loads.

Ultimate Limit State:
Equation 6.10a shown in equation II.9:

$$1.20 \times G + (1.35 \times 0 \times q_r + 1.35 \times 0 \times q_s + 0.9 \times 0 \times q_{we} + 0.9 \times 0 \times q_{wi)} = 1.20G \quad \text{(II.9)}$$

Equation 6.10b shown in equations II.10 until II.13:

$$1.10 \times G + 1.35 \times q_r + (1.35 \times 0 \times q_s + 0.9 \times 0 \times q_{we} + 0.9 \times 0 \times q_{wi}) = 1.10G + 1.35q_r \quad \text{(II.10)}$$

$$1.10 \times G + 1.35 \times q_s(i) + (0.9 \times 0 \times q_{we} + 0.9 \times 0 \times q_{wi} + 1.35 \times 0 \times q_r) = 1.10G + 1.35q_s(i) \quad \text{(II.11)}$$

$$1.10 \times G + 1.35 \times q_s(ii) + (0.9 \times 0 \times q_{we} + 0.9 \times 0 \times q_{wi} + 1.35 \times 0 \times q_r) = 1.10G + 1.35q_s(ii) \quad \text{(II.12)}$$

$$0.9 \times G + 1.35 \times q_{we} + 1.35 \times q_{wi} + (1.35 \times 0 \times q_r + 1.35 \times 0 \times q_s) = 0.9G + 1.35q_{we} + 1.35q_{wi} \quad \text{(II.13)}$$

Serviceability Limit State:
Load combination conform table A2.6 shown in equations II.14 until II.17

$$1.0 \times G + 1.0 \times q_r + (1.0 \times 0 \times q_s + 1.0 \times 0 \times q_{we} + 1.0 \times 0 \times q_{wi}) = 1.0G + 1.0q_r \quad \text{(II.14)}$$

$$1.0 \times G + 1.0 \times q_s(i) + (1.0 \times 0 \times q_{we} + 1.0 \times 0 \times q_{wi} + 1.0 \times 0 \times q_r) = 1.0G + 1.0q_s(i) \quad \text{(II.15)}$$

$$1.0 \times G + 1.0 \times q_s(i) + (1.0 \times 0 \times q_{we} + 1.0 \times 0 \times q_{wi} + 1.0 \times 0 \times q_r) = 1.0G + 1.0q_s(ii) \quad \text{(II.16)}$$

$$1.0 \times G + 1.0 \times q_{we} + 1.0 \times q_{wi} + (1.0 \times 0 \times q_r + 1.0 \times 0 \times q_s) = 1.0G + 1.0q_{we} + 1.0q_{wi} \quad \text{(II.17)}$$

II.7 Calculation arched truss

II.7.1 Ultimate Limit State

Internal forces

All load cases have been implemented in a SCIA model. In appendix D.5 these inputs can be found. In the visualisations the other structural data is shown as well. First of all, the supports are all hinged connections. Three of the four are sliding hinges. The curved beams are continuous members, and all the diagonals are connected in a hinged way in between. The dimensions of the model are the same as in figure II.1.
All the ULS and SLS load combinations, II.9 until II.17, are inserted in the SCIA model. The SLS load combinations will be discussed later in the report.
Now that all the input is known, the structural model is calculated. The extreme stresses found in the members are shown in appendix D.6. For the diagonals only the members with the highest (tensile) and the lowest (compressive) stresses are shown. The curved beams are continuous, so here the peak stresses (both positive and negative) are shown.

Diagonals

First, the diagonals are checked on tension and compression.
The design tensile strength is:

$$k_{mod} \times \frac{f_{t,0,k}}{\gamma_m} = f_{t,0,d} = 36.04 N/mm^2 \quad \text{(II.18)}$$

where $f_{t,0,k}$ is multiplied with factor k_l (see appendix D.1).
The design compressive strength is:

$$k_{mod} \times \frac{f_{c,0,k}}{\gamma_m} = f_{c,0,d} = 35.53 N/mm^2 \quad \text{(II.19)}$$

$$\eta = \frac{\sigma_{t,0,max}}{f_{t,0,d}} = \frac{2.07}{36.04} = 0.06 \leq 1.0 \quad \text{(II.20)}$$

$$\eta = \frac{\sigma_{c,0,max}}{f_{c,0,d}} = \frac{3.59}{35.53} = 0.10 \leq 1.0 \quad \text{(II.21)}$$

Both tensile as compression forces in the diagonals will not lead to failure of the truss.

The diagonals are connected by hinges, so only axial forces are conducted through the elements.

Curved beams
First, the beams are checked on the maximal tension and compression. The design strengths are the same as in the diagonals, because the orientation of the elements does not affect the tensile and compressive strengths.

$$\eta = \frac{\sigma_{t,0,max}}{f_{t,0,d}} = \frac{2.66}{36.04} = 0.07 \leq 1.0 \tag{II.22}$$

$$\eta = \frac{\sigma_{c,0,max}}{f_{c,0,d}} = \frac{3.20}{35.53} = 0.09 \leq 1.0 \tag{II.23}$$

Both tensile as compression forces in the beams will not lead to failure of the truss.

Then the shear and bending stresses will be checked. The most extreme value (positive or negative) out of the values in appendix D.6 are taken. The material used is orthotropic, so has a plane of symmetry in the middle of the section. So if the most extreme stress meets the requirement, the other will as well.

The design shear strength is:

$$k_{mod} \times \frac{f_{v,k}}{\gamma_m} = f_{v,d} = 5.20 N/mm^2 \tag{II.24}$$

The design bending strength is:

$$k_{mod} \times \frac{f_{m,0,k}}{\gamma_m} = f_{m,0,d} = 40.00 N/mm^2 \tag{II.25}$$

$$\eta = \frac{\sigma_{v,max}}{f_{v,d}} = \frac{2.06}{5.20} = 0.40 \leq 1.0 \tag{II.26}$$

$$\eta = \frac{\sigma_{m,0,max}}{f_{m,0,d}} = \frac{1.97}{40.00} = 0.05 \leq 1.0 \tag{II.27}$$

The shear forces and bending moments will not lead to failure of the truss.

Buckling

The last check for internal forces is the buckling check of the diagonals.

$$\lambda = L \times \sqrt{\frac{A}{I}} = 40.8 \tag{II.28}$$

$L = 1178.5mm$
$A = 10000mm^2$
$I = 8.3 \times 10^6 mm^4$

Equation II.29 is conform NEN-EN 1995-1-1 expression 6.21:

$$\lambda_{rel} = \frac{\lambda}{\pi} \times \sqrt{\frac{f_{c,0,k}}{E_{0,05}}} = 0.86 \tag{II.29}$$

$f_{c,o,k} = 53.3 N/mm^2$
$E_{0.05} = 12200 N/mm^2$

Equation II.30 is conform NEN-EN 1995-1-1 expression 6.27:

$$k = 0.5 \times (1 + \beta_c \times (\lambda_{rel} - 0.3) + \lambda_{rel}^2) = 0.90 \tag{II.30}$$

$\beta_c = 0.1$

Equation II.31 is conform NEN-EN 1995-1-1 expression 6.25:

$$k_c = \frac{1}{k + \sqrt{k^2 - \lambda_{rel}^2}} = 0.86 \tag{II.31}$$

Equations II.32 and II.33 are confrom NEN-EN 1995-1-1 expressions 6.23 abd 6.24:

$$\frac{\sigma_{c,0,d}}{k_c \times f_{c,0,d}} + \frac{\sigma_{m,y,d}}{f_{m,y,d}} + k_m \times \frac{\sigma_{m,z,d}}{f_{m,z,d}} \leq 1 \tag{II.32}$$

$$\frac{\sigma_{c,0,d}}{k_c \times f_{c,0,d}} + k_m \times \frac{\sigma_{m,y,d}}{f_{m,y,d}} + \frac{\sigma_{m,z,d}}{f_{m,z,d}} \leq 1 \tag{II.33}$$

$\sigma_{m,y,d}$ and $\sigma_{m,z,d} = 0 N/mm^2$ so:

$$\frac{\sigma_{c,0,d}}{k_c \times f_{c,0,d}} \leq 1 \tag{II.34}$$

$\sigma_{c,0,d} = 3.59 N/mm^2$
$f_{c,0,d} = 35.53 N/mm^2$

$$\frac{\sigma_{c,0,d}}{k_c \times f_{c,0,d}} = 0.12 \leq 1 \tag{II.35}$$

Buckling will not cause failure of the structure.

Detail

In this section the connection of the diagonal members to the bottom and top member will be checked. First the connection will be checked for the maximal compression, then it will be checked for tension. The connection is cut in an angle of 35.5° at the bottom of the diagonal, and 45° in the top of the diagonal. The 35.5° will calculated elaborate and then the unity check is performed on both connections.

35.5° joint

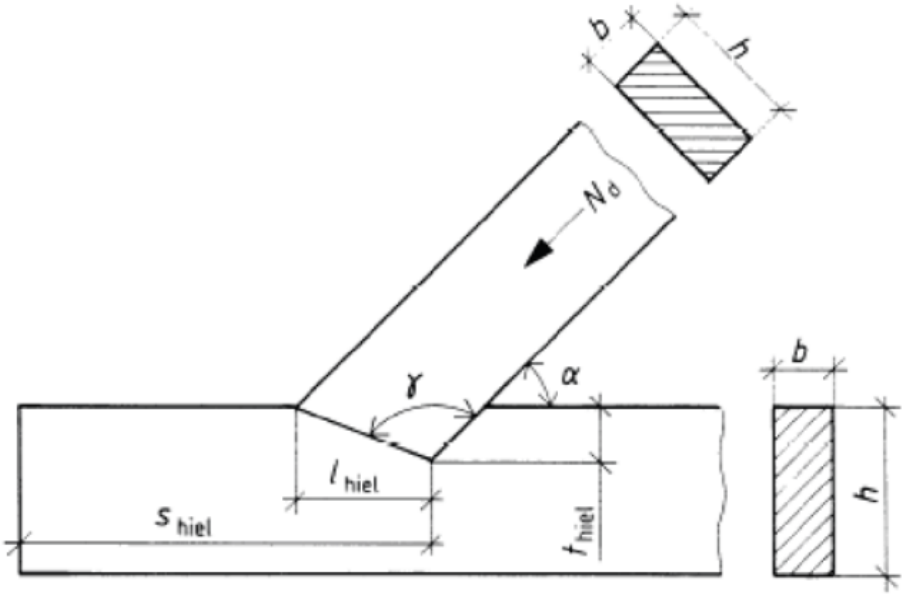

Figure II.6: Tooth joint conform NEN-EN 1995-1-1 figure NB.4

In figure II.6 the *hiel* is replaced by *amb* in the formulas below.
$N_{c,d} = \sigma_{c,0,d} \times A = 35900N$
$b = 100mm$
$s_{amb} = 152mm$
$t_{amb} = \sin(180 - 90 - 35.5) \times 100 = 81.4mm$
$l_{amb} = \cos(180 - 90 - 35.5) \times 100 = 58.1mm$
$\alpha = 35.5°$

Equations II.36 until II.38 are conform NEN-EN 1995-1-1 expressions NB.8.4, NB.8.5 and NB.8.6.

$$\sigma_{c,0,d} \leq f_{c,0,d}$$
$$\sigma_{c,0,d} = \frac{N_{c,d} \times \cos\alpha}{t_{amb} \times b} = 3.59N/mm^2 \tag{II.36}$$

$$\sigma_{c,90,d} \leq f_{c,90,d}$$
$$\sigma_{c,90,d} = \frac{N_{c,d} \times \sin\alpha}{l_{amb} \times b} = 3.59N/mm^2 \tag{II.37}$$

$$\tau_{v,d} \leq f_{v,d}$$
$$\tau_{v,d} = \frac{N_{c,d} \times \cos\alpha}{s_{amb} \times b} = 1.93N/mm^2 \tag{II.38}$$

$$f_{c,0,d} = k_{mod} \times \frac{f_{c,0,k}}{\gamma_m} = 35.53 N/mm^2 \tag{II.39}$$

$$f_{c,90,d} = k_{mod} \times \frac{f_{c,90,k}}{\gamma_m} = 12.67 N/mm^2 \tag{II.40}$$

$$f_{v,d} = k_{mod} \times \frac{f_{v,k}}{\gamma_m} = 5.20 N/mm^2 \tag{II.41}$$

35.5° joint:

$$\eta = \frac{\sigma_{c,0,d}}{f_{c,0,d}} = \frac{3.59}{35.53} = 0.10 \leq 1.0 \tag{II.42}$$

$$\eta = \frac{\sigma_{c,90,d}}{f_{c,90,d}} = \frac{3.59}{12.67} = 0.28 \leq 1.0 \tag{II.43}$$

$$\eta = \frac{\sigma_{v,d}}{f_{v,d}} = \frac{1.93}{5.20} = 0.37 \leq 1.0 \tag{II.44}$$

45° joint:

$$\eta = \frac{\sigma_{c,0,d}}{f_{c,0,d}} = \frac{3.59}{35.53} = 0.10 \leq 1.0 \tag{II.45}$$

$$\eta = \frac{\sigma_{c,90,d}}{f_{c,90,d}} = \frac{3.59}{12.67} = 0.28 \leq 1.0 \tag{II.46}$$

$$\eta = \frac{\sigma_{v,d}}{f_{v,d}} = \frac{1.68}{5.20} = 0.32 \leq 1.0 \tag{II.47}$$

For compression both connections meets all requirements.

For tension in a tooth joint no ULS-checks are provided by the Eurocode. The most probable failure mechanisms will therefore be analyzed in both the diagonals and edge beams details. First the diagonals are checked.
In the diagonal the two most probable failure modes are tension in the reduced section ($\sigma_{t,0,d}$) and shear of the 'teeth' ($\tau_{v,d}$). In figure II.7 these failure modes are shown in the left part. Due to the fact that the detail is 'sandwiched' in the beam, no other deformations can occur. So there will be pure shear in the detail. Note that the representation is 2D but the calculation is three-dimensional. Equations II.48 until II.55 check whether the diagonal resists the stresses.

$$\begin{aligned} &\sigma_{t,0,d} \leq f_{t,0,d} \\ &\sigma_{t,0,d} = \frac{F}{A} = 15.92 N/mm^2 \end{aligned} \tag{II.48}$$

$F = \sigma_{t,0,d} \times A = 20700N$
$A = 13 \times 100 = 1300 mm^2$

$$f_{t,0,d} = k_{mod} \times \frac{f_{t,0,k}}{\gamma_m} = 34.00 N/mm^2 \tag{II.49}$$

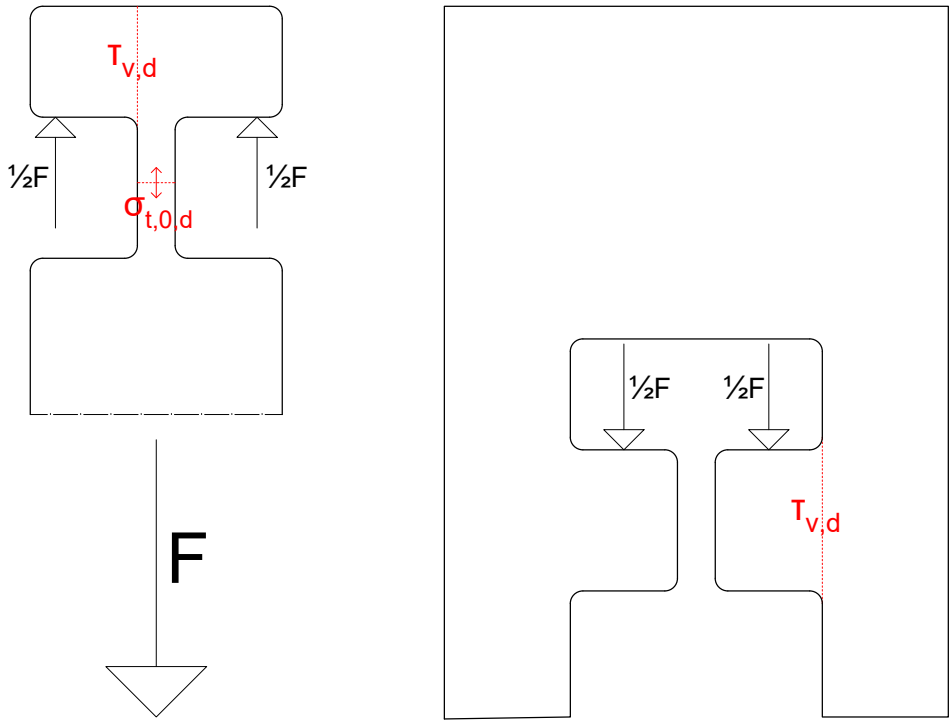

Figure II.7: 2D representation of detail with probable failure modes

$$\begin{aligned} \tau_{v,d} &\leq f_{v,d} \\ \tau_{v,d} &= \frac{V}{A} = 2.41 N/mm^2 \end{aligned} \tag{II.50}$$

$V = F/2 = 10350N$
$A = 43 \times 100 = 4300mm^2$

$$f_{v,d} = k_{mod} \times \frac{f_{v,k}}{\gamma_m} = 5.20 \quad N/mm^2 \tag{II.51}$$

35.5° joint:

$$\eta = \frac{\sigma_{t,0,d}}{f_{t,0,d}} = \frac{15.92}{34.00} = 0.47 \leq 1.0 \tag{II.52}$$

$$\eta = \frac{\sigma_{t,0,d}}{f_{t,0,d}} = \frac{2.41}{5.20} = 0.46 \leq 1.0 \tag{II.53}$$

45° joint:

$$\eta = \frac{\sigma_{t,0,d}}{f_{t,0,d}} = \frac{13.80}{34.00} = 0.41 \leq 1.0 \tag{II.54}$$

$$\eta = \frac{\tau_{v,d}}{f_{v,d}} = \frac{2.35}{5.20} = 0.45 \leq 1.0 \tag{II.55}$$

Tension in both details of the diagonal will not lead to failure of the structure.

For the calculation of the beam it is important to notice that the section shown in figure II.7 on the right is cut in an angle of 35.5 degrees at the bottom. This means that the forces do not act in the direction of the beam, but slanted compared towards the grain direction. To calculate whether the beam meets the requirements, the forces are resolved in both x (parallel to the grain) and y (perpendicular to the grain) direction. Looking at the figure, it might be expected that tension in the narrowest parts of the beam might also lead to great stresses. However, the beam is only this narrow where the section is made. Right next to the connection the full beam's area is able to resist stresses. Therefore this will not be one of the possible failure modes. For the shear force both the x and the y direction are considered. In case of a force in the y direction this causes a rolling shear. Equations II.56 until II.61 check whether the beam resists the stresses.

$$\begin{aligned} \tau_{v,d} &\leq f_{v,d} \\ \tau_{vR,d} &\leq f_{vR,d} \\ \tau_{v,d} &= \frac{V_x}{A} = 1.20 N/mm^2 \\ \tau_{vR,d} &= \frac{V_y}{A} = 0.86 N/mm^2 \end{aligned} \tag{II.56}$$

$V_x = \cos 35.5 \times \frac{1}{2}F = 8426N$
$V_y = \sin 35.5 \times \frac{1}{2}F = 6010N$
$A = 7020mm^2$

$$\begin{aligned} f_{v,d} &= k_{mod} \times \frac{f_{v,k}}{\gamma_m} = 2.53 N/mm^2 \\ f_{vR,d} &= k_{mod} \times \frac{f_{vR,k}}{\gamma_m} = 2.53 N/mm^2 \end{aligned} \tag{II.57}$$

35.5° joint:

$$\eta = \frac{\tau_{v,d}}{f_{v,d}} = \frac{1.20}{2.53} = 0.47 \leq 1.0 \tag{II.58}$$

$$\eta = \frac{\tau_{vR,d}}{f_{vR,d}} = \frac{0.86}{2.53} = 0.34 \leq 1.0 \tag{II.59}$$

45° joint:

$$\eta = \frac{\tau_{v,d}}{f_{v,d}} = \frac{1.14}{2.53} = 0.45 \leq 1.0 \tag{II.60}$$

$$\eta = \frac{\tau_{vR,d}}{f_{vR,d}} = \frac{1.14}{2.53} = 0.45 \leq 1.0 \tag{II.61}$$

Tension in both details of the beam will not lead to failure of the structure.

II.7.2 Serviceability Limit State

Load combination SLS	Deflection middle of roof		
	U_x	U_z	U_{total}
B.14	1.4 mm	1.4 mm	1.9 mm
B.15	2.7 mm	2.7 mm	3.8 mm
B.16	2.5 mm	2.6 mm	3.6 mm
B.17	3.4 mm	2.0 mm	3.9 mm

Table II.3: Deflections due to load combinations

In table II.3 the calculated deflections found in the middle of the roof are shown. Note that the X-direction is horizontal and the Z-direction is vertical. The span of the roof is 10 meters, so the found deflections are acceptable.

The joint itself will deflect as well, so the total deflections will increase. In the previous calculated roof the increase due to this effect was less than 10 percent. The current diagonal has two different joints. However, the 35.5° joint is stronger than the 45° joint. So the effect will be even smaller than the previous calculated roof. Therefore it is assumed that the deflections in the roof will be tolerable.

Appendix A

Abaqus

A.1 User defined materials

The values for the material below are obtained from Green et al., 1999.

Name:	Western white	
Model:	Elastic orthotropic	
E_1 Young's modulus:	11110	N/mm^2
E_2 Young's modulus:	422.18	N/mm^2
E_3 Young's modulus:	866.58	N/mm^2
ν_{12} Poisson's ratio:	0.329	
ν_{13} Poisson's ratio:	0.344	
ν_{23} Poisson's ratio:	0.410	
G_{12} Shear modulus:	577.72	N/mm^2
G_{13} Shear modulus:	533.28	N/mm^2
G_{23} Shear modulus:	55.55	N/mm^2
Density:	432.5	kg/m^3
Friction coefficient:	0.3	
Size beam:	$100 \times 100mm$	
Size diagonal:	$50 \times 50mm$	

A.2 Input Abaqus designed connections

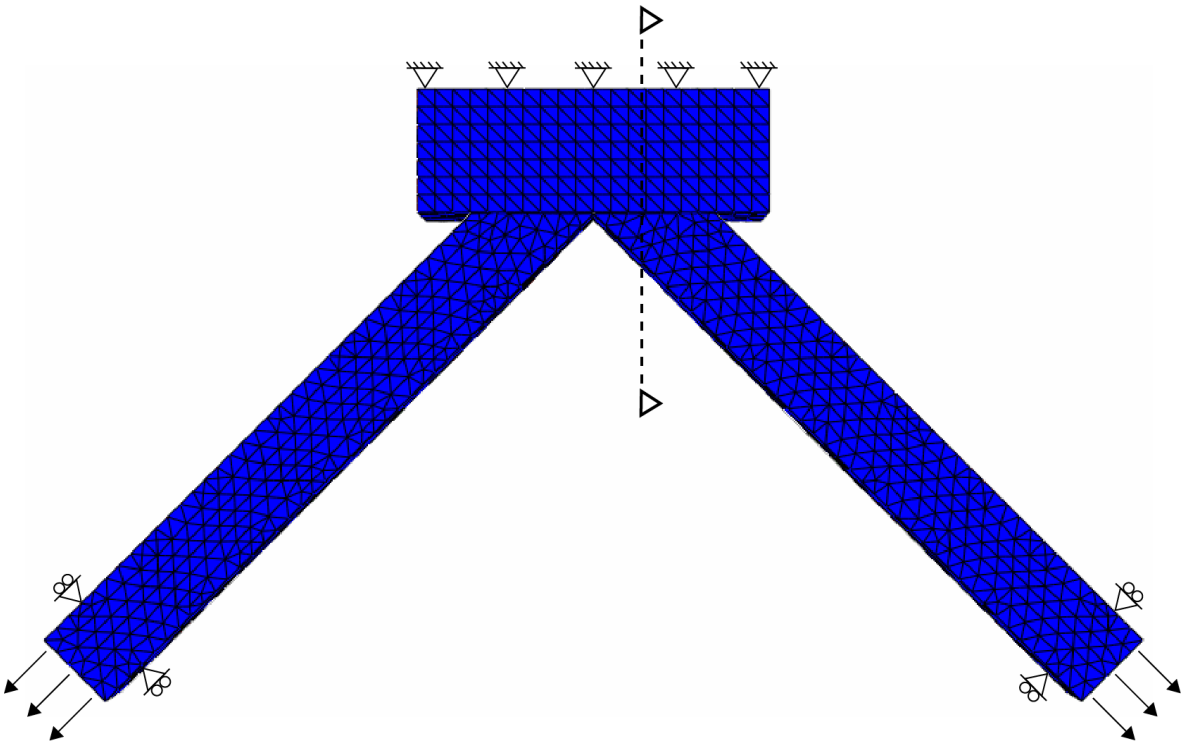

Figure A.1: Input Abaqus dovetail connection

Boundary conditions:	All translations of top surface are 0. The diagonals can only move in the direction of the applied force.
Loads:	Loads are applied as a pressure of $2N/mm^2$ which is equal to $5kN$ per diagonal in this case.
Section:	The sections on the next page are as shown in figure A.1.

A.3 Results Abaqus dovetail connection

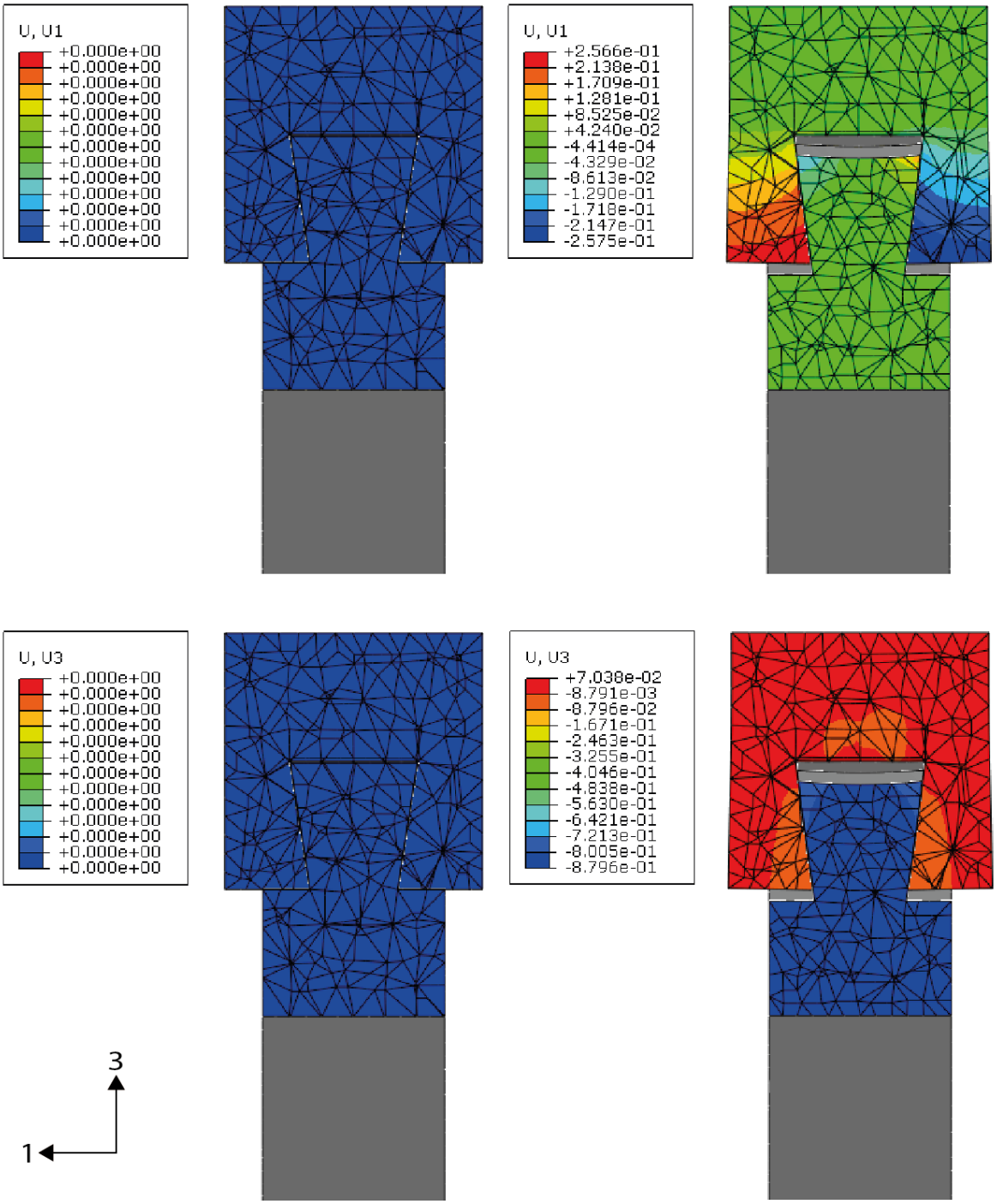

Figure A.2: Displacements Abaqus dovetail connection

The visualisations of the deformations have a scale factor of 4.

A.4 Results Abaqus gooseneck connection

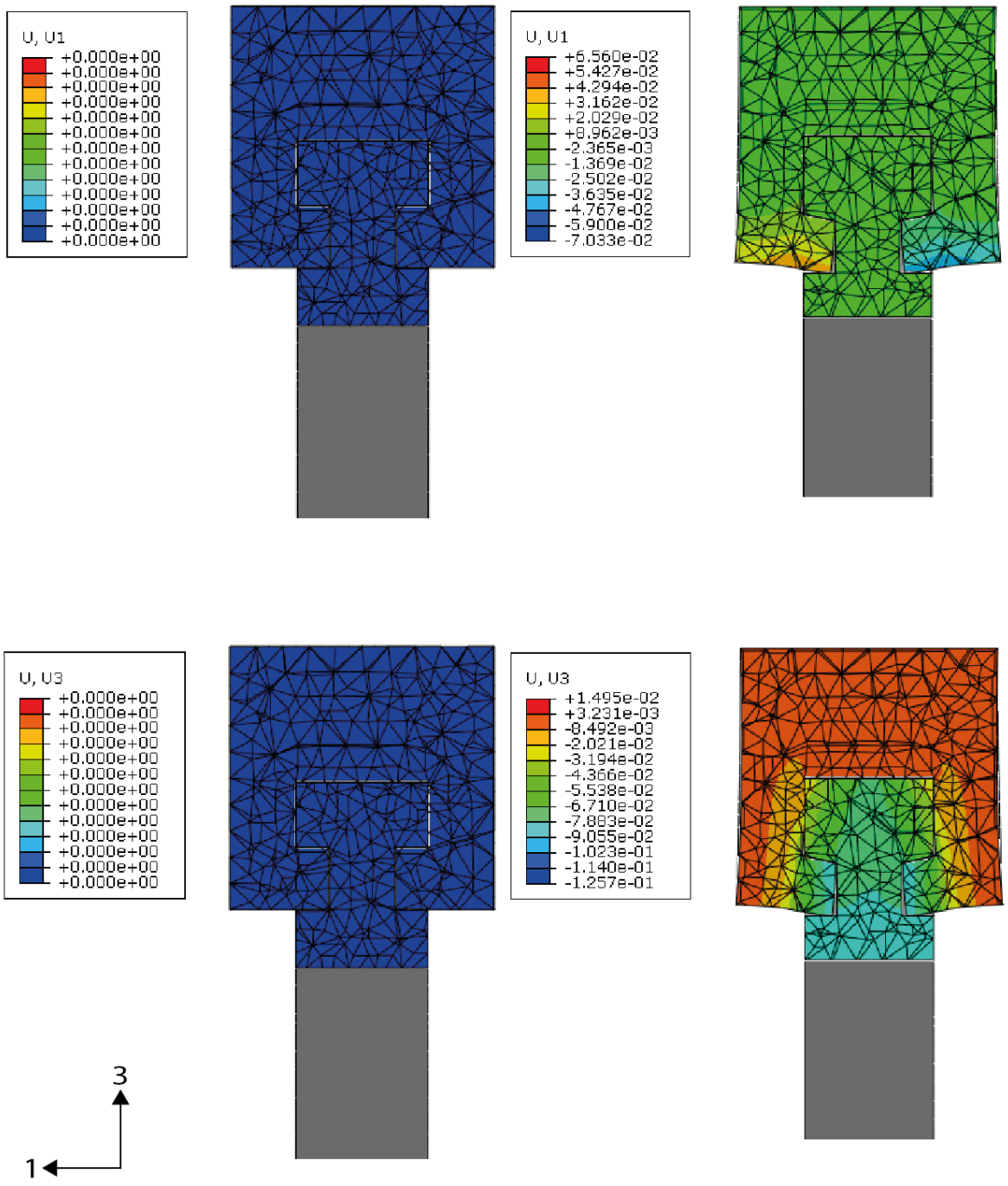

Figure A.3: Displacements Abaqus gooseneck connection

The visualisations of the deformations have a scale factor of 50.

A.5 Critical stresses Abaqus

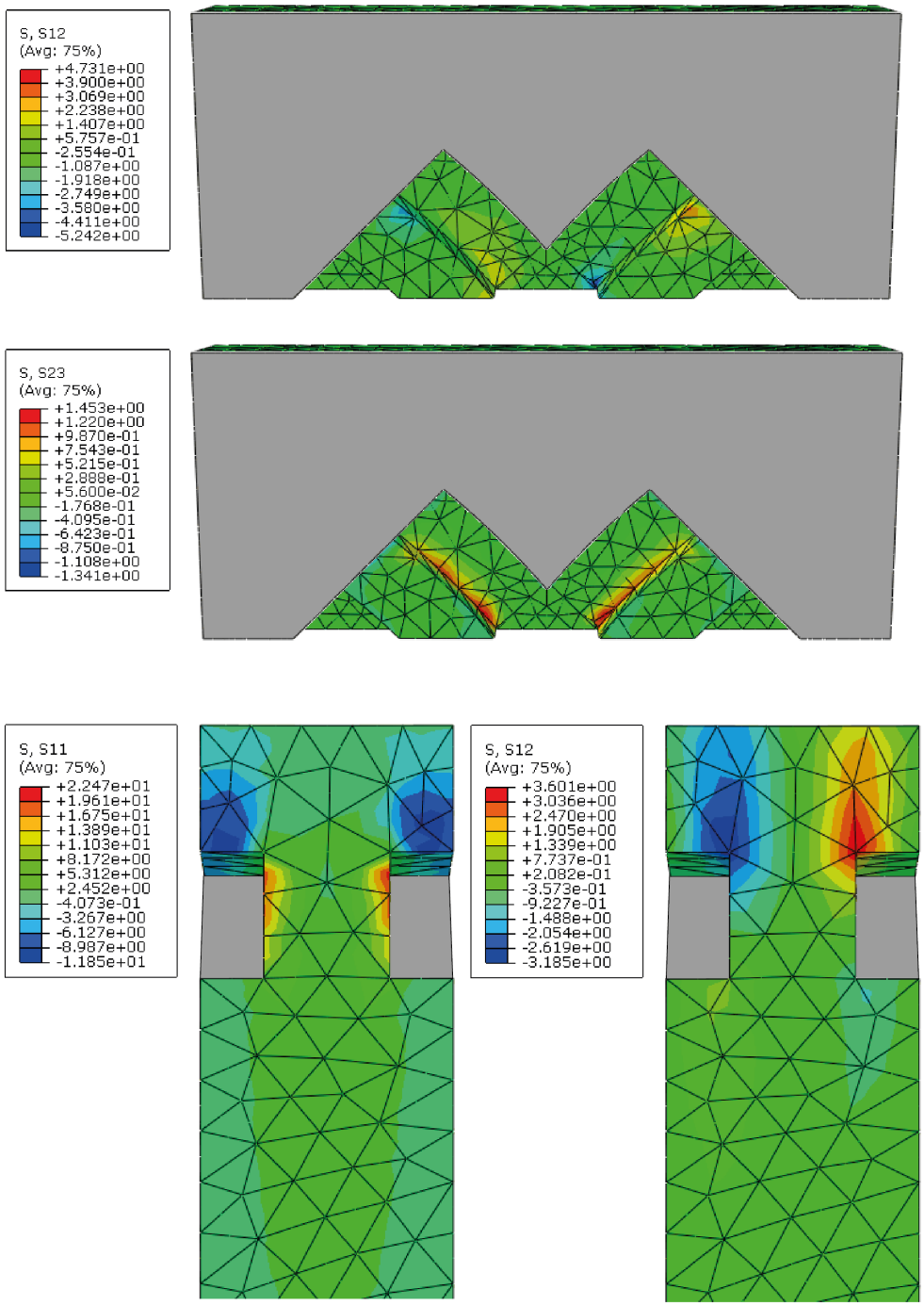

Figure A.4: Critical stresses in the beam and the diagonal

The visualisations of the deformations have a scale factor of 1.

Appendix B

Structural design

B.1 Bolt connection laboratory test

Bearing strength
Equations B.1 until B.3 are all conform NEN-EN 1995-1-1 equations 8.31 to 8.33.

$$k_{90} = 1.30 + 0.015 \times d = 1.66 \qquad for \quad LVL \tag{B.1}$$

$d = 24mm$

$$f_{h,o,k} = 0.082 \times (1 - 0.01 \times d) \times \rho_k = 29.9N/mm^2 \tag{B.2}$$

$\rho_k = 480kg/m^3$

$$f_{h,\alpha,k} = \frac{f_{h,o,k}}{k_{90} \times sin^2\alpha + cos^2\alpha} = 22.5N/mm^2 \tag{B.3}$$

$\alpha = 45^o$

Diagonal: $f_{h,o,k} = 29.9Nmm^2$
Beam: $f_{h,45,k} = 22.5Nmm^2$

Characteristic strength bolt connection
Equations B.4 is conform NEN-EN 1995-1-1 equation 8.13.

$$F_{v,Rk} = 0.5 \times f_{h,\alpha,k} \times t_2 \times d \tag{B.4}$$

$t_{2,diagonal} = 68mm$
$t_{2,beam} = 136mm$
$d = 24mm$

Diagonal: $F_{v,Rk} = 24.4kN$
Beam: $F_{v,Rk} = 36.7kN$

B.2 Structural optimization

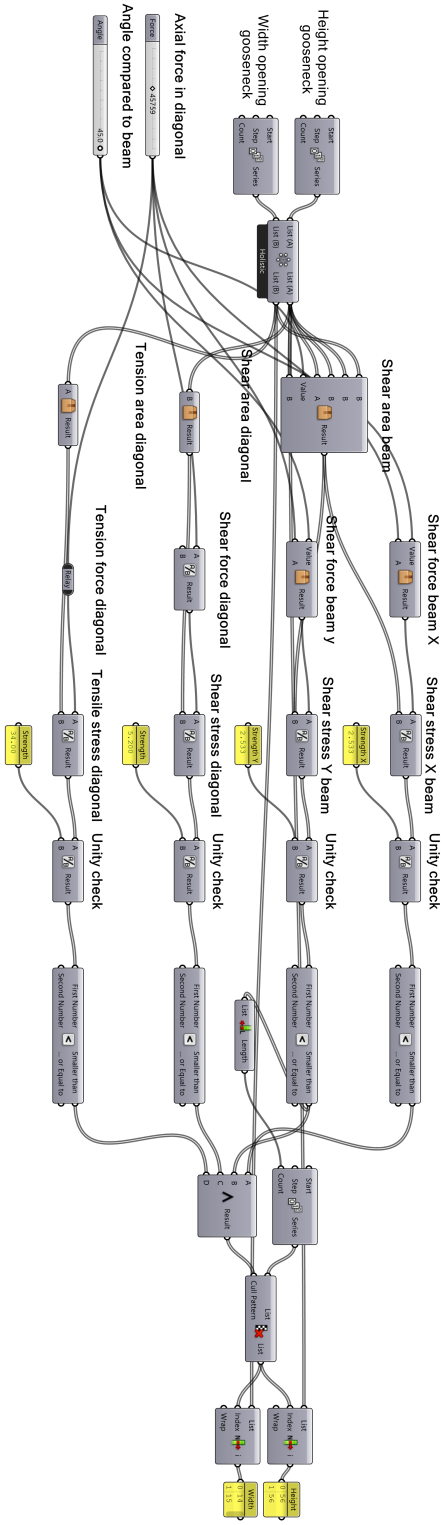

Figure B.1: Optimization in Grasshopper

Appendix C

Robot tests

C.1 Test specimens

C.1.1 Specimen 1

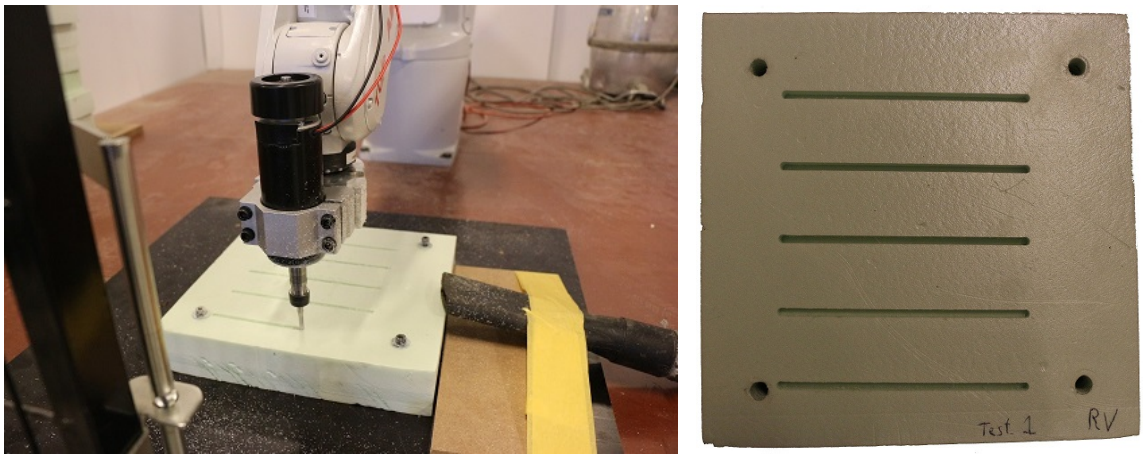

Figure C.1: Milling specimen 1

Specimen 1	Line 1	Line 2	Line 3	Line 4	Line 5
Moving speed [mm/s]	100	100	100	100	100
Milling speed [mm/s]	10	10	10	10	10
Milling depth [mm]	2	4	6	8	10
Layers	6	3	2	1	1
Total milling depth [mm]	12	12	12	8	10

Table C.1: Variables specimen 1

C.1.2 Specimen 2

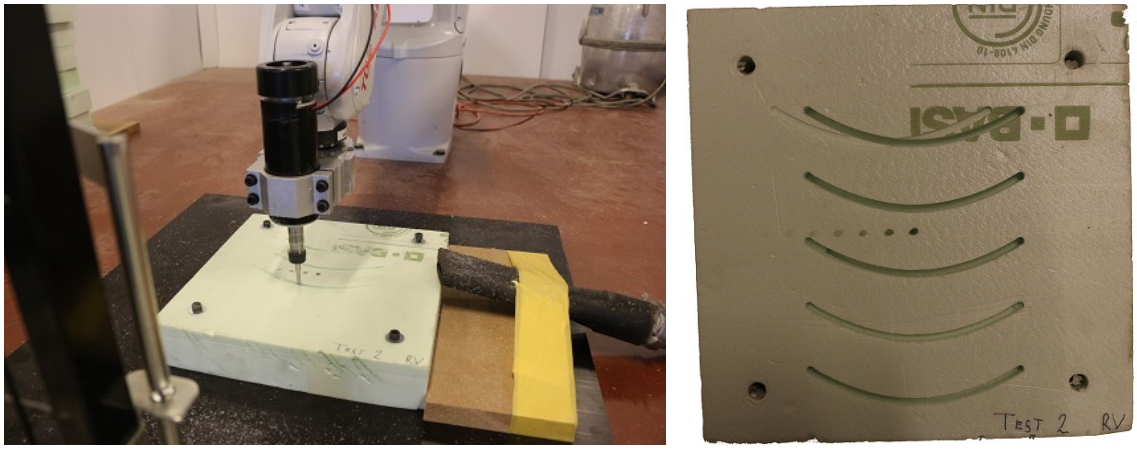

Figure C.2: Milling specimen 2

Specimen 1	Line 1	Line 2	Line 3	Line 4	Line 5
Moving speed [mm/s]	50	50	50	50	50
Milling speed [mm/s]	10	10	10	10	10
Milling depth [mm]	2	4	6	8	10
Layers	6	3	2	1	1
Total milling depth [mm]	12	12	12	8	10

Table C.2: Variables specimen 2

C.1.3 Specimen 3

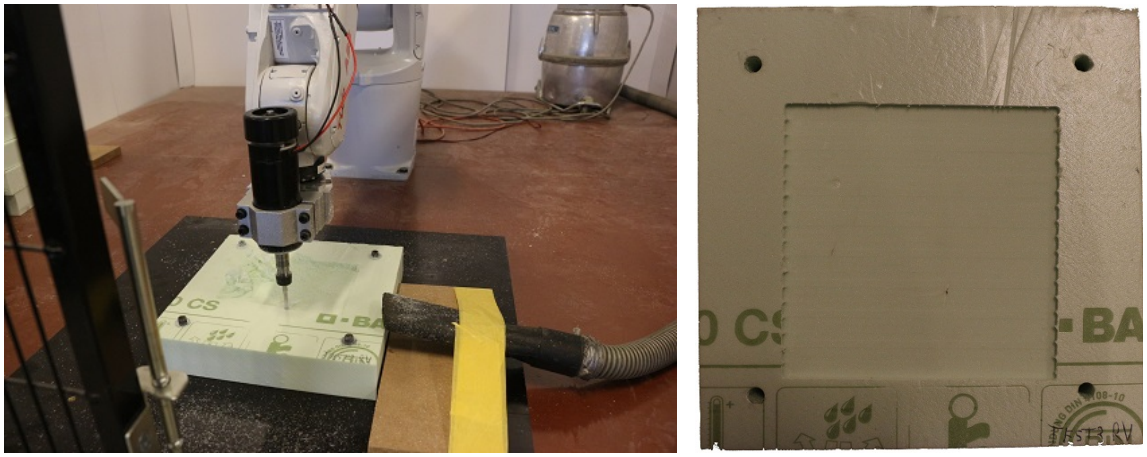

Figure C.3: Milling specimen 3

Specimen 3	
Moving speed [mm/s]	50
Milling speed [mm/s]	10
Milling depth [mm]	5
Distance between lines [mm]	4.5

Table C.3: Variables specimen 3

C.1.4 Specimen 4

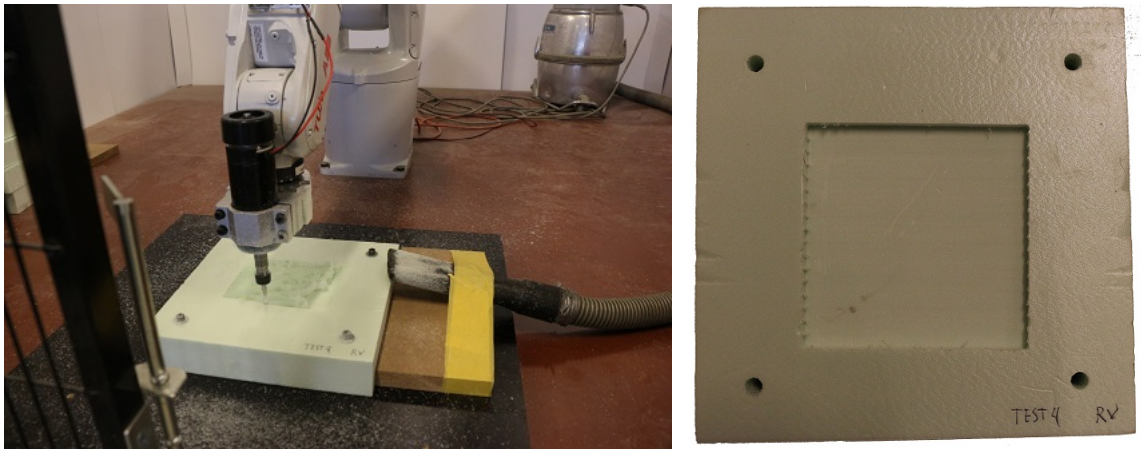

Figure C.4: Milling specimen 4

Specimen 4	
Moving speed [mm/s]	50
Milling speed [mm/s]	10
Milling depth [mm]	10
Distance between lines [mm]	4

Table C.4: Variables specimen 4

C.1.5 Specimen 5

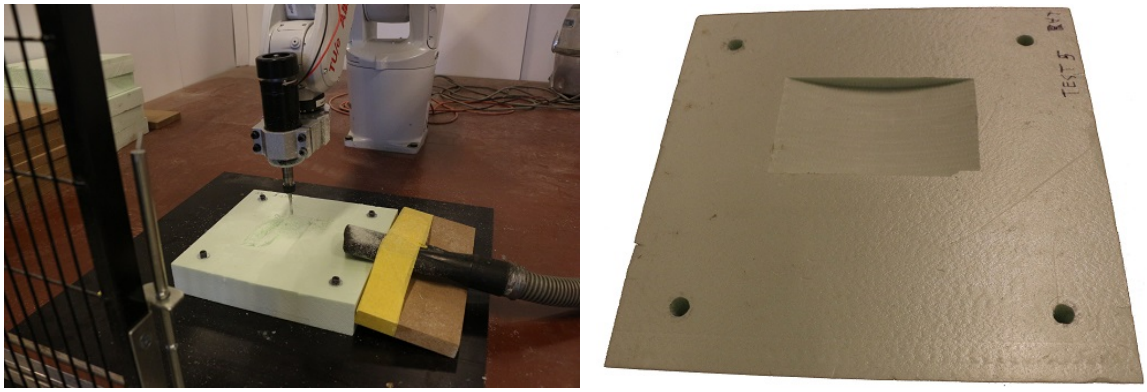

Figure C.5: Milling specimen 5

Specimen 5	
Moving speed [mm/s]	50
Milling speed [mm/s]	10
Maximal milling depth [mm]	10
Distance between lines [mm]	4.5

Table C.5: Variables specimen 5

C.1.6 Specimen 6

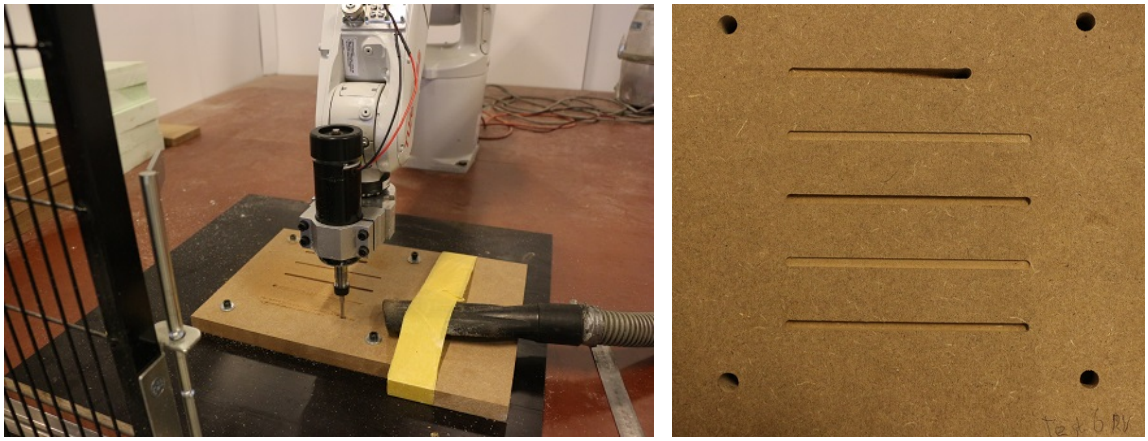

Figure C.6: Milling specimen 6

Specimen 1	Line 1	Line 2	Line 3	Line 4	Line 5
Moving speed [mm/s]	50	50	50	50	50
Milling speed [mm/s]	10	5	10	5	5
Milling depth [mm]	2	0.5	0.5	1	1
Layers	-	4	10	2	5
Total milling depth [mm]	-	2	5	2	5

Table C.6: Variables specimen 6

C.1.7 Specimen 7

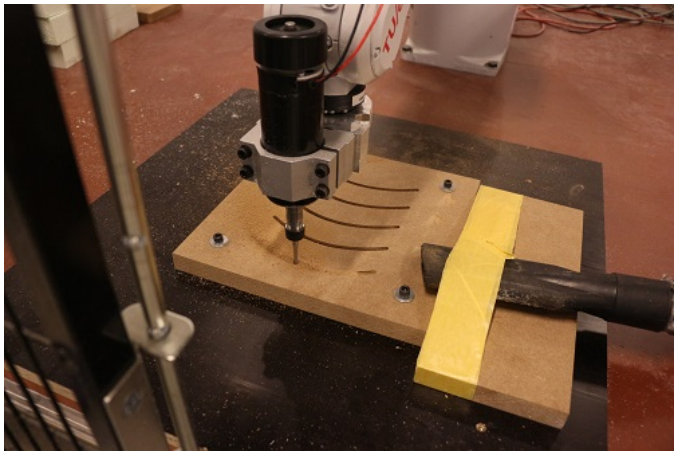

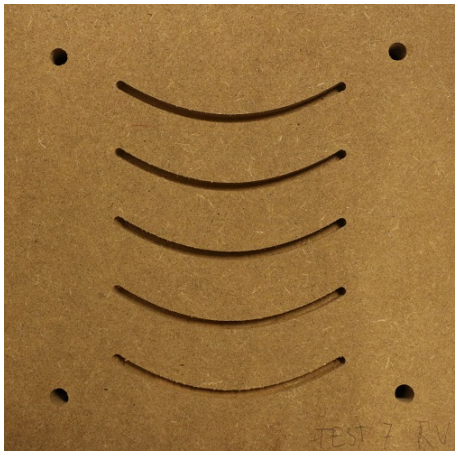

Figure C.7: Milling specimen 7

Specimen 1	Line 1	Line 2	Line 3	Line 4	Line 5
Moving speed [mm/s]	50	100	50	50	50
Milling speed [mm/s]	10	10	5	5	5
Milling depth [mm]	0.5	1	1.5	2	3
Layers	20	10	7	5	3
Total milling depth [mm]	10	10	10.5	10	9

Table C.7: Variables specimen 7

C.1.8 Specimen 8

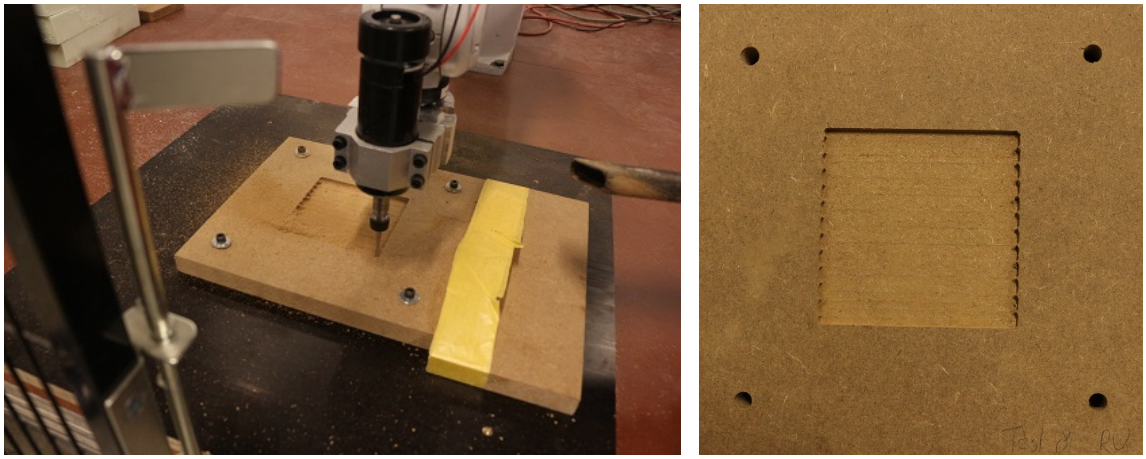

Figure C.8: Milling specimen 8

Specimen 8	
Moving speed [mm/s]	50
Milling speed [mm/s]	5-10
Milling depth [mm]	5
Distance between lines [mm]	4.5

Table C.8: Variables specimen 8

C.1.9 Specimen 9

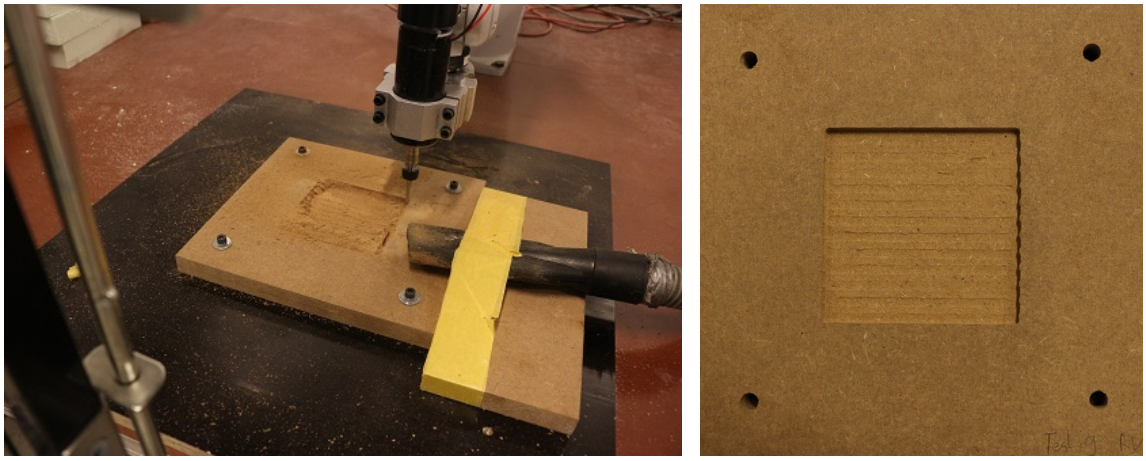

Figure C.9: Milling specimen 9

Specimen 9	
Moving speed [mm/s]	50
Milling speed [mm/s]	5-10
Milling depth [mm]	7.5
Distance between lines [mm]	4.5

Table C.9: Variables specimen 9

C.2 Milling designed connection

C.2.1 Beam

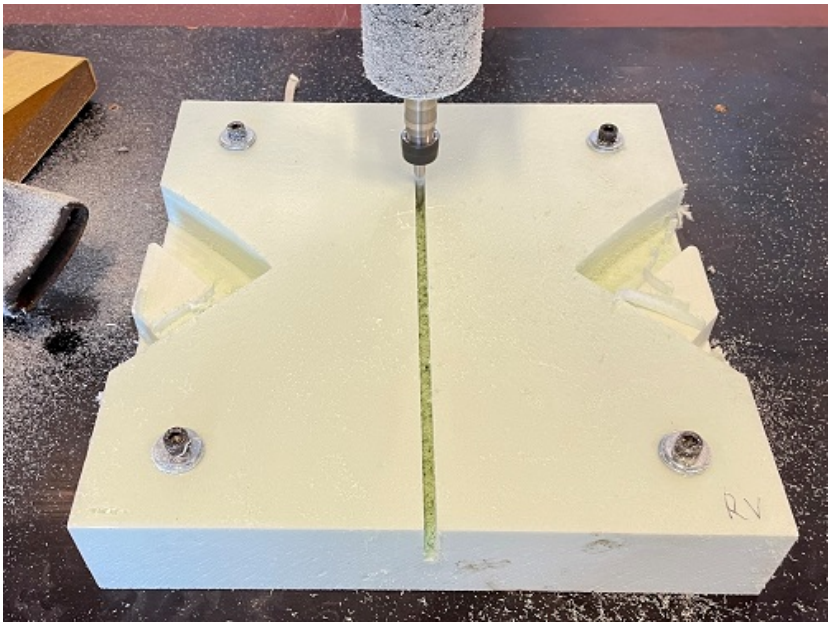

Figure C.10: Milling designed beam

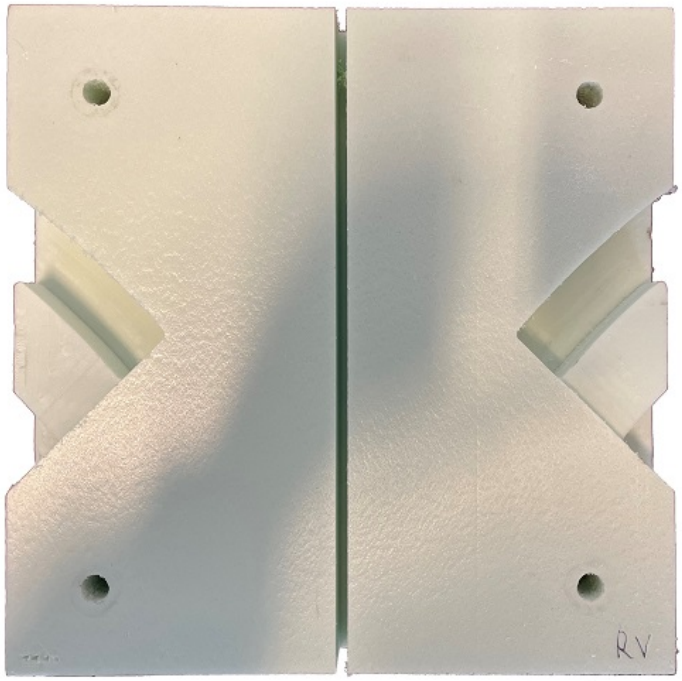

Figure C.11: Milled designed beam

C.2.2 Diagonal

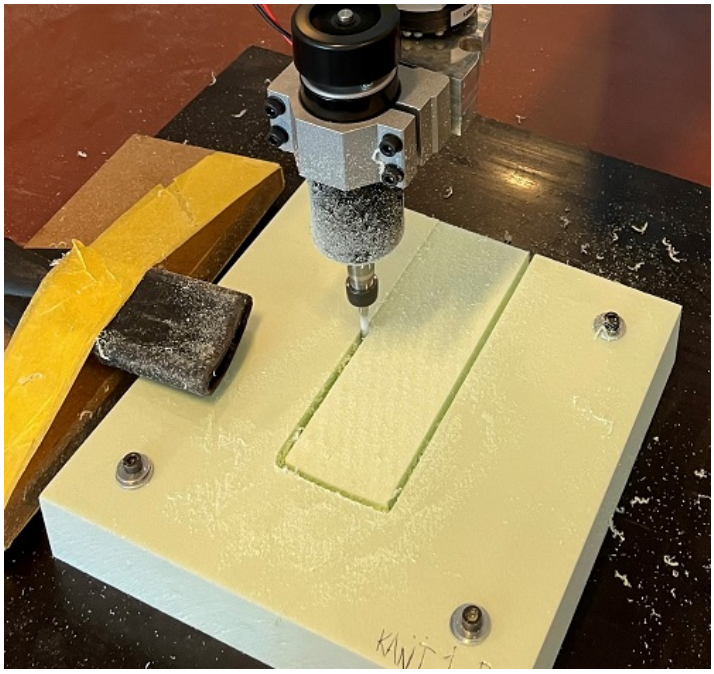

Figure C.12: Milling designed diagonal

Figure C.13: Milled designed diagonal

Appendix D

Structural report

D.1 Board BauBuche Q

Table 10: Characteristic values for Board BauBuche Q with nominal thickness 30 mm ≤ B ≤ 80 mm in N/mm²

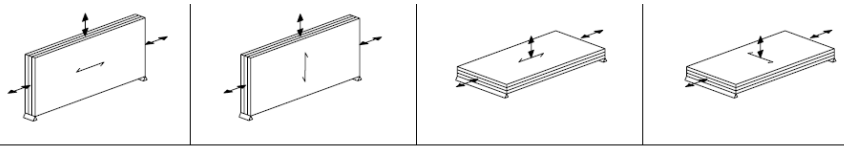

Characteristic strength values in N/mm²					
Bending	$f_{m,0,k}$	(51.9) - 60.0[a]		75.0	
	$f_{m,90,k}$		(8.6) - 10.0[a]		20.0
Tension	$f_{t,0,k}$	(44.0) - 51.0[b] - (56.1)		(44.0) - 51.0[b] - (56.1)	
	$f_{t,90,edge,k}$		8.0		8.0
Compression	$f_{c,0,k}$	53.3[d] - (63.9)		53.3[d] - (63.9)	
	$f_{c,90,edge,k}$		19.0[d] - (22.8)		19.0[d] - (22.8)
	$f_{c,90,flat,k}$				13.0[d] – (15.6)
Shear	$f_{v,k}$	7.8	7.8	3.8	
Rolling shear	$f_{vR,k}$				3.8
Stiffness values in N/mm²					
Modulus of elasticity	$E_{0,mean}$	13,200		13,200	
	$E_{0,05}$	12,200		12,200	
	$E_{90,mean}$		2,200		2,200
	$E_{90,05}$		2,000		2,000
Shear modulus	G_{mean}	820	820	430	430
	G_{05}	540	540	360	360
Density values in kg/m³					
	ρ_k	730			
	ρ_{mean}	800			

Figure D.1: Characteristic values for Board BauBuche Q

For the material safety coefficient of BauBuche, the value to be used for ongoing and temporary design situation $\gamma_M = 1.20$. The modification factor and the deformation factor with a medium load duration in at least climate class two will be $k_{mod} = 0.80$ and $k_{def} = 0.80$ (Blaß and Streib, 2017).

$f_{t,0,k}$ is to be multiplied by $k_l = min[(3,000/l)^{s/2}; 1.1]$ where s = 0.12 so $k_l = 1.06$

D.2 Input SCIA truss flat roof

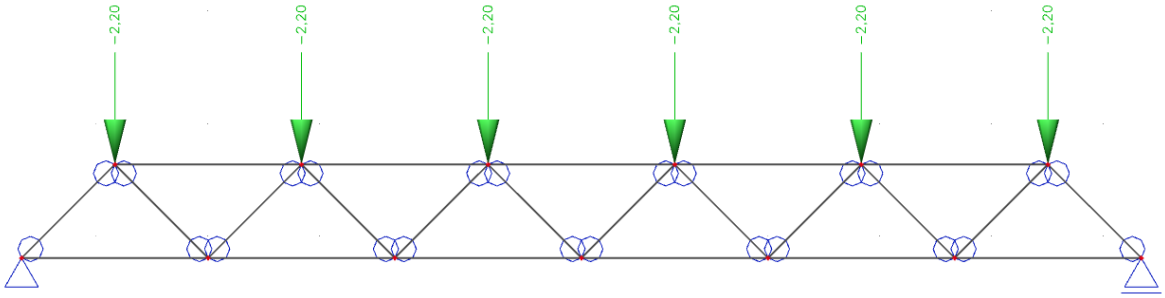

Figure D.2: Input SCIA permanent loads (G)

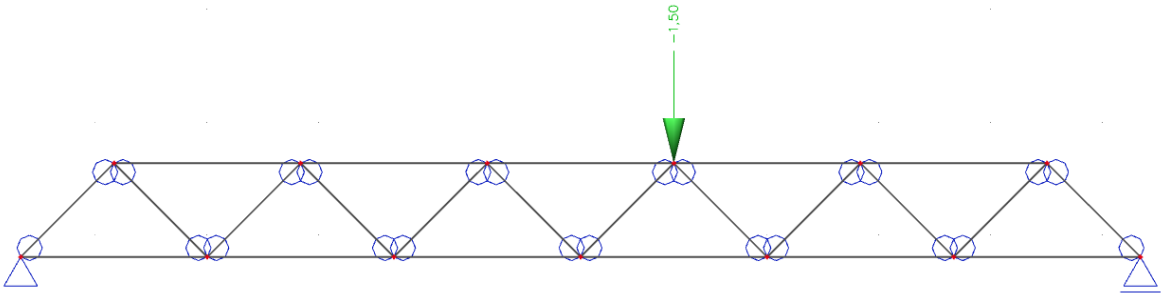

Figure D.3: Input SCIA imposed load (q_r)

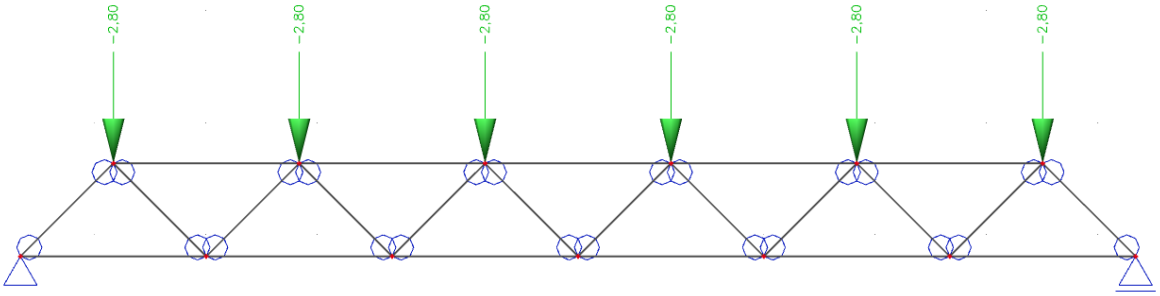

Figure D.4: Input SCIA snow load (q_s)

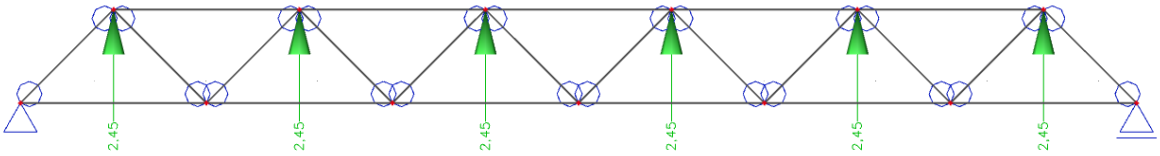

Figure D.5: Input SCIA wind load ($q_w(i)$)

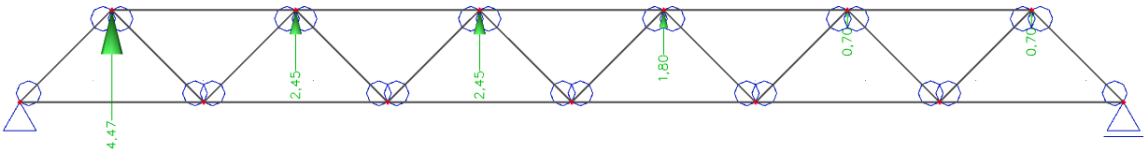

Figure D.6: Input SCIA wind load ($q_w(ii)$)

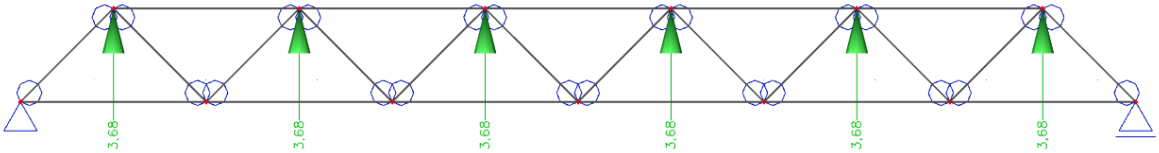

Figure D.7: Input SCIA internal pressure ($q_w(i)$)

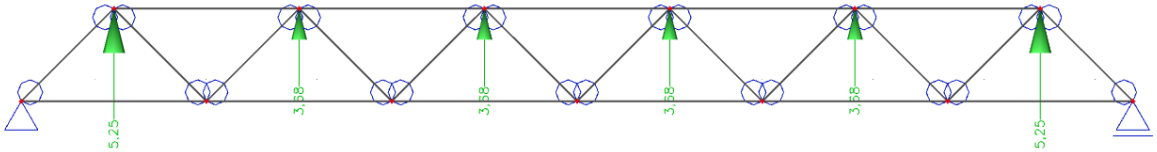

Figure D.8: Input SCIA internal pressure ($q_w(ii)$)

D.3 Results SCIA truss flat roof

Load combination	Extreme stresses diagonals				Extreme stresses beams			
ULS	Member	Normal stress	Member	Normal stress	Normal stress		Shear stress		Bending stress
A.9	BC	0.71 N/mm^2	AB	-1.10 N/mm^2	0.77 N/mm^2	-0.76 N/mm^2	0.03 N/mm^2	-0.03 N/mm^2	0.19 N/mm^2
A.10	BC	0.82 N/mm^2	AB	-1.18 N/mm^2	0.90 N/mm^2	-0.90 N/mm^2	0.03 N/mm^2	-0.04 N/mm^2	0.25 N/mm^2
A.11	BC	1.67 N/mm^2	AB	-2.59 N/mm^2	1.80 N/mm^2	-1.79 N/mm^2	0.08 N/mm^2	-0.08 N/mm^2	0.44 N/mm^2
A.12	AB	3.46 N/mm^2	BC	-2.23 N/mm^2	2.38 N/mm^2	-2.41 N/mm^2	0.11 N/mm^2	-0.11 N/mm^2	0.14 N/mm^2
A.13	AB	3.94 N/mm^2	BC	-2.03 N/mm^2	2.29 N/mm^2	-2.33 N/mm^2	0.11 N/mm^2	-0.10 N/mm^2	0.14 N/mm^2

Figure D.9: Extreme stresses retrieved from SCIA

D.4 Calculations SLS

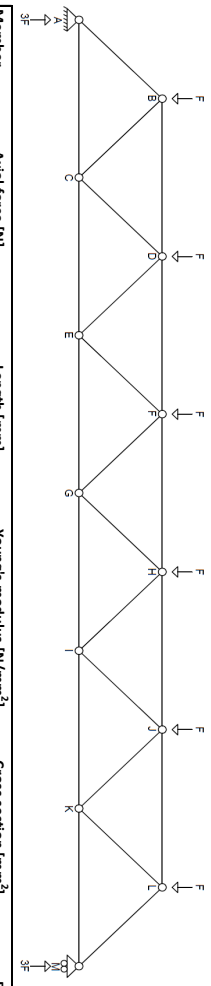

Member	Axial force [N]	Length [mm]	Young's modulus [N/mm²]	Cross section [mm²]	Elongation [mm]	New length [mm]	Stress [N/mm²]
AB	-21213.2	1178.5	13200.0	10000.0	-0.19	1178.3	-2.12
AC	15000.0	1666.7	13200.0	40000.0	0.05	1666.7	0.38
BC	14142.1	1178.5	13200.0	10000.0	0.13	1178.6	1.41
BD	-25000.0	1666.7	13200.0	40000.0	-0.08	1666.6	-0.63
CD	-14142.1	1178.5	13200.0	10000.0	-0.13	1178.4	-1.41
CE	35000.0	1666.7	13200.0	40000.0	0.11	1666.8	0.88
DE	7071.1	1178.5	13200.0	10000.0	0.06	1178.6	0.71
DF	-40000.0	1666.7	13200.0	40000.0	-0.13	1666.5	-1.00
EF	-7071.1	1178.5	13200.0	10000.0	-0.06	1178.4	-0.71
EG	45000.0	1666.7	13200.0	40000.0	0.14	1666.8	1.13
FG	0.0	1178.5	13200.0	10000.0	0.00	1178.5	0.00
FH	-45000.0	1666.7	13200.0	40000.0	-0.14	1666.5	-1.13
GH	0.0	1178.5	13200.0	10000.0	0.00	1178.5	0.00
GI	45000.0	1666.7	13200.0	40000.0	0.14	1666.8	1.13
HI	-7071.1	1178.5	13200.0	10000.0	-0.06	1178.4	-0.71
HJ	-40000.0	1666.7	13200.0	40000.0	-0.13	1666.5	-1.00
IJ	7071.1	1178.5	13200.0	10000.0	0.06	1178.6	0.71
IK	35000.0	1666.7	13200.0	40000.0	0.11	1666.8	0.88
JK	-14142.1	1178.5	13200.0	10000.0	-0.13	1178.4	-1.41
JL	-25000.0	1666.7	13200.0	40000.0	-0.08	1666.6	-0.63
KL	14142.1	1178.5	13200.0	10000.0	0.13	1178.6	1.41
KM	15000.0	1666.7	13200.0	40000.0	0.05	1666.7	0.38
LM	-21213.2	1178.5	13200.0	10000.0	-0.19	1178.3	-2.12

Figure D.10: Calculations used for SLS

D.5 Input SCIA arched truss

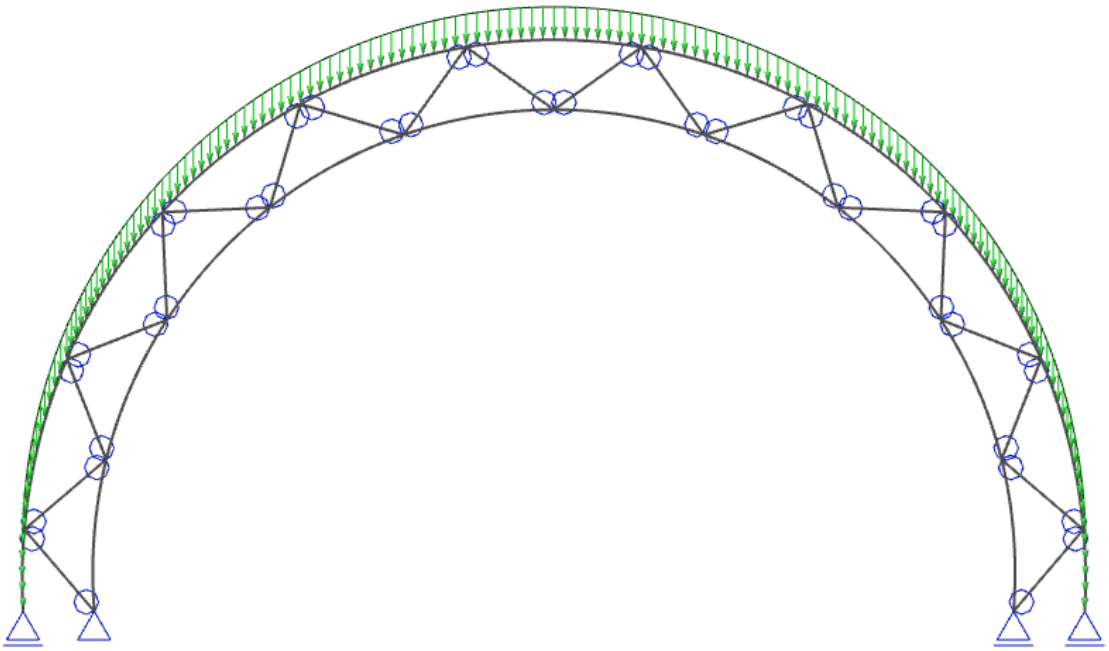

Figure D.11: Input SCIA permanent loads (G)

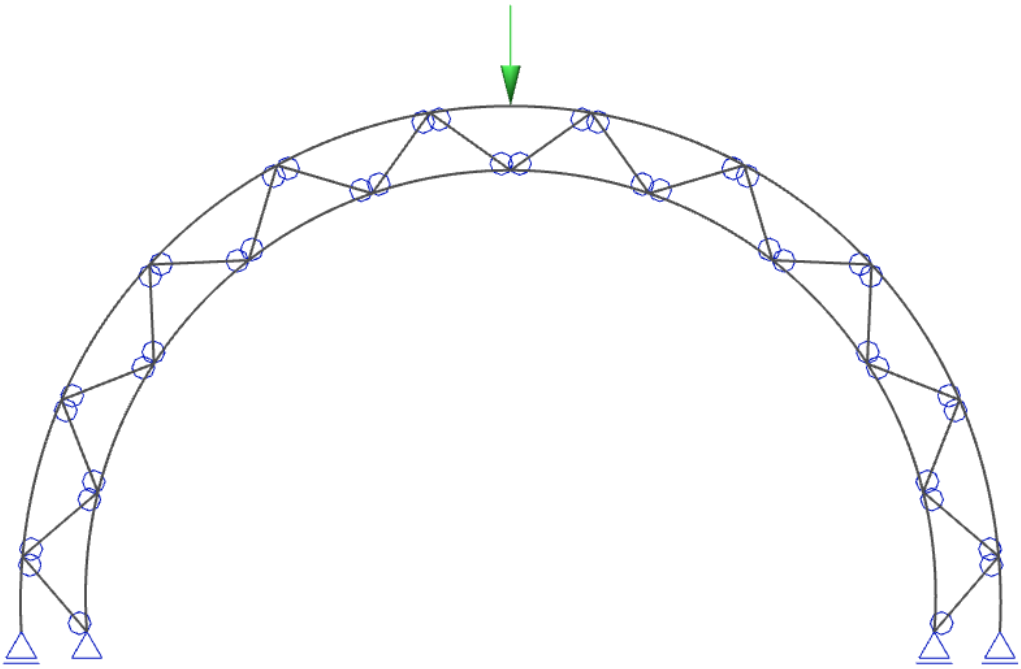

Figure D.12: Input SCIA imposed load (q_r)

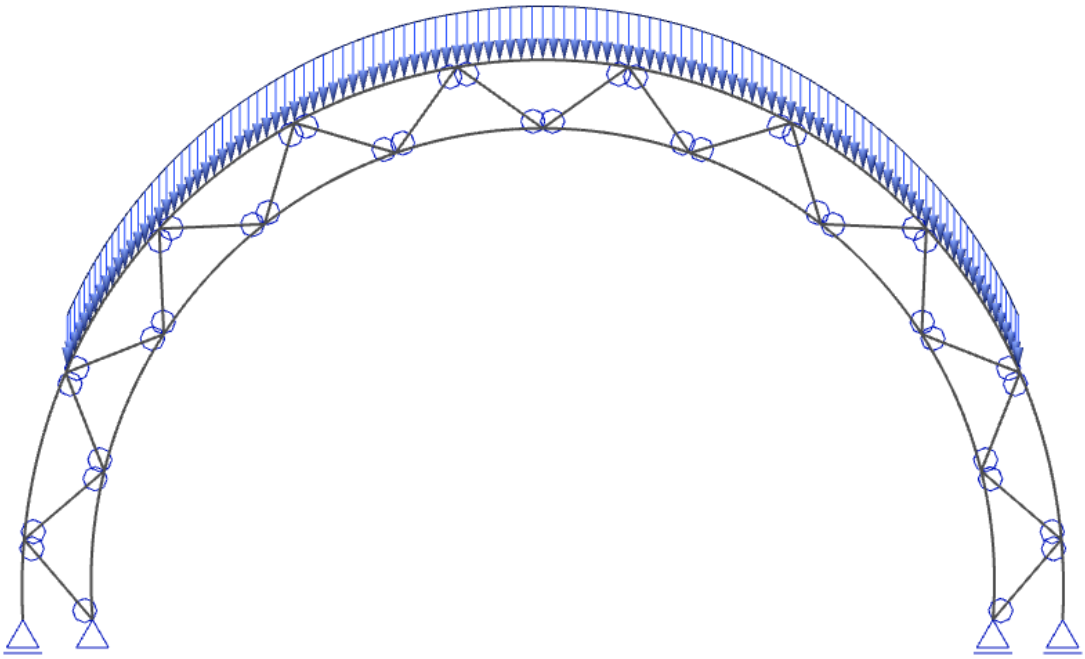

Figure D.13: Input SCIA snow load ($q_s(i)$)

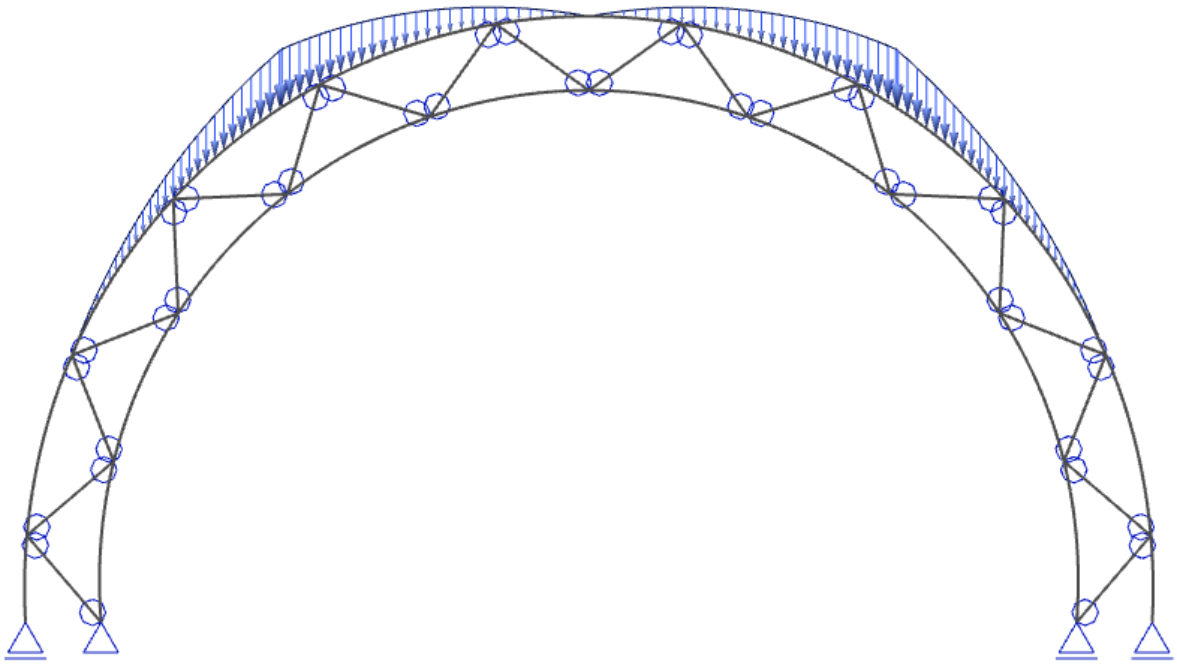

Figure D.14: Input SCIA snow load ($q_s(ii)$)

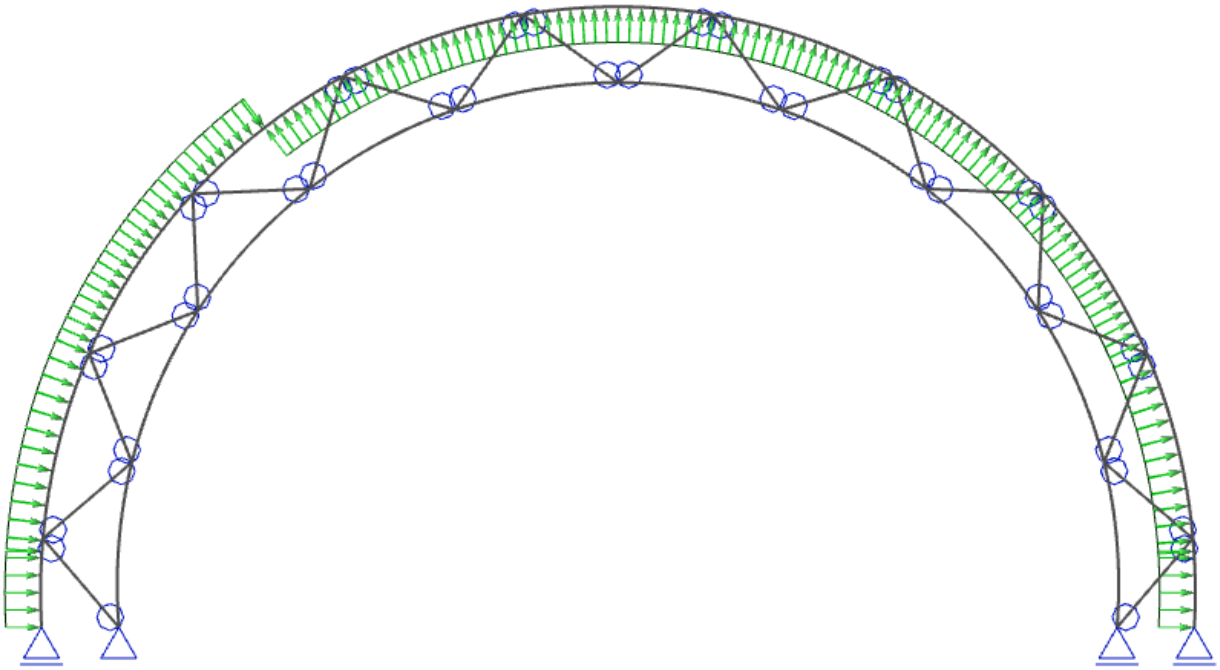

Figure D.15: Input SCIA wind load (q_{we})

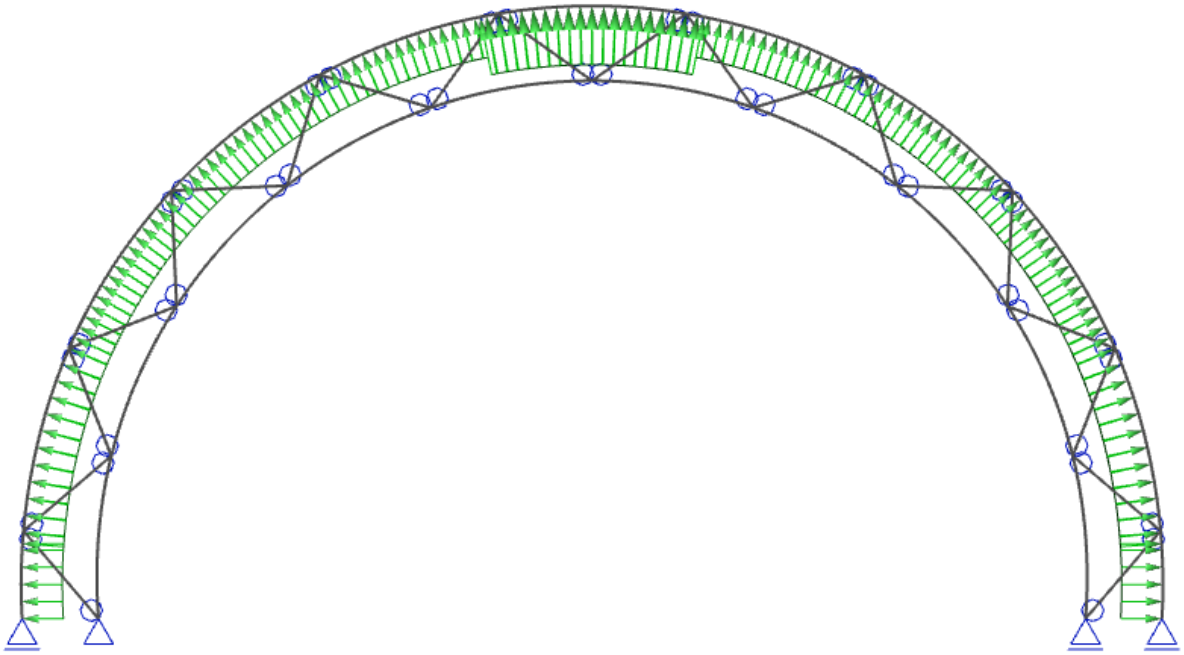

Figure D.16: Input SCIA internal pressure (q_{wi})

D.6 Results SCIA arched truss

Load combination	Extreme stresses diagonals				Extreme stresses curved beams					
ULS	Member	Normal stress	Member	Normal stress	Normal stress		Shear stress		Bending stress	
B.9	PQ	0.75 N/mm^2	ST	-0.95 N/mm^2	0.88 N/mm^2	-1.32 N/mm^2	0.85 N/mm^2	-0.85 N/mm^2	0.65 N/mm^2	-0.81 N/mm^2
B.10	NO	0.88 N/mm^2	ST	-0.98 N/mm^2	1.01 N/mm^2	-1.38 N/mm^2	0.89 N/mm^2	-0.89 N/mm^2	0.68 N/mm^2	-1.30 N/mm^2
B.11	PQ	1.77 N/mm^2	ST	-2.15 N/mm^2	2.07 N/mm^2	-3.01 N/mm^2	1.95 N/mm^2	-1.95 N/mm^2	1.48 N/mm^2	-1.85 N/mm^2
B.12	PQ	2.07 N/mm^2	QR	-2.32 N/mm^2	2.00 N/mm^2	-3.20 N/mm^2	2.06 N/mm^2	-1.75 N/mm^2	1.58 N/mm^2	-1.97 N/mm^2
B.13	EF	2.07 N/mm^2	AC	-3.59 N/mm^2	2.66 N/mm^2	-2.89 N/mm^2	1.72 N/mm^2	-1.66 N/mm^2	1.75 N/mm^2	-1.73 N/mm^2

Figure D.17: Extreme stresses retrieved from SCIA